STAMP

TECHNICAL RELEASE REQUEST

WHC-CM-3-4

Complete for all Types of Release

Purpose
- ☐ Speech or Presentation
  - ☐ Full Paper
  - ☐ Summary
  - ☐ Abstract
  - ☐ Visual Aid
- ☐ Speakers Bureau
- ☐ Poster Session
- ☐ Reference
- ☑ Technical Report
- ☐ Thesis or Dissertation
- ☐ Manual
- ☐ Brochure/Flier
- ☐ Software/Database
- ☐ Controlled Document
- ☐ Other: _____

Intended Audience
- ☑ Public
- ☐ Sponsor-limited
- ☐ Internal

New Document Number (Document Clearance Administration will assign): WHC-EP-0332

Existing Identification Number:

If Previously Cleared, List Document No.:

Date Clearance Required: 5/15/90

Title: Simulations of Infiltration of Meteoric Water and Contaminant Plume Movement in the Vadose Zone at Single-Shell Tank 241-T-106 at the Hanford Site

Lead Author/Name	Impact Level	Phone	MSIN	Other Author(s) Name (s)
REQUESTOR JERRY D. DAVIS	2	6-8919	H4-54	

Project or Program: ~~DEFENSE WASTE~~ Per phone call with Jerry Davis on 6/15/90 - Program to Restoration-N.S.

Lead Org Code: 81210

Sponsor Agency: (DOE,) DOT, NRC, USGS,

Editor Name: S. JANICEK

Phone: 6-2386

DOE/HQ Assistant Secretary For: DP, EH, (ER,) EM, RW, NE

New or novel (patentable) subject matter? ☑ No ☐ Yes
If "Yes", has disclosure been submitted by WHC or other company?
☐ No ☐ Yes Disclosure No(s).

Information received from others in confidence, such as proprietary data, trade secrets, and/or inventions?
☑ No ☐ Yes (Identify)

Copyrights? ☑ No ☐ Yes
If "Yes", has written permission been granted?
☐ No ☐ Yes (Attach Permission)

Trademarks?
☑ No ☐ Yes (Identify)

Complete for Speech or Presentation

Complete Title of Conference or Meeting: NA

Group or Society Sponsoring: NA

Dates of Conference or Meeting: NA

City/State: NA

Will a Proceedings be Published? ☐ Yes ☐ No
Will you hand out material at the meeting? ☐ Yes ☐ No

For a journal submission, provide complete title of journal: NA

Cognizant Line Management

		Date
Author/REQUESTOR J.D. DAVIS	J.D. Davis	4/26/90
Peer Review J.W. CAMMANN	N.R. Wing for	6/14/90
Cognizant Manager L.C. BROWN	M.A. Adams for	6/14/90

Auth. Derivative Classifier

	Yes	No
Unclassified	☒	☐
Classified	☐	☒
UCNI	☐	☒

Date: 6/14/90

WHC Technical Program — Date: 6/14/90

	Yes	No	
Applied Technology	☒	☐	☒ Approve
Limited Disclosure	☐	☐	☐ Disapprove

RD Wojtasek for

Comments (Please Initial)
Per S. Janicek this document is being jointly cleared through DP&S. 6/15/90.

Add to Distribution → Ward Staubitz, USGS, 1201 Pacific Ave, Suite 600, Tacoma, WA 98402
added 7/19/90 S.A. Janicek

Document Clearance Administration

General Counsel — Date: 6/14/90

	Remove	Affix	
Copyright License Notice	☐	☐	☒ Approve
Purpose and Use	☐	☐	
Patent Status	☐	☐	
Legal Disclaimer	☐	☒	☐ Disapprove
Proprietary Information	☐	☐	
Computer Software Notice	☐	☐	

DOE Technical Program — Date: 7/07/90
☒ Approve ☐ Disapprove

Communications — Date:
☐ Approve N/A ☐ Disapprove

Publications Services — Date: 7/19/90
☐ Editorial Review Only ☒ Approve ☐ Disapprove

Other — Date: 7/19/90
NA N. Solis
☐ Approve ☐ Disapprove

Document Clearance Administration Release Stamp

APPROVED FOR RELEASE OFFICIAL DOCUMENT NS Date 7/19/90

EP

DOE F 1332.15 (5-88) | U.S. DEPARTMENT OF ENERGY | OMB Control No. 1910-1400

DOE AND MAJOR CONTRACTOR RECOMMENDATIONS FOR ANNOUNCEMENT AND DISTRIBUTION OF DOCUMENTS

1. DOE Report No.	2. DOE Contract No.	3. DOE 8 and R code(s)	4. OSTI UC or C Category No.
WHC-EP-0332	DE-AC06-87RL-10930		

5. Title SIMULATIONS OF INFILTRATION OF METEORIC WATER AND CONTAMINANT PLUME MOVEMENT IN THE VADOSE ZONE AT SINGLE-SHELL TANK 241-T-106 AT THE HANFORD SITE

6. Type of Document ("x" one)

a. Scientific and technical report: ☐ monthly ☐ quarterly ☐ annual ☐ final ☐ topical ☐ other

b. Conference paper: Name of conference (no abbreviations) _____

Location (city/st/ctry) _____

Date (mo/day/yr) _____ Sponsor _____

Contents: ☐ proceedings ☐ viewgraphs ☐ paper ☐ poster sessions

c. Computer Media:

Document is accompanied by ☐ magnetic tape(s) _____

☐ diskette(s) _____

☐ other (specify) _____

d. Other (e.g., journal article, manuscript, manual, etc.) (specify) _____

7. Copies Transmitted to OSTI ("x" one or more)

☐ a. Copies transmitted for unclassified distribution.
☐ b. Copies transmitted for special distribution.
☒ c. Two reproducible copies transmitted.
☐ d. Ten copies transmitted for OSTI processing and NTIS sales.
☐ e. Copies transmitted for classified distribution as defined in M-3679.
☐ f. One copy transmitted for OSTI classified processing.

8. Document contains information pertaining to any of the following:

☐ Yes ("x" one or more) ☒ No (if no, unlimited distribution may be made within the U.S. In addition, copies may be made available to Foreign requestors through exchange agreements or NTIS sales.)

☐ a. Classified
(Announce to addresses in M-3679)
☐ b. Official Use Only (OUO)
☐ c. Export Control/ITAR/EAR
☐ d. Proprietary Information
☐ e. Small Business Innovation Research (SBIR)
☐ f. Unclassified Controlled Nuclear Information (UCNI)
☐ g. Patent Sensitivity
☐ h. Translations of copyrighted material
(Boxes b—h will be announced to Government agencies and their contractors)
☐ i. Other (explain) _____
(This designation must be in accordance with written DOE Program Office guidance)

Upon demand, OSTI will make distribution of these documents in accordance with existing laws, regulations, and/or written program office guidance.

9. Patent and Copyrighted Information

a. ("x" one) ☒ 1. DOE patent clearance has been granted by responsible DOE patent group.
☐ 2. Document has been sent to responsible DOE patent group for clearance.
☐ 3. Patent clearance not required.

b. Does this material contain copyrighted information? ☐ No ☐ Yes
If yes, has release been obtained for DOE reproduction? ☐ No ☐ Yes
(attach release)

10. Additional information, remarks, and special handling instructions. (*Do not* identify Sigma categories for Nuclear Weapon Data reports, and *do not* provide additional instructions which are inconsistent with item 8 above.) (Continue on separate sheet, if necessary)

11. Submitted by (Name and Position) (Please print or type)		Phone
CHRISITINE WILLINGHAM, CLERK		509-376-5194 FTS 88-444-5194
(Organization) INFORMATION RESOURCE MANAGEMENT	Signature Christine Willingham	Date 8/17/90

Battelle
Pacific Northwest Laboratories

CLEARANCE OF PUBLICATIONS AND PRESENTATIONS

CLEARANCE

Complete for all Types of Release

Type of Release
- ☒ Technical Report
- ☐ Speech or Presentation
  - ☐ Full Paper
  - ☐ Summary
  - ☐ Abstract
  - ☐ Slides
  - ☐ Poster Session
- ☐ Journal Article
- ☐ Book or Book Chapter
- ☐ Thesis or Dissertation
- ☐ Software Documentation
- ☐ Instruction Manual
- ☐ Brochure/Flier
- ☐ Trade Show Exhibit
- ☐ Other:

Document Number (Clearance Administration will assign): PNL-7401

Other Number (e.g., NUREG/CR):

JUN 20 1990

OSTI RECV'D

If Previously Cleared, List Document No.:

Date Clearance Required:

Title: Simulations of Infiltration of Meteoric Water and Contaminant Plume Movement in the Vadose Zone at Single-Shell Tank 241-T-106 at the Hanford Site

Lead Author Name, Payroll Number, Phone, Mailstop (MSIN): J. L. Smoot/30157/376-1352/K6-77

Other Author(s) Name(s): JE Szecsody, B. Sagar, GW Gee, and CT Kincaid

Project or Program Title: Simulate the Plume Under T-106 Single-Shell Tank in 200W

Lead Org. Code: D7D32

Editor Name (if edited), Phone: J. Sprouse 376-1896

Client (Four Digit Code):

If 1830, Project No. and B&R No.: 16016 820201000 (ED 9644)

If Related Services, TD No. (and FIN No. if NRC):

If Non-1830, Contract No.:

Speech, Article, Presentation

Complete Title of Conference:

Group or Society Sponsoring:

Dates of Conference:

City/State:

Will a Proceedings be Published? ☐ Yes ☐ No

Will you hand out material at the meeting? ☐ Yes ☐ No

For a journal submission, provide complete title of journal:

Brochure, Flier

Intended Audience:

Purpose of Publication/Presentation:

Quantity	Production Cost	How will it be distributed?

I HAVE REVIEWED THE ATTACHED DOCUMENT AND HAVE CONSIDERED ALL OF THE APPROPRIATE ITEMS IN THE CHECKLIST ON THE BACK OF THIS FORM.

Author: JL Smoot JL Smoot 5/29/90	Program Manager: Date
Peer Reviewer: MP Bergeron MP Bergeron 6/15/90	Other: Date
Editorial Reviewer: PC Hays KE Hanson for PC Hays 6-15-90	Reviewers' Comments (Please initial): This document is being published by WHC and is going through WHC clearance also. The document will be published as WHC-EP-0332. Please note distribution Comments. (12 copies to OSTI. 1 to Technical Report files) RL Skaggs
Section Manager: RL Skaggs RL Skaggs 6/15/90 Date	
Department Manager: RL Skaggs RL Skaggs 6/15/90 Date	
Authorized Derivative Classifier: RL Skaggs 6/15/90 Date	

☒ Unclassified
☐ Classified
☐ This document may contain UCNI
☐ Restricted distribution because of:

Administration Will Route

Patent Reviewer: Paul W. Simmelink 6/22/90 Date

DOE-RL: Date

Approved for Release: Date

Publication Services: 6/25/90

Attention Patent Services: This document may contain or disclose:

Initials

54-1100-022 (10-88)

WHC-EP-0332

Simulations of Infiltration of Meteoric Water and Contaminant Plume Movement in the Vadose Zone at Single-Shell Tank 241-T-106 at the Hanford Site

Prepared for the U.S. Department of Energy
Assistant Secretary for Environmental Restoration
and Waste Management

Westinghouse
Hanford Company Richland, Washington

Hanford Operations and Engineering Contractor for the
U.S. Department of Energy under Contract DE-AC06-87RL10930

RECORD COPY

Approved for Public Release

DISCLAIMER

This report was prepared as an account of work sponsored by an agency of the United States Government. Neither the United States Government nor any agency thereof, nor any of their employees, nor any of their contractors, subcontractors or their employees, makes any warranty, expressed or implied, or assumes any legal liability or responsibility for the accuracy, completeness, or any third party's use or the results of such use of any information, apparatus, product, or process disclosed, or represents that its use would not infringe privately owned rights. Reference herein to any specific commercial product, process, or service by trade name, trademark, manufacturer, or otherwise, does not necessarily constitute or imply its endorsement, recommendation, or favoring by the United States Government or any agency thereof or its contractors or subcontractors. The views and opinions of authors expressed herein do not necessarily state or reflect those of the United States Government or any agency thereof.

Available from
U.S. Department of Commerce
National Technical Information Service
5285 Port Royal Road
Springfield, VA 22161

NTIS Price Codes:
Microfiche Copy: A01
Printed Copy:

Pages	Price Codes	Pages	Price Codes
001-025	A02	301-325	A14
026-050	A03	326-350	A15
051-075	A04	351-375	A16
076-100	A05	376-400	A17
101-125	A06	401-425	A18
126-150	A07	426-450	A19
151-175	A08	451-475	A20
176-200	A09	476-500	A21
201-225	A10	501-525	A22
226-250	A11	526-550	A23
251-275	A12	551-575	A24
276-300	A13	576-600	A25

Printed in the United States of America

DISCLM-1.CHP (2-89)

RECORD COPY

WHC-EP-0332

Simulations of Infiltration of Meteoric Water and Contaminant Plume Movement in the Vadose Zone at Single-Shell Tank 241-T-106 at the Hanford Site

J. L. Smoot
J. E. Szecsody
B. Sagar
G. W. Gee
C. T. Kincaid
Pacific Northwest Laboratory

Date Manuscript Complete
November 1989

Prepared for the U.S. Department of Energy
Assistant Secretary for Environmental Restoration
and Waste Management

Westinghouse Hanford Company
P.O. Box 1970
Richland, Washington 99352

Hanford Operations and Engineering Contractor for the
U.S. Department of Energy under Contract DE-AC06-87RL10930

Approved for Public Release

Reference herein to any trademark, manufacturer, or otherwise, does not necessarily constitute or imply its endorsement, recommendation, or favoring by the United States Government or any agency thereof.

SIMULATIONS OF INFILTRATION OF METEORIC WATER AND CONTAMINANT PLUME MOVEMENT IN THE VADOSE ZONE AT SINGLE-SHELL TANK 241-T-106 AT THE HANFORD SITE

ABSTRACT

Contaminant plume migration in the vadose zone from a leak at Tank 241-T-106 on the Hanford Site was modeled to determine the effect of coarse backfill covers on the infiltration of meteoric water and the subsequent transport of contaminants. Infiltration through the upper 2 m of soil cover was simulated for the period of 1947 to 2020 using hydraulic properties estimated for the backfill sediments. The infiltration simulations indicate that approximately 77 percent (13.1 cm/yr) of annual precipitation infiltrates below a depth of 2 m. Evaporation averaged 20 percent (3.4 cm) of annual precipitation. Reducing the hydraulic conductivity tenfold resulted in a drainage of 68 percent of annual precipitation, whereas increasing the hydraulic conductivity tenfold resulted in a drainage of 86 percent of annual precipitation. When a 0.15-m-thick layer of silt loam soil was added to the surface, the drainage was reduced to less than 1 percent of the annual precipitation after 5 yr. The infiltration simulations suggest that coarse backfill sediments, kept free of vegetation, allow a significant portion of the annual precipitation to infiltrate and drain to the subsurface.

The Tank 241-T-106 leak was simulated for the period 1960 to 1990 using an infiltration average of 77 percent of precipitation. The results of the simulations indicate that increased meteoric water infiltration because of

the presence of coarse surface sediments increases the rate of movement of ^{106}Ru. The simulations show the ^{106}Ru plume approaching the water table in the early 1980's, but subsequent radioactive decay appears to preclude the plume from moving into the saturated zone. The simulated ^{137}Cs plume migrates considerably less distance than the ^{106}Ru plume because of greater sorption.

The increased plume mobility compared to previous simulations at lower infiltration rates implies that remedial action, in the form of an infiltration barrier, could be an effective means to inhibit the movement of the plume.

EXECUTIVE SUMMARY

Contaminant plume migration in the vadose zone from a leak at Tank 241-T-106 on the Hanford Site was modeled with the inclusion of infiltration of meteoric water. The purpose of this modeling effort was to determine the effect of coarse backfill covers overlying the buried single-shell tank farms on infiltration of meteoric water and the subsequent transport of contaminants from a leak at Tank 241-T-106.

Infiltration through the upper 2 m of soil cover was simulated for the period of 1947 to 2020 to determine the amount of water available for deep percolation towards the water table. The results of the infiltration simulation were used to simulate the antecedent and subsequent moisture distribution relative to the 1973 leak at Tank 241-T-106. The movement of ^{106}Ru and ^{137}Cs plumes resulting from this leak were simulated through the subsurface layered sediments.

Using hydraulic properties estimated for the backfill sediments, the infiltration simulations indicate that approximately 77 percent (13.1 cm/yr) of annual precipitation infiltrates below a depth of 2 m. Evaporation averaged 20 percent (3.4 cm) of annual precipitation. Reducing the hydraulic conductivity tenfold resulted in a drainage of 68 percent of annual precipitation, whereas increasing the hydraulic conductivity tenfold resulted in a drainage of 86 percent of annual precipitation. This indicates that the estimate of drainage for the backfill may be reasonable, given some spatial variation in soil properties. Different surface modifications were simulated to evaluate potential methods for reducing drainage. When a 0.15-m-thick layer of silt loam soil was added to the surface, the drainage was reduced to less than 1 percent of the annual precipitation after 5 yr. In contrast, a surface of clean gravel increased the drainage to 95 percent of precipitation. When an impermeable barrier was placed over the tank farm sediments, the drainage at a 2-m depth decreased to less than 0.05 cm/yr after 8 yr, for cases of either a backfill or a clean graveled surface.

The infiltration simulations suggest that coarse backfill sediments, kept free of vegetation, allow a significant portion of the annual precipitation to infiltrate and drain to the subsurface. Drastic improvement in infiltration control is obtained using a 0.15-m-thick fine-grained (silt loam) soil cover. A surface covering (either a fine-grained soil or an impermeable material) will ensure that low infiltration rates can be achieved in the near future.

The Tank 241-T-106 leak was simulated for the period 1960 to 1990 using an infiltration average of 77 percent of precipitation. The results of the simulations indicate that the increased meteoric water infiltration, because of the presence of coarse surface sediments, increases the rate of movement of the ^{106}Ru plume. The simulations show the ^{106}Ru plume approaching the water table in the early 1980's, but subsequent radioactive decay appears to preclude the plume from moving into the saturated zone. The simulated ^{137}Cs plume migrates considerably less distance than the ^{106}Ru plume because of a greater sorption to subsurface sediments and becomes essentially stationary after approximately 50 days.

These contaminant plume simulations show increased mobility because of the relatively high infiltration rates compared to previous simulations at lower infiltration rates. This fact implies that remedial action, in the form of an infiltration barrier, could be an effective means to inhibit the movement of the plume. However, the results are very preliminary because much of the input used for both model simulations was based on estimates of physical and chemical properties of the tank farm sediments. At present, no direct measurements of these properties have been made on the tank farm sediments. Laboratory measurements of these properties, as well as field experiments verifying water fluxes and sorption characteristics at various depths, may ultimately be required to verify the simulation results.

CONTENTS

1.0 INTRODUCTION 1

2.0 INFILTRATION SIMULATIONS OF METEORIC WATER INTO SURFACE SEDIMENTS AT THE 241-T TANK FARM 1
2.1 CONDITIONS SIMULATED 3
2.2 MODEL INPUT PARAMETERS 3
2.3 INFILTRATION SIMULATION RESULTS 9
2.3.1 Infiltration of Meteoric Water 9
2.3.2 Hydraulic Conductivity Alteration 13
2.3.3 Surface Soil Conditions Alteration 14
2.3.4 Precipitation Timing and Intensity 18
2.3.5 Barrier Simulations 18
2.4 INFILTRATION SIMULATION CONCLUSIONS 21

3.0 SIMULATIONS OF CONTAMINANT PLUME MOVEMENT IN THE VADOSE ZONE AT TANK 241-T-106 22
3.1 CONCEPTUAL MODEL FOR THE SIMULATIONS 22
3.2 CONTAMINANT PLUME SIMULATION RESULTS 27
3.2.1 Ruthenium-106 Movement 28
3.2.2 Cesium-137 Movement 34
3.3 CONTAMINANT PLUME SIMULATION CONCLUSIONS 34

4.0 REFERENCES 36

APPENDIXES:

A. Hydraulic Property Characterization of the Grout Site . . . . A-i
B. Physical Analysis for Grout Study . . . . . B-i
C. Grout Site Sediment Sample Analyses . . . . . C-i

LIST OF FIGURES

1 Location of the Hanford Site and the T Tank Farm 2

2 Cross-Sectional View of the 241-T Tank Farm. 4

3 Grain-Size Distributions of Hanford Site Sediments 6

4 Precipitation and Drainage for Backfill (Case 1) 9

5 Yearly Fluxes for Backfill (Case 1) 12

6 Effect on Drainage of a Change in Hydraulic Conductivity 15

7 Effect on Drainage of the Addition of a Surface Soil or Gravel . . . 17

8 Yearly Drainage for Impermeable Surface Barrier Cases 20

9 Cumulative Drainage at 2-m Depth for Impermeable Surface Barrier Cases 20

10 Plan and Vertical Cross-Sectional Views of the 1973 ^{137}Cs, ^{144}Ce, and ^{106}Ru (1 μCi/L) Volumetric Isopleths 24

11 Plan and Vertical Cross-Sectional Views of the 1973 and 1978 ^{106}Ru (1 μCi/L) Volumetric Isopleths 25

12 Textures and Thicknesses of the Five Stratigraphic Zones at the T Tank Farm 26

13 Saturated Hydraulic Conductivity and Saturated Moisture Content Values for the Five Stratigraphic Layers Identified at the T Tank Farm 27

14 PORFLO-3 Simulation of Relative Saturation in 1969 29

15 PORFLO-3 Simulation of Relative Saturation in 1974 30

16 PORFLO-3 Simulation of the Vertical Extent of the ^{106}Ru (1 μCi/L) Volumetric Isopleth for Varying Infiltration Rates at Early Simulation Times 31

17 PORFLO-3 Simulation of the Vertical Extent of the ^{106}Ru (1 μCi/L) Volumetric Isopleth for a Constant 0.05 m/yr Infiltration Rate at Early Simulation Times (Days) 32

LIST OF FIGURES (cont.)

18 PORFLO-3 Simulation of the Vertical Extent of the ^{106}Ru (1 μCi/L) Volumetric Isopleth for Varying Infiltration Rates at Late Simulation Times 33

19 PORFLO-3 Simulation of the Vertical Extent of the ^{137}Cs (1 μCi/L) Volumetric Isopleth for Varying Infiltration Rates 35

LIST OF TABLES

1 Conditions Used for the Infiltration Cases Simulated 5

2 Hydraulic Properties, Reported as van Genuchten Functions 7

3 Results for Backfill (Case 1) 11

4 Results for Hydraulic Conductivity Changes 14

5 Effect on Drainage of the Addition of a Surface Soil 16

6 Results for the Addition of an Impermeable Surface Barrier 19

7 Radionuclide Inventory of the Tank 241-T-106 Supernatant Solution 23

This page intentionally left blank.

1.0 INTRODUCTION

An understanding of the infiltration of meteoric water through sediments at the single-shell tank farms and the impact of this transient infiltration on contaminant plume movement is important for evaluating alternative remedial actions for leaking single-shell tanks at the Hanford Site. Two modeling studies are described in this report: (1) a one-dimensional simulation of the infiltration of meteoric water into surface sediments and (2) a three-dimensional simulation of contaminant plume migration in the vadose zone at Tank 241-T-106. The evaluation of infiltration through sediments at single-shell tank farms in the 200 West Area at the Hanford Site (Figure 1) is in support of environmental remediation activities being conducted at the Hanford Site to comply with the *Resource Conservation and Recovery Act of 1976* (RCRA); the *Comprehensive Environmental Response, Compensation, and Liability Act of 1980* (CERCLA); and the *Hanford Federal Facility Agreement and Consent Order*, hereinafter referred to as the Tri-Party Agreement (Ecology et al. 1989). This work is sponsored by the U.S. Department of Energy through the aegis of the Westinghouse Hanford Company (Westinghouse Hanford) Environmental Restoration/Remedial Action Program Office.

The varying of infiltration rates may be expected to affect the transport of contaminants from single-shell tank leaks to the water table. The simulation of the infiltration of meteoric water through 2 m of surface sediments above the buried tank were made using the one-dimensional computer code UNSAT-H Version 2.0 (Fayer and Jones 1990). The results were used as a surface boundary condition for three-dimensional simulations of contaminant plume movement in the entire vadose zone using the code PORFLO-3 Version 1.0* (Runchal and Sagar 1989; Sagar and Runchal 1990). The results include ^{106}Ru and ^{137}Cs plume migration over time with transient infiltration.

Infiltration simulations with UNSAT-H Version 2.0 included evaluation of the sensitivity of the predictions and evaluation of potential methods for reducing drainage by the addition of surface barriers. The proposed use of temporary barriers would be considered an interim remedial action according to the provisions of the Tri-Party Agreement (Ecology et al. 1989).

2.0 INFILTRATION SIMULATIONS OF METEORIC WATER INTO SURFACE SEDIMENTS AT THE 241-T TANK FARM

The results of a one-dimensional simulation of water balance of the surface sediments of the 241-T Tank Farm are described in the following paragraphs. Water balance is simulated with UNSAT-H Version 2.0 (Fayer and Jones 1990) to a depth of 2 m using daily meteorological input and estimated sediment hydraulic properties.

---

*PORFLO-3 is a copyright of Analytic & Computational Research, Incorporated.

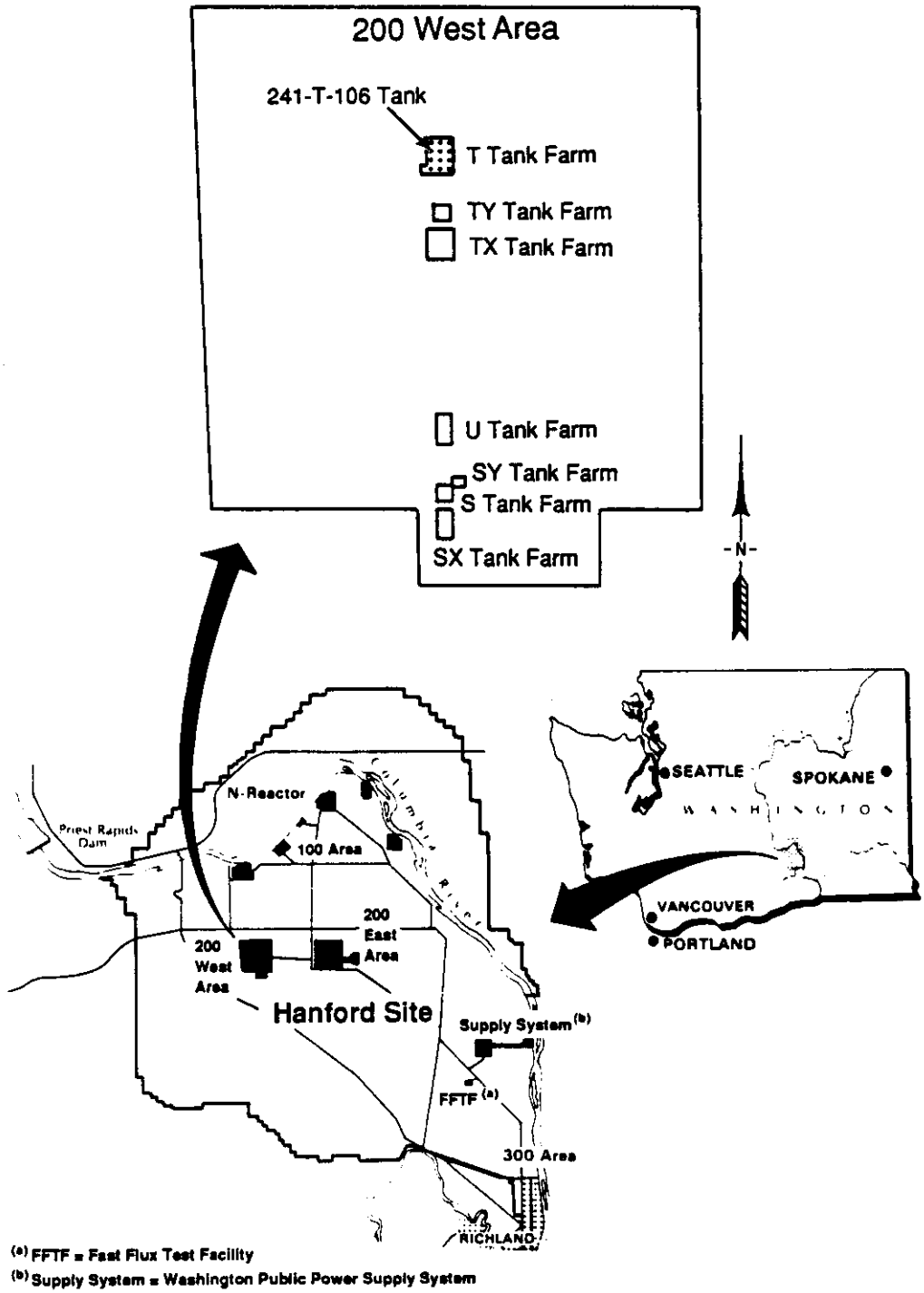

Figure 1. Location of the Hanford Site and the T Tank Farm.

The purpose of this simulation was to predict the downward flux of meteoric water over time at the depth of the approximate top of the buried single-shell waste tanks (Figure 2). The moisture conditions and the downward flux of meteoric water at a 2-m depth have been estimated at the 241-T Tank Farm since the beginning of tank operations in 1944. Future drainage is also predicted for the next 31 yr (1990 through 2020) given the data currently available. The drainage fluxes were used as input for the upper-boundary condition in subsequent simulations using PORFLO-3 (Runchal and Sagar 1989; Sagar and Runchal 1990). The water flux at a 2-m depth will hereinafter be referred to as drainage.

2.1 CONDITIONS SIMULATED

The surface water balance was simulated for the period of time beginning January 1947, near the start of use of the 241-T Tank Farm (Brown et al. 1979). Surface water balances were also simulated from 1973 to present, as well as future water balance conditions through December 2020 (over 31 yr from the present). The following specific cases are described in this report.

Case 1: Unimpeded infiltration into the backfill from January 1947 through December 2020 (74 yr). No action is taken to divert precipitation.

Cases 2 and 3: Sensitivity to a change in hydraulic conductivity from case 1 (saturated hydraulic conductivity [K_{sat}] = 4.46 cm/h). Simulations of 0.1 x K_{sat} (case 2) and 10 x K_{sat} (case 3) for 11 yr.

Cases 4 and 5: Addition of a surface soil layer: 0.15-m-thick surface silt loam (case 4) or clean gravel (case 5).

Case 6: Effect of precipitation timing for conditions of case 5.

Cases 7 and 8: Addition of an infiltration barrier for the conditions of case 1 (case 7) or case 5 (case 8).

Cases 2 through 8 (Table 1) test the sensitivity of the predictions made in case 1 to unimpeded water infiltration through the upper 2 m of coarse-grain sediments and include several options of surface modification to minimize drainage. A smaller amount of drainage through this zone should result in a smaller potential for contaminant migration at a greater depth. The simulations for the top 2 m of soil incorporate daily meteorological data to calculate the change in water flux over time. Time increments range from 10^{-2} to 1 h, with a reduction to 10^{-8} h when precipitation commences.

2.2 MODEL INPUT PARAMETERS

The one-dimensional simulations of infiltration at the 241-T Tank Farm cover the zone from the land surface to a depth of 2 m, corresponding to the approximate top of the buried single-shell tanks (Figure 2). Backfill material (silty, sandy gravel) composed of mixed sediments, largely from the

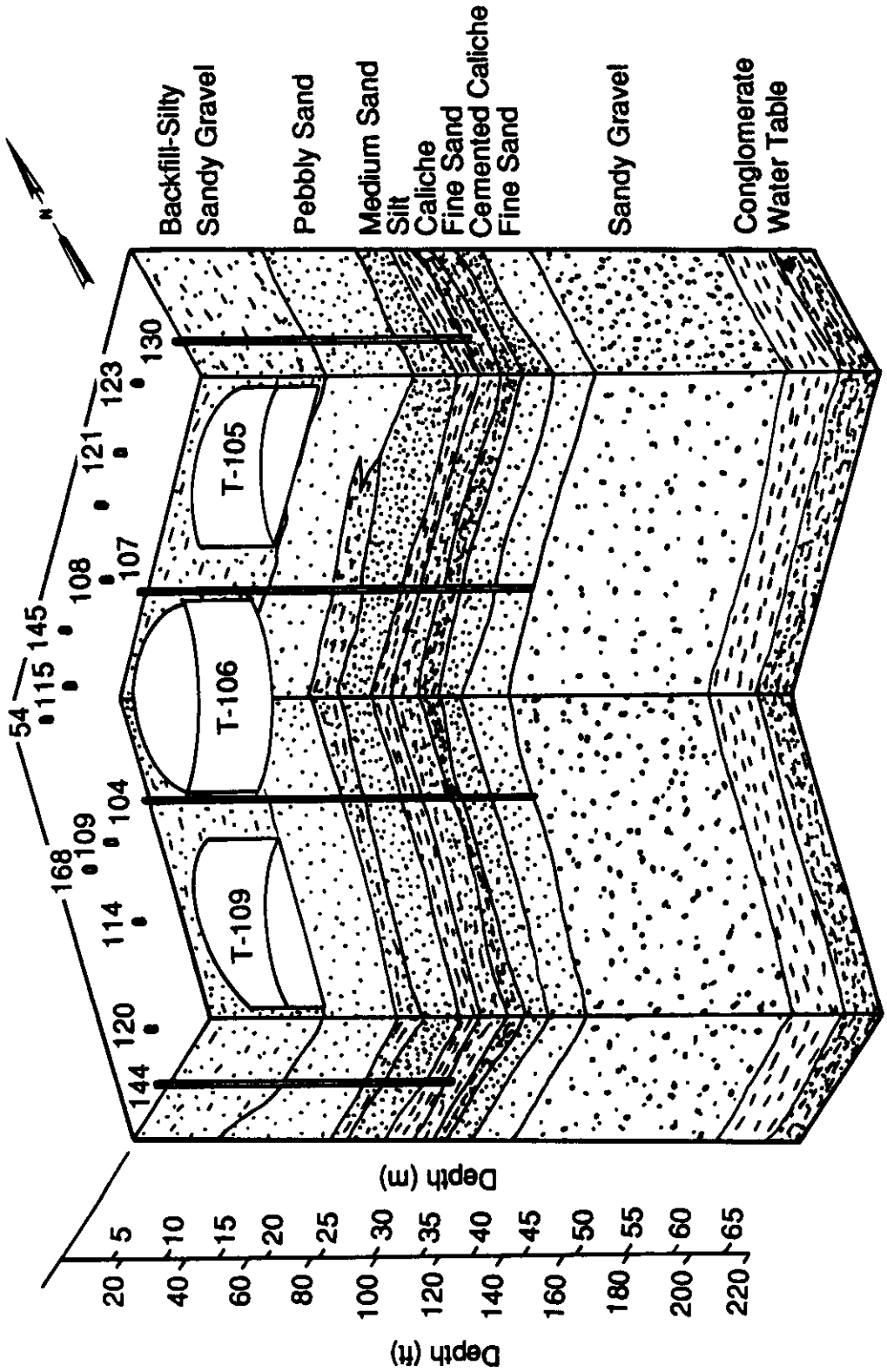

Figure 2. Cross-Sectional View of the 241-T Tank Farm.

Table 1. Conditions Used for the Infiltration Cases Simulated.

Case	Time period simulated	Material	K_{sat} (cm/h)	Change in precipitation	Impermeable barrier
1	1947-2020	Backfill	4.46	no	no
2	1980-1990	Low-K backfill	0.446	no	no
3	1980-1990	High-K backfill	44.6	no	no
4	1957-1966	Silt loam and backfill	2.50, 4.46	no	no
5	1957-1966	Clean gravel and backfill	1,261, 4.46	no	no
6	1957-1966	Clean gravel and backfill	1,261, 4.46	yes	no
7	1990-2010	Backfill	4.46	no	yes
8	1990-2010	Clean gravel and backfill	1,261, 4.46	no	yes

Hanford formation (Routson et al. 1979), was used to bury the tanks at the 241-T Tank Farm (Figure 2). Some of the other tank farm surfaces have been locally covered with a layer of clean gravel. This situation is simulated in case 5.

Grain-size distributions for several samples of backfill were provided by the Westinghouse Hanford staff. Surface samples from 17 tank farm locations (nine from the 200 West Area and eight from the 200 East Area) were collected and analyzed for their grain-size distribution in early August 1989. Sample 9-025 (taken from the 241-U Tank Farm surface) and sample 9-029 (taken from the 241-S Tank Farm surface) represent the upper and lower extremes of the grain-size distributions for samples from the 200 West Area, where Tank T-106 is located.

The size distributions for these samples are plotted in Figure 3 with size distributions for clean gravel (see Appendix A) and soils from the 300 Area lysimeter sites, the 200 East Area lysimeter site, and the McGee Ranch site (Gee 1987; Gee and Kirkham 1984). Also plotted is the size distribution for sandy gravel, designated as AP-1g, taken from the AP Tank Farm, which has been characterized for hydraulic properties (see Appendix C). The grain-size distribution for unit AP-1g (Figure 3) is similar to the surface materials at the 200 West Area Tank Farms, but sieve analyses indicate that AP-1g may have a somewhat larger proportion of fine-grained material than the surface samples (9-025 and 9-029). With a higher percentage of

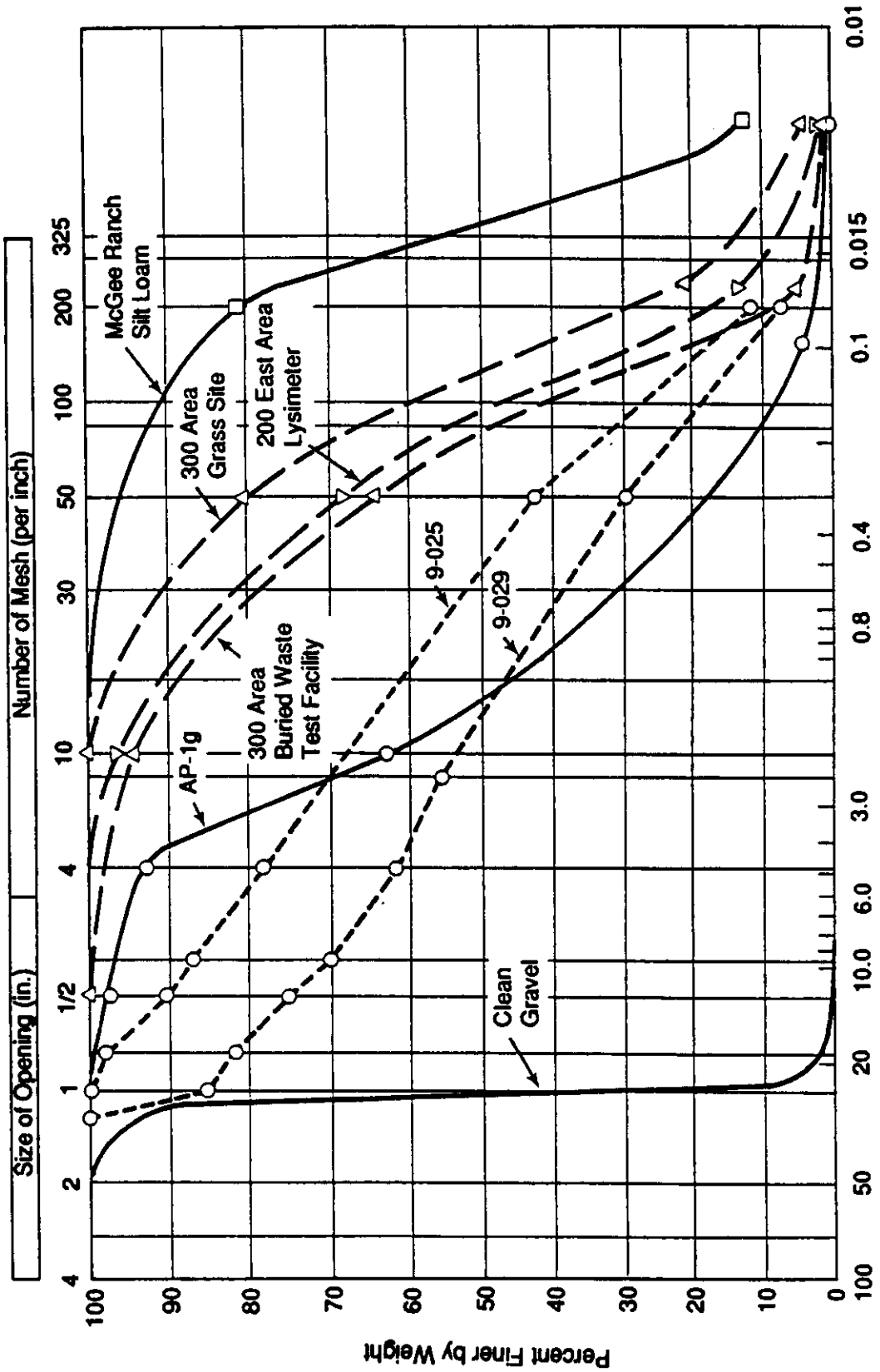

Figure 3. Grain-Size Distributions of Hanford Site Sediments.

fine-grain sediment, the saturated hydraulic conductivity may be larger for unit AP-1g than for the backfill sediments at the 200 West Area tank farms. However, hydraulic conductivity and water retention data are not available for the actual backfill at the 241-T Tank Farm, so data from unit AP-1g were used to represent the backfill properties. Properties for the entire 2-m depth of backfill were simulated using hydraulic properties of the AP-1g soil.

The hydraulic properties used for the backfill (i.e., those of unit AP-1g), as well as the properties of the soils used in the other cases, are represented by van Genuchten functions (van Genuchten 1980) as shown in Table 2. These parameters are fitted values obtained from laboratory data. In the simulations for the silt loam, the soil water suction (tension) was allowed to vary from 0.0 (saturated) to 10^5 cm (dry) for a range of hydraulic conductivity from 2.5 to 10^{-27} cm/h, respectively. The backfill and the clean gravel had extremely steep desaturation curves. Therefore, it was necessary to restrict the maximum suction to 500 cm to be within the limits of single-precision calculations on the VAX* computer. These constraints do not affect the overall water flux, because the water content at 500 cm is essentially equal to the water content of residual moisture (i.e., suction is very large). The K_{sat} for each sediment type in Table 2 are discussed in terms of baseline hydraulic conductivity (K_o) for subsequent simulations. A unit gradient was assumed for the lower boundary condition.

Table 2. Hydraulic Properties, Reported as van Genuchten Functions.

Sediment type	θsat, saturated water content (cm^3/cm^3)	θr, residual water content (cm^3/cm^3)	α coefficient (1/cm)	n power index	K_{sat} hydraulic conductivity (cm/h)
Clean gravel	0.4190	0.0308	4.695	2.572	1,261.0
Backfill (AP-1g)	0.2585	0.0200	0.1008	2.922	4.46
McGee silt loam	0.4520	0.0000	0.00828	1.419	2.50

The initial soil suction for case 1 was 100 cm for the profile (24 nodes); 100 cm was chosen as an estimate of relatively dry backfill sediments because it was known that this unit dried on the surface during tank emplacement. Other cases were initiated at later times, so their initial conditions were the final conditions of the previous year in the case 1 simulation. Given the relatively fast transport of water in the backfill or

*VAX is a trademark of the Digital Equipment Corporation.

the clean gravel, any choice of initial conditions should be of little consequence after a short time (less than 1 yr). However, an accurate representation of the precipitation (frequency and amount) is important to avoid accumulating errors in water fluxes.

The model used in this simulation [UNSAT-H Version 2.0 (Fayer and Jones 1990)] is a one-dimensional, finite-difference, unsaturated zone water flow code. Because the UNSAT-H Version 2.0 was used in the isothermal mode in this study, it is equivalent to UNSAT-H Version 1.0, in which the accuracy of the code has been verified (Fayer et al. 1986). This model uses meteorological data including precipitation to simulate water and vapor movement in the sediments and evaporation at the surface. Actual precipitation records from the Hanford Meteorological Station were used from 1947 to 1988. Simulated values used for future events were generated based on the average and variation from 1957 to 1988 using WGEN, a Markov chain exponential model (Richardson 1981). This model produces precipitation values that vary randomly but maintain the same statistical features (mean, variance, and timing) as the actual data.

The temporal resolution of WGEN output was a day; thus the hour of initiation of precipitation events could not be simulated. Therefore, application of precipitation starting at midnight was used at a rate of 1 cm/h. Because the hour of precipitation differed from actual events, and the simulated intensity was greater than most events, this water application method was compared to actual precipitation timing and intensity. The comparison is reported in Section 2.3.4.

Additional daily meteorological data were needed, including maximum and minimum temperatures, dew point temperature, net solar radiation, wind velocity, and cloud cover. The Hanford Meteorological Station data were used for 1947 and 1957 through 1988. The model WGEN (Richardson 1981) was used to synthesize data for maximum and minimum temperatures and net solar radiation for 1948 to 1956 and 1989 to 2020. The input parameters for WGEN were calculated from the Hanford Meteorological Station data from 1957 to 1988. Average monthly values for wind velocity for 1945 to 1980 and cloud cover for 1946 to 1980 (Stone et al. 1983) were used in the simulations, and a weekly average was used for dew point temperature, because these parameters could not be generated stochastically.

The rate of evaporation depends on both the potential evaporation rate and the mass of water at the sediment surface (i.e., in the uppermost element). The maximum (potential) evaporation rate is calculated with the Penman equation, which is a theoretical approach that includes both radiant energy and aerodynamic (wind and vapor pressure deficit) terms (Doorenbos and Pruitt 1977). As water is removed from the surface element by evaporation, a soil suction gradient develops, which results in water being transported up from deeper in the sediments. When this vertical water transport rate to the surface is smaller than the potential evaporation rate, the actual evaporation becomes limited by the water transport rate and, as a result, the surface dries out. Evaporation eventually becomes negligible as the water transport rate becomes small. The potential evaporation rate can also limit the actual evaporation rate, because meteorological conditions at the surface change hourly and seasonally.

Plant transpiration was not simulated in this study because a herbicide currently is used on the surface at the 241-T Tank Farm, and the plant density and herbicide timing over the life of the tank farm are not known. Although UNSAT-H Version 2.0 (Fayer and Jones 1990) can solve cases of linked moisture and heat flux, no change in heat flux was considered, to reduce the complexity of the simulation. Vapor flux of water (assuming constant heat flux) was included in the simulation because it may be significant, given the large air porosities that are present most of the time in the gravel. The diffusion coefficient for water vapor (0.246 cm^2/s) was calculated at the average annual sediment temperature (11.5 °C) with the Wilke-Chang equation (Bird et al. 1960).

2.3 INFILTRATION SIMULATION RESULTS

2.3.1 Infiltration of Meteoric Water

The relationship between daily precipitation and drainage at a depth of 2 m for simulation case 1 is shown in Figure 4, where the two largest precipitation events (at 61 and 271 days) are shown to reach the 2-m depth in an average of 31 and 22 days, respectively. Because water is also redistributed throughout the sediments, the volume of downward flux also depends on

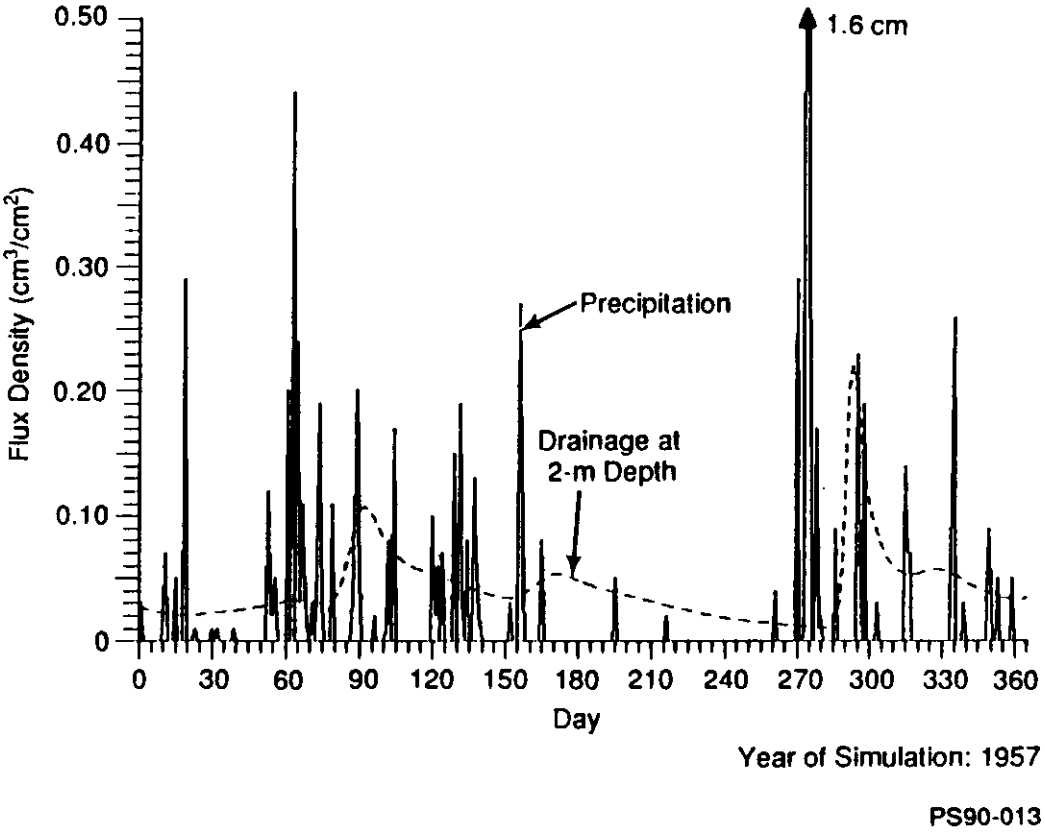

Figure 4. Precipitation and Drainage for Backfill (Case 1).

the antecedent moisture conditions. Smaller precipitation events do not produce clear drainage peaks, as a result of the redistribution of the precipitation pulse. For example, the third largest drainage peak (at 171 days) is probably the result of the combination of precipitation grouped around days 130 and 155. Without closer examination of the hourly flux profiles, further resolution is not possible. In general, Figure 4 shows that water transport in the upper vadose zone is relatively fast (within a month) for this backfill. Therefore, summed over a long period such as a year, the flux at the 2-m depth would not show a significant lag compared to precipitation. However, because a significant portion of precipitation occurs in December, the variation between yearly precipitation and drainage may be caused by late-year precipitation events that result in drainage early in the following year.

The results of the 74-yr simulation of infiltration (case 1) for the years 1947 through 2020 are presented in terms of yearly cumulative fluxes in Table 3. The precipitation simulated over the 74 yr averaged 16.88 ± 4.41 cm, compared to an average of 16.02 ± 4.41 cm for the years 1912 through 1980 (Stone et al. 1983) and an average of 16.72 ± 4.87 cm for the years 1947 to 1988. While these are in reasonable agreement, the combined generated and actual precipitation average does not equal either of the other averages exactly because the number of values of generated data is relatively small (31 yr) and the entire historical record (1912-1980) is not completely generated.

The evaporation averaged 3.41 ± 0.78 cm/yr in the 74-yr simulation (case 1, with unimpeded infiltration) or about 20.2 percent of the total annual precipitation. About 77 percent of the annual precipitation or 13.1 ± 3.03 cm/yr ended up as drainage at a depth of 2 m. The net storage (final storage minus initial storage) in the backfill was 6.25 cm and accounted for 0.5 percent of the total precipitation for the 74-yr test period. Surface runoff averaged 1.8 percent per year and the mass-balance error averaged 0.2 percent per year, which accounted for the remaining flux.

The surface runoff component is produced during the initial phases of the rain events and is apparently an artifact of the water entry calculation. Therefore, this error could be lumped with the mass-balance error. A combined annual mass-balance error of 2 percent accounts for the water balances failing to agree exactly in Table 3. A preliminary double-precision version of UNSAT-H (Fayer et al. 1986) was used to calculate fluxes for 2 yr in the backfill. The surface runoff component was eliminated in this simulation; most of the surface runoff flux resulted in increased drainage at a depth of 2 m (80.0 percent of precipitation) and a small decrease in evaporation (18.3 percent of precipitation).

The high infiltration rates in the backfill caused the actual evaporation (3.41 cm/yr) to be small compared to the potential evaporation. Potential evaporation averaged 165 cm/yr for years when actual precipitation data were available and for the years 2011 to 2020, and it averaged 114 cm/yr for other years in which the meteorological data were generated. The difference in potential evaporation was caused by an error in generating estimates of the dew point temperature. This apparently did not affect the results, because the average evaporation in years with high potential evaporation

Table 3. Results for Backfill (Case 1).

Year	Precip. (cm/yr)	Evap. (cm/yr)	Drainage (cm)	Storage (cm)	Year	Precip. (cm/yr)	Evap. (cm/yr)	Drainage (cm/yr)	Storage (cm)
Initial				4.56					
1947	23.70	5.19	12.51	10.49	1985	12.95	2.47	10.66	10.12
1948	25.27	5.61	18.97	10.88	1986	18.01	3.44	13.56	10.85
1949	10.46	2.48	8.95	9.83	1987	12.90	2.81	9.68	11.22
1950	28.90	5.75	21.86	10.82	1988	10.59	2.49	9.18	9.79
1951	17.78	3.86	13.70	10.34	1989	15.29	3.30	10.85	10.64
1952	10.57	2.84	9.06	8.96	1990	16.94	3.61	12.68	10.99
1953	17.65	3.88	11.81	10.02	1991	14.68	3.13	10.41	11.96
1954	14.53	3.07	11.55	9.56	1992	20.07	3.92	16.38	11.50
1955	18.57	4.11	11.56	12.42	1993	18.03	3.85	12.84	12.51
1956	14.22	3.28	13.66	9.48	1994	13.11	3.32	11.96	10.28
1957	21.06	4.25	15.48	9.80	1995	19.48	3.79	13.51	12.28
1958	22.20	4.27	15.80	11.52	1996	16.92	3.72	14.36	10.81
1959	17.96	3.62	16.32	9.29	1997	16.26	3.29	12.58	11.10
1960	13.77	3.46	8.95	10.59	1998	19.51	4.09	15.36	10.73
1961	17.37	3.27	14.62	10.04	1999	16.87	3.38	13.09	10.82
1962	15.39	2.91	11.83	10.42	2000	15.98	3.55	12.59	10.23
1963	16.03	2.89	11.83	10.72	2001	21.56	3.95	16.57	10.65
1964	13.69	2.58	7.06	14.45	2002	16.03	3.25	12.65	10.65
1965	9.27	2.01	11.48	10.12	2003	12.95	2.91	8.64	12.02
1966	15.06	3.07	11.49	10.25	2004	16.13	3.27	13.40	11.10
1967	8.28	2.15	8.21	8.09	2005	18.72	3.97	15.27	10.54
1968	14.38	3.13	8.37	10.78	2006	21.79	3.75	15.83	12.51
1969	16.16	3.10	12.29	10.77	2007	14.91	2.75	14.11	10.14
1970	16.08	2.74	13.91	9.70	2008	19.41	3.86	13.26	12.33
1971	16.00	2.75	11.35	11.16	2009	16.33	3.54	12.60	12.34
1972	16.23	2.59	12.90	11.42	2010	22.50	4.51	18.17	12.11
1973	21.01	1.75	15.74	14.14	2011	17.40	3.47	14.36	11.55
1974	13.46	2.72	13.67	10.85	2012	12.55	3.13	10.79	9.74
1975	18.95	3.75	14.92	10.55	2013	14.78	3.13	10.28	11.09
1976	7.06	1.95	8.43	7.53	2014	16.84	3.04	12.91	11.91
1977	16.26	3.24	7.95	11.22	2015	16.89	3.65	13.56	11.22
1978	16.61	3.51	14.20	10.02	2016	15.39	2.90	12.88	10.52
1979	14.05	2.90	9.81	11.31	2017	22.50	4.10	16.37	12.34
1980	24.56	4.24	18.35	12.09	2018	19.94	3.57	14.97	13.34
1981	17.88	3.19	14.36	11.93	2019	11.91	2.23	13.77	9.20
1982	20.27	3.94	15.74	12.43	2020	15.29	3.37	10.10	10.81
1983	27.12	5.35	22.52	12.31					
1984	18.44	4.32	15.84	10.52					
					average	16.88	3.41	13.07	10.93
					standard deviation	±4.09	±0.78	±3.03	±1.19

(3.22 ± 0.78) was actually less than the average evaporation in years with low potential evaporation (3.66 ± 0.70), probably because slightly more precipitation occurred.

The small evaporation estimate is reasonably accurate for the conditions of this simulation, given that the yearly mass-balance error was low and the effect of a change in hydraulic conductivity was small (see Section 2.3.2). The small mass-balance error was achieved by using a large number of time steps (16,000 to 100,000/yr), which caused the simulations to use considerable computer time (70 to 250 central processing unit min/yr simulated). A double-precision version of UNSAT-H was tested and found to run even slower (300 central processing unit min/yr), so all of the test runs (Cases 1 through 8) were run with the single-precision version of UNSAT-H.

A plot of the yearly cumulative fluxes (Figure 5) shows that the drainage has no noticeable lag relative to precipitation. The average for evaporation of 20 percent of precipitation is in the same range as the 15 to 35 percent rate measured in field lysimeters containing clean gravel that have been in operation for 3 yr (Gee 1987). When the precipitation and drainage at a 2-m depth (Figure 5) are compared, the yearly change in storage should also be

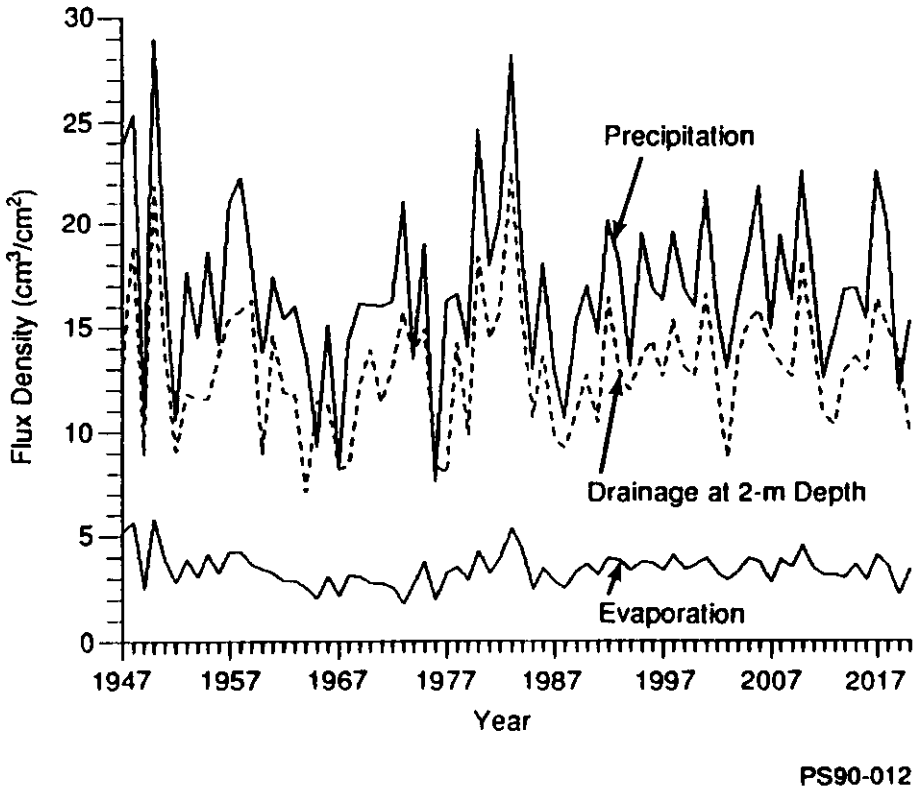

Figure 5. Yearly Fluxes for Backfill (Case 1).

considered (Table 3), because of the lag for the drainage from year-end precipitation. The years in which the drainage exceeds precipitation are usually accompanied by a decrease in storage. Yearly average storage in the backfill averaged 10.93 ± 1.19 cm/yr; this value can be converted into volumetric water content by dividing by the soil profile depth (200 cm). Thus the average volumetric water content in the backfill was 5.47 ± 0.006 percent.

The precipitation input varies on an hourly basis, but as a result of some damping, the drainage (Figure 4) appears to vary in terms of days (i.e., hourly resolution is not necessary). When the data are summed on a yearly basis (Figure 5), the resolution of changes in drainage from specific precipitation events is lost; therefore, the plot varies as a step function from year to year. Consequently, a plot of the actual daily drainage values for the 74 yr (27,000 points) would show smoother transitions than those in Figure 5, although the values would have greater extremes.

The sensitivity of the flux predictions to changes in hydraulic conductivity and surface sediment properties is discussed in the following paragraph. An evaluation of the timing of precipitation also is discussed because simulated precipitation events began at midnight, while actual events occur more randomly.

2.3.2 Hydraulic Conductivity Alteration

Two variations of case 1 were simulated for an 11-yr period to test the sensitivity of the evaporation and drainage predictions. Using the hydraulic properties (other than conductivity) of the backfill (Table 2), the drainage through a backfill with a tenfold smaller hydraulic conductivity (low-K backfill) was simulated in case 2. The flux through a backfill with a tenfold larger hydraulic conductivity (high-K backfill), was simulated in case 3. The results of this water-flux modeling (Table 4) show that there was more evaporation (27 percent) for the simulated low-K backfill (case 2) than the backfill in case 1 (20 percent). There was slightly less evaporation (19 percent) in the simulated high-K backfill (case 3) than the evaporation in backfill (case 1). Drainage averaged 87 percent of precipitation for the high-K backfill (case 3, K_{sat} = 44.6 cm/h), 77 percent for the backfill (case 1, K_{sat} = 4.46 cm/h), and 71 percent for the low-K backfill (case 2, K_{sat} = 0.446 cm/h).

The relationship between precipitation and drainage at a 2-m depth for the three cases is more clearly shown on a daily basis (Figure 6). Two precipitation events at 23 and 34 days (shown in the lower graph of Figure 6) will reach the 2-m depth at different times, depending on the hydraulic conductivity. In the higher conductivity (high-K) backfill (case 3), water infiltrates faster and with greater volume (represented by the area under the curve), whereas water flow is slower in the lower-conductivity (low-K) backfill (case 2) and less volume reaches the 2-m depth. A precipitation event at day 255 does not appear in the drainage of the low-K backfill (case 2), probably because evaporation is much greater at this warmer time of year than for earlier precipitation events.

Table 4. Results for Hydraulic Conductivity Changes.

Year	Precip. (cm/yr)	Case 2 Backfill with 0.1 x K_o			Case 3 Backfill with 10 x K_o		
		Evap. (cm/yr)	Drainage (cm/yr)	Storage (cm)	Evap. (cm/yr)	Drainage (cm/yr)	Storage (cm)
Initial				11.47			11.47
1980	24.56	5.41	14.54	16.70	3.77	26.14	8.54
1981	17.88	4.08	11.75	17.50	2.87	14.98	7.90
1982	20.27	5.12	11.89	19.66	3.56	16.87	7.46
1983	28.12	7.02	18.62	20.39	4.74	21.48	8.64
1984	18.44	5.73	16.81	16.57	3.78	15.68	7.36
1985	12.95	3.14	9.30	16.19	2.21	11.51	6.53
1986	18.01	4.65	13.76	15.16	3.14	13.66	7.39
1987	12.90	3.68	9.06	14.94	2.54	10.37	7.15
1988	10.59	3.10	8.45	13.46	2.31	8.19	7.01
1989	15.29	4.42	6.89	16.59	3.11	11.58	7.42
1990	16.94	4.61	11.55	16.75	3.33	13.39	7.12
Average	16.18	4.63	12.06	16.72	3.21*	14.90*	7.50
±s	±3.75	±1.16	±3.62	±1.98	±0.74	±5.16	±0.64

*Excludes 1980.

Another observation that can be made from Figure 6 is that the redistribution of water (i.e., the damping of water flux) is greater in the low-K backfill (case 2). Considering water infiltrating from the two precipitation peaks at 25 and 45 days, the high-K backfill (case 3) shows two large and distinct drainage peaks, in contrast to the backfill (case 1), which has two smaller and less distinct peaks. The low-K backfill (case 2) shows one peak at 85 days (the peak at 35 days is probably from the previous year's precipitation).

Even with a change of two orders of magnitude in the soil hydraulic conductivity, by modeling the estimated sediment and meteorological conditions of the Hanford Site, evaporation is estimated to be 19 to 27 percent of precipitation, and 71 to 87 percent of precipitation reaches the 2-m depth. Using hydraulic data from the actual backfill at the tank farms would make it possible to obtain a better estimate of the drainage.

2.3.3 Surface Soil Conditions Alteration

Two simulations of 10-yr periods were performed assuming the addition of a 0.15-m layer of clean gravel (case 5) or silt loam (case 4) to the surface of the existing backfill. The purpose of the clean gravel simulation was to provide a comparative estimate of drainage for such a condition because a relatively clean gravel is locally present at some tank farms at the Hanford Site, such as the TX and TY Tank Farms. The silt loam simulation was included

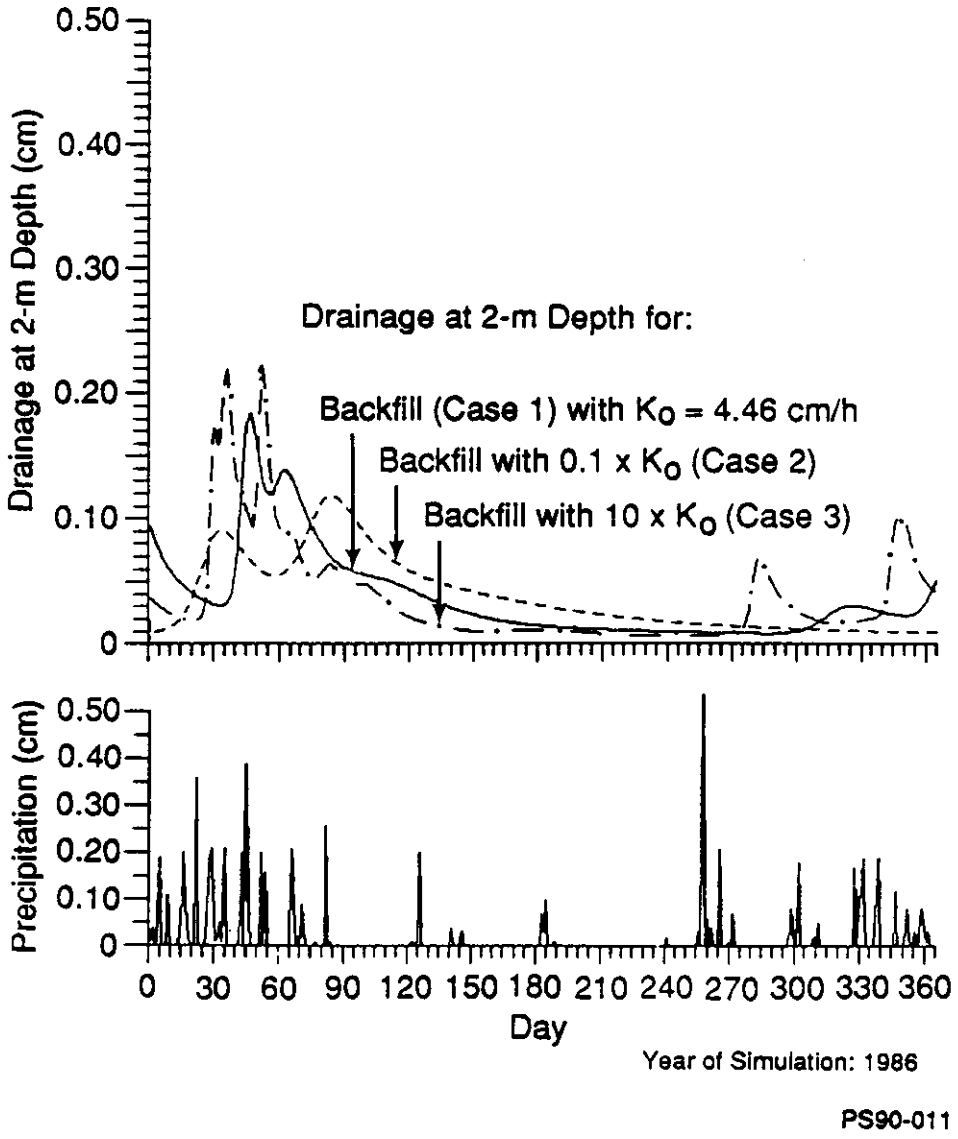

Figure 6. Effect on Drainage of a Change in Hydraulic Conductivity.

to evaluate the efficiency of this material in reducing the infiltration of meteoric water. The hydraulic properties used for these simulations are listed in Table 2.

The results are similar to those described in Section 2.3.2, in which the silt loam soil, with smaller hydraulic conductivity, exhibits less drainage at a depth of 2 m and more evaporation, and the clean gravel exhibits greater drainage. More specifically, evaporation from the surface silt loam (case 4 in Table 5) was significantly greater than from the backfill (95 percent versus 20 percent), and the silt loam also had significantly less drainage to a depth of 2 m (1 percent versus 77 percent). This indicates that the

addition of a fine-grained silt loam surface soil could significantly reduce the drainage of water. This small amount of drainage can be reduced further by the emplacement of an impermeable barrier, as described in the next section.

Table 5. Effect on Drainage of the Addition of a Surface Soil.

Year	Precip. (cm/yr)	Case 4 Silt loam on surface			Case 5 Clean gravel on surface		
		Evap. (cm/yr)	Drainage (cm/yr)	Storage (cm)	Evap. (cm/yr)	Drainage (cm/yr)	Storage (cm)
Initial				9.48			9.48
1957	21.06	26.10	3.788	7.01	0.602	20.01	10.05
1958	22.20	18.82	0.464	9.88	0.704	20.08	11.35
1959	17.96	17.82	0.464	6.64	0.599	19.11	9.53
1960	13.77	12.64	0.215	7.52	0.526	12.03	10.65
1961	17.37	17.81	0.132	6.91	0.543	16.73	10.67
1962	15.39	15.40	0.092	6.78	0.470	14.76	10.73
1963	16.03	14.76	0.069	7.94	0.474	15.20	11.01
1964	13.69	10.14	0.055	11.14	0.441	10.26	13.92
1965	9.27	14.04	0.045	6.59	0.327	12.67	10.13
1966	15.06	12.54	0.037	9.04	0.520	14.18	10.40
Average	16.18	14.89*	0.175*	7.94	0.52	15.50	10.84
Standard deviation	±3.75	±2.89	±0.173	±1.57	±0.10	±3.43	±1.20

*Excludes 1957.

The simulated addition of a layer of clean gravel to the surface results in decreased evaporation compared to the backfill (3 percent versus 20 percent) and increased drainage to a depth of 2 m (96 percent versus 77 percent). These results suggested that a larger volume of water should be expected to infiltrate the sediments at the tank farms that locally have clean gravel at the surface.

A plot of the drainage at a depth of 2 m for cases 1, 4, and 5 (Figure 7) indicates that the simulations predict more rapid drainage for a clean gravel surface (case 5) than for the backfill. At a 2-m depth for conditions in which a silt loam is on the surface (case 4), there is little relationship between precipitation and drainage because of the significant amount of evaporation that occurs. The initial conditions for all 3 cases were identical, so drainage as shown in Figure 7 was initially the same.

Because the precipitation fluxes do not appear as drainage peaks for the silt loam case (Figure 7), it is difficult to estimate the travel time for comparison to the gravel cases. However, the yearly drainage for the silt

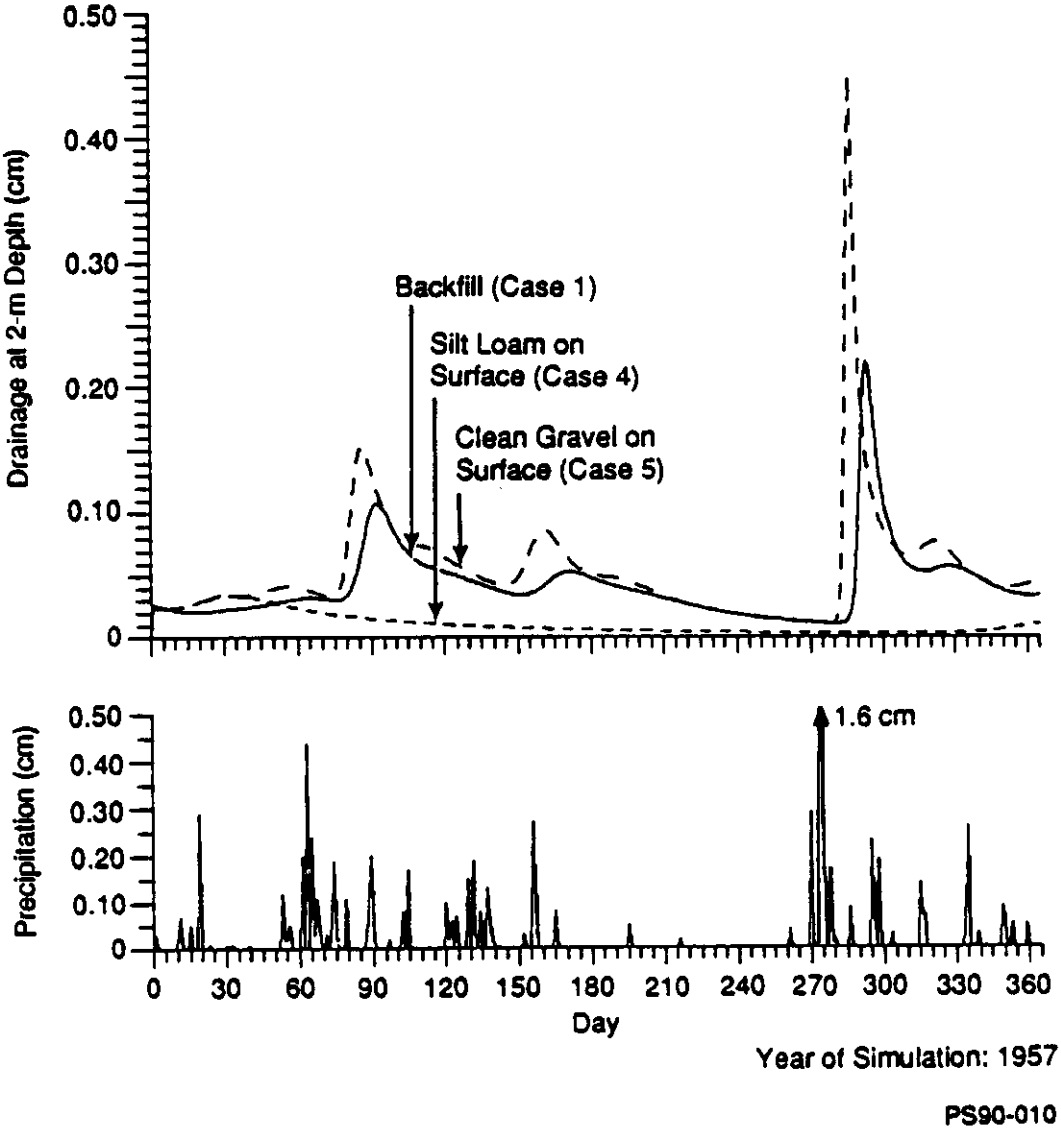

Figure 7. Effect on Drainage of the Addition of a Surface Soil or Gravel.

loam (Table 5) shows that it took several years to eliminate the effects of the initial conditions, which suggests that water transport through the silt loam could take considerably longer than in the backfill.

2.3.4 Precipitation Timing and Intensity

The effect of the timing and intensity of precipitation was investigated for 10 yr of records (1957 to 1966) for the conditions of case 5 (surface covered by a clean gravel). In case 5, precipitation was simulated as beginning at midnight at 1 cm/h; for case 6, the actual hour and intensity of rainfall were used. The results indicate a small increase in evaporation (4.9 percent versus 3.2 percent of annual precipitation) for the actual versus the simulated precipitation timing (i.e., cases 6 and 5, respectively). This results in a 0.9 percent decrease in the drainage at 2 m. Although this relationship was not evaluated in the other cases, precipitation timing and intensity should affect surfaces covered with finer materials to an equal or greater extent. However, an additional factor that may increase drainage is infiltration beneath a snowpack; this phenomenon is not presently simulated with UNSAT-H Version 2.0 (Fayer and Jones 1990).

2.3.5 Barrier Simulations

The results of the simulations of the 20-yr effect of an impermeable surface barrier are presented in Table 6 for the backfill (case 7) and the clean graveled surface (case 8). In each case, the drainage decreased significantly to about 4.5 cm for the first year after barrier emplacement, and 0.5 cm the second year. Within 3 yr, the drainage was less than 0.25 cm/yr, and after 5 yr the drainage was less than 0.1 cm/yr. The continued flux is due to the drainage of the water remaining in the 2-m backfill (about 5 cm or 2.5 percent). The residual (minimum) soil moisture for the backfill is 2 percent (listed as residual water content in Table 2), so drainage would asymptotically approach this value, subject to water table boundary conditions deeper in the sediments.

The decrease in the drainage is illustrated in Figure 8 for these two cases. The area under each curve represents the total drainage volume. There is very little difference in the drainage between the two barrier cases. Given that the drainage drops to a relatively small amount within 3 yr, a reasonable estimate for the drainage reduction from barrier emplacement is equal to the average yearly drainage of 13.1 cm/yr for the backfill and 16.2 cm/yr for the clean graveled surface.

The cumulative drainage at a depth of 2 m (Figure 9) graphically shows this decrease in water volume for the two impermeable barrier cases. The slopes of the lines before barrier emplacement are equal to the flux rates, and the variation in each line is caused by the temporal variation of precipitation. Over a long time (e.g., decades), the data show that the temporal variation in drainage might reasonably be ignored and an average

Table 6. Results for the Addition of an Impermeable Surface Barrier.

Year	Precip. (cm/yr)	Case 7 Backfill			Case 8 Clean gravel on surface		
		Evap. (cm/yr)	Drainage (cm/yr)	Storage (cm)	Evap. (cm/yr)	Drainage (cm/yr)	Storage (cm)
1989	15.29	3.30	10.85	10.64	3.30	10.85	10.64
1990	0.0	0.0	4.455	6.18	0.0	4.819	6.21
1991	0.0	0.0	0.499	5.69	0.0	0.469	5.74
1992	0.0	0.0	0.239	5.45	0.0	0.224	5.51
1993	0.0	0.0	0.149	5.30	0.0	0.139	5.37
1994	0.0	0.0	0.105	5.19	0.0	0.098	5.28
1995	0.0	0.0	0.000	5.11	0.0	0.074	5.20
1996	0.0	0.0	0.063	5.05	0.0	0.059	5.14
1997	0.0	0.0	0.052	5.00	0.0	0.048	5.09
1998	0.0	0.0	0.044	4.95	0.0	0.041	5.05
1999	0.0	0.0	0.037	4.92	0.0	0.035	5.02
2000	0.0	0.0	0.033	4.88	0.0	0.030	4.99
2001	0.0	0.0	0.029	4.86	0.0	0.027	4.96
2002	0.0	0.0	0.026	4.83	0.0	0.024	4.94
2003	0.0	0.0	0.023	4.81	0.0	0.021	4.92
2004	0.0	0.0	0.021	4.79	0.0	0.019	4.90
2005	0.0	0.0	0.019	4.77	0.0	0.018	4.88
2006	0.0	0.0	0.017	4.75	0.0	0.016	4.86
2007	0.0	0.0	0.016	4.73	0.0	0.015	4.85
2008	0.0	0.0	0.015	4.72	0.0	0.014	4.84
2009	0.0	0.0	0.014	4.71	0.0	0.013	4.82
2010	0.0	0.0	0.013	4.69	0.0	0.012	4.81

used with very little loss in accuracy. This suggestion is not appropriate, however, for short periods of time in which the combination of large precipitation events and rapid transport of water in the sediments leads to variation in daily drainage, as shown in Figure 4.

The reduction of water flux into contaminated sediments under Tank 106 in the 241-T Tank Farm should reduce the potential for radionuclide transport from near the tank to deeper parts of the vadose zone. The effect will be more clearly defined by subsequent three-dimensional simulations.

2.4 INFILTRATION SIMULATION CONCLUSIONS

The simulations using UNSAT-H Version 2.0 (Fayer and Jones 1990) show that the annual water balance of the top 2 m of cover placed over the tank farms is highly dependent on the hydraulic properties of the cover materials and less dependent on the variations in annual precipitation. The simulated climatic changes cause precipitation to vary around a mean value of about 17 cm, or 1 cm higher than the long-term average for the Hanford Site.

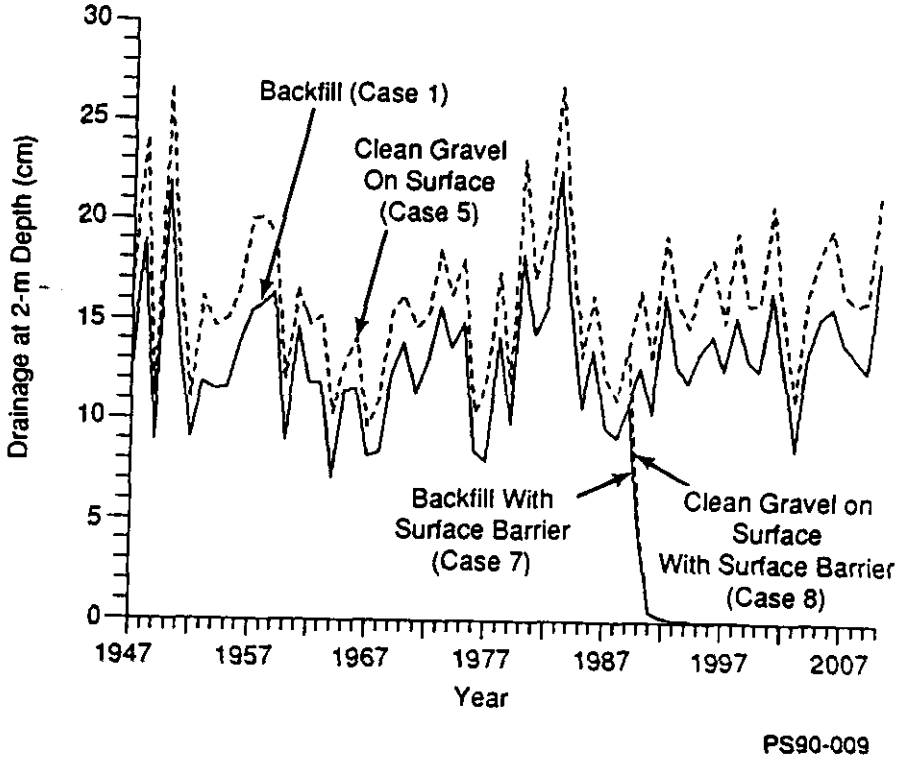

Figure 8. Yearly Drainage for Impermeable Surface Barrier Cases.

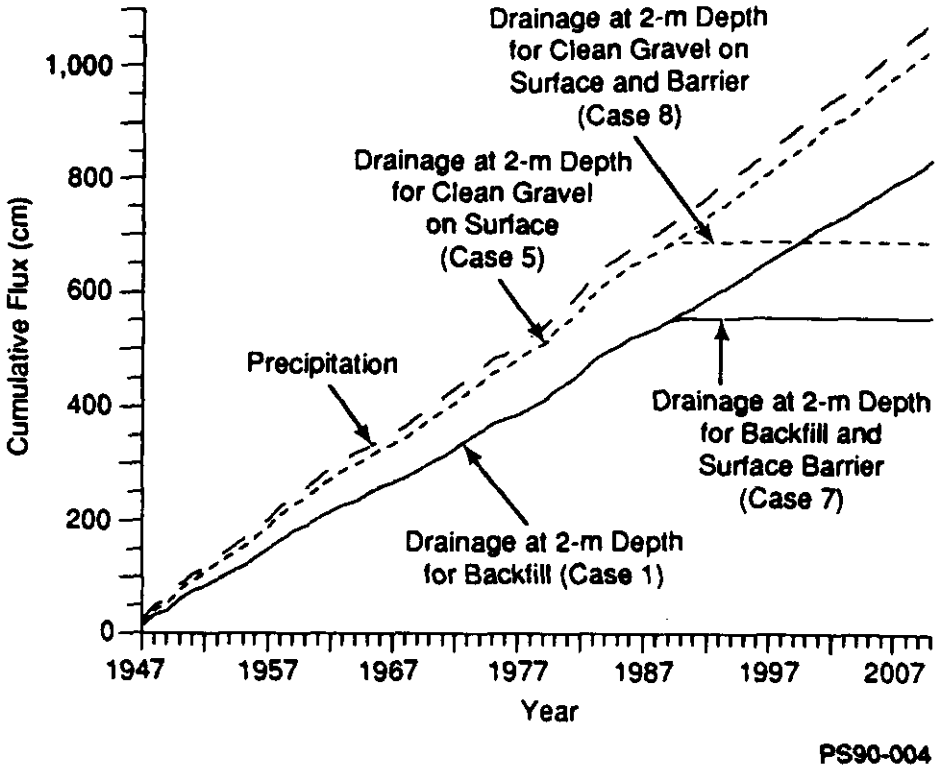

Figure 9. Cumulative Drainage at 2-m Depth for Impermeable Surface Barrier Cases.

Using a hydraulic property approximation of the backfill (sample AP-1g) at the 241-T Tank Farm, a simulation indicated that 20 percent of the annual precipitation evaporated, and 77 percent reached a depth of 2 m for a period of 74 yr. Simulations of a two-orders-of-magnitude change in the hydraulic conductivity of the backfill showed that 68 percent to 86 percent of the annual precipitation reached the 2-m depth when these changes in hydraulic properties were simulated for an 11-yr period (1980 to 1990). With a thin layer of clean gravel or a silt loam soil on the surface, the water flux at a 2-m depth varied from about 95 percent to 1 percent of the annual precipitation for a 10-yr (1957 to 1966) simulation period. Essentially, surfaces covered with coarse backfill materials enhance infiltration, while surfaces covered with silt loam materials significantly reduce infiltration.

No direct measurements of hydraulic properties have been made on the upper 2 m of tank farm sediments. Hydraulic property measurements are necessary to substantiate the model simulations. Direct measurements of water flux at a 2-m depth ultimately may be required to verify the model simulation results. However, the results are in general agreement with recharge measurements at lysimeters in the 300 Area on the Hanford Site.

3.0 SIMULATIONS OF CONTAMINANT PLUME MOVEMENT IN THE VADOSE ZONE AT TANK 241-T-106

3.1 CONCEPTUAL MODEL FOR THE SIMULATIONS

The 241-T-106 single-shell tank is located in the 200 West Area of the Hanford Site, in southcentral Washington State (Figure 1). The problem of leaking single-shell tanks is well documented, most recently by the U.S. General Accounting Office (GAO 1989). The major features of the problem are summarized below.

The Tank 241-T-106 leak was first documented in 1973 (ARHCO 1973). A report by the U.S. Atomic Energy Commission (AEC 1973) provides a detailed chronology of the leakage that began on or about April 20, 1973. Leakage stopped on June 10, 1973, when the pumpable liquid contents of the tank were removed. The total duration of the leak was approximately 52 days, during which 115,000 gal of supernate were lost from the tank.

The radionuclide inventory of the supernate solution within the tank is shown in Table 7. Most of the inventory consists of ^{144}Ce and ^{144}Pr, ^{137}Cs, ^{89}Sr and ^{90}Sr, and ^{106}Ru and ^{106}Rh, with lesser amounts of the other radionuclides (Routson et al. 1979). With the exception of ^{106}Ru and ^{106}Rh, the inventory is characterized by long half-lives and high sorption coefficients. The inventory in Table 7 corresponds to 2.67×10^5 total Ci of ^{106}Ru and 3.85×10^4 total Ci of ^{137}Cs that leaked from the tank. The ^{106}Ru has a half-life of 1 yr and sorption coefficients are generally approximately zero; the ^{137}Cs has a half-life of 30.17 yr (Walker et al. 1984) and is highly sorbed by Hanford Site soils. The movement of ^{106}Ru is of interest because its transport should be essentially concurrent with the fluid front.

The leak apparently occurred on the southeast side of the tank because the contaminant plume is centered around this area. Figure 10 shows a plan view and a vertical cross-sectional view of the plume as measured in the summer of 1973, after the leak had been detected and the tank pumped out. The concentrations shown in the figure were measured on a per-liter-volume-of-soil basis. The contaminant transport is shown for ^{106}Ru, ^{144}Ce, and ^{137}Cs. The ^{106}Ru is the most mobile of the three radionuclides and traveled the farthest; the ^{137}Cs is the least mobile and was contained within a small zone around the base of the tank. The configuration of the ^{106}Ru plume appears to be approximately circular, with a radius of about 15 to 20 m in plan view and a maximum depth of about 20 m.

Figure 11 shows the measured ^{106}Ru 1-μCi/L isopleths for 1973 versus 1978; the ^{106}Ru 1-μCi/L isopleth appears to have migrated about 5 to 7 m downward at dry wells 107 and 108, but shows little movement elsewhere. Because of its relatively short (1-yr) half-life, ^{106}Ru would decay from the estimated 2.7×10^{11} μCi leaked from the tank in 1973 to about 8.4×10^9 μCi in 1978. However, the decay process alone is not sufficient to explain the relative stationarity of the 1 μCi/L isopleth of ^{106}Ru observed in 1978.

Table 7. Radionuclide Inventory of the Tank 241-T-106 Supernatant Solution.

Radioactive component	μCi/L[a]	μCi/gal[b]
Cerium-144/praseodymium-144	1.18×10^4	4.48×10^4
Cesium-137	8.85×10^4	3.35×10^5
Europium-155	1.69×10^3	6.40×10^3
Cesium-134	1.32×10^3	5.00×10^3
Antimony-125	1.12×10^4	4.24×10^3
Strontium-89/strontium-90	2.98×10^4	1.13×10^5
Ruthenium-106/rhodium-106	6.12×10^5	2.32×10^6
Plutonium-239	9	34
Plutonium-240	2	8
Americium-241	2	6

[a]After Routson et al. (1979).
[b]After AEC (1973).

Based primarily on the work of Price and Fecht (1976), but in general agreement with more recent work, five stratigraphic subdivisions are assumed for the unsaturated zone in the vicinity of the 241-T Tank Farm. These zones are shown in Figure 12. The total section is 61 m thick. Beginning at the water table, the vadose zone consists of about 23 m of sandy gravel overlain by 14 m of calcareous, silty, fine-grained to very-fine-grained sand that may include a caliche layer. Above this are 4 m of coarse-grained to medium-grained sand overlain by 8 m of pebbly, very-coarse-grained to medium-grained sand, and capped by about 12 m of backfill (a silty, sandy gravel).

In the horizontal plane, the model domain encompasses an area of about 6,000 m^2 approximately centered on Tank 241-T-106. The model domain extends vertically to about 81 m below the land surface (205 m), including 61 m of the vadose zone and 20 m of the saturated zone. At this scale, each stratigraphic subdivision within the domain is assumed to be of constant thickness. No flow is allowed across the vertical (sides and ends) boundaries of the vadose zone. Groundwater flow in the vicinity of the 241-T Tank Farm is to the north, with a gradient of about 1×10^{-3} (Last et al. 1989). These conditions are imposed on the saturated zone in the model. The saturated zone was arbitrarily terminated by a no-flow boundary at an elevation of 124 m.

Infiltration through the top surface of the model is based on the results of the UNSAT-H Version 2.0 modeling studies (Table 3). These numbers were tabulated directly into the input for the PORFLO-3 simulation. The tank

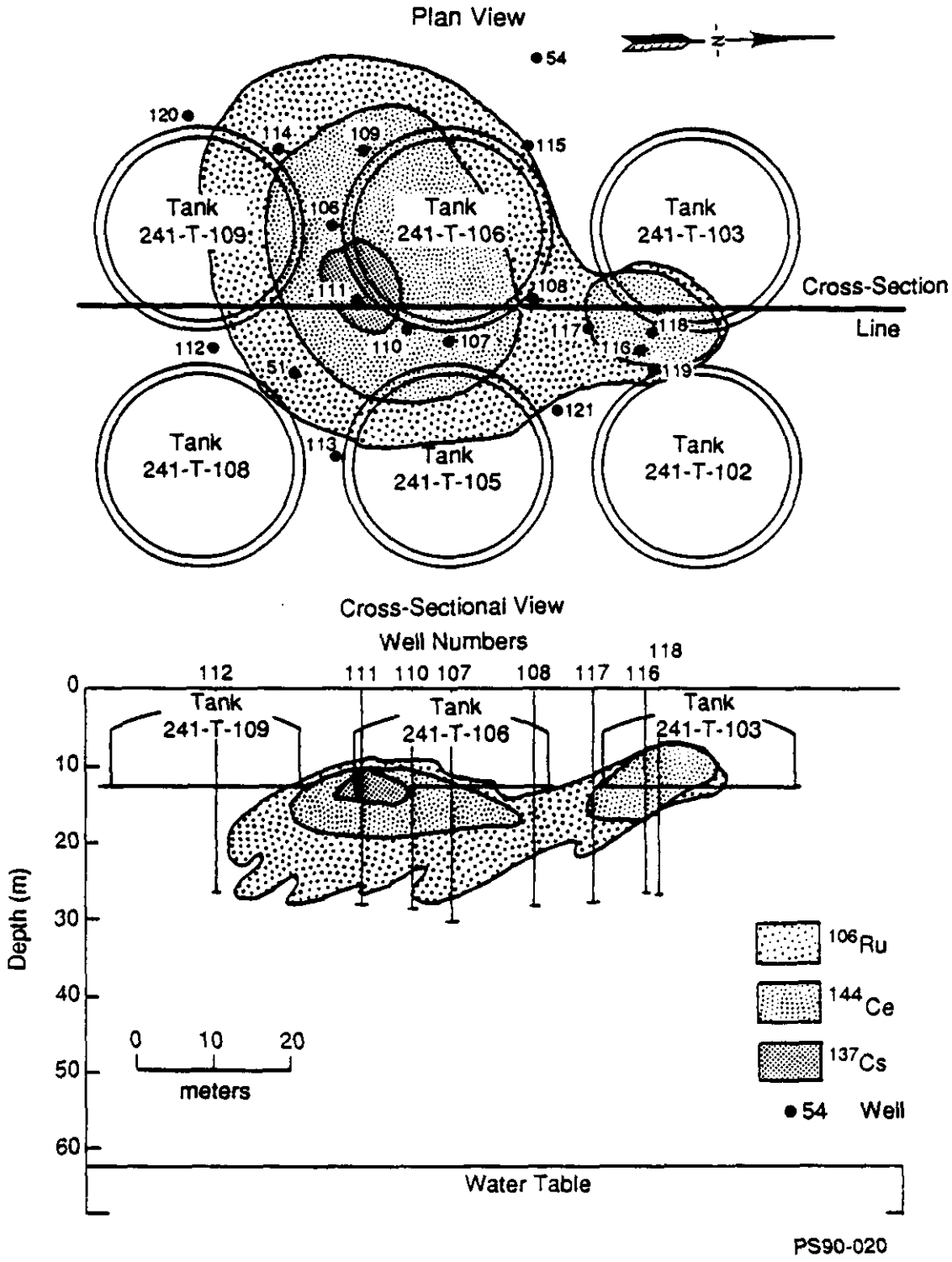

Figure 10. Plan and Vertical Cross-Sectional Views of the 1973 ^{137}Cs, ^{144}Ce, and ^{106}Ru (1 μCi/L) Volumetric Isopleths.

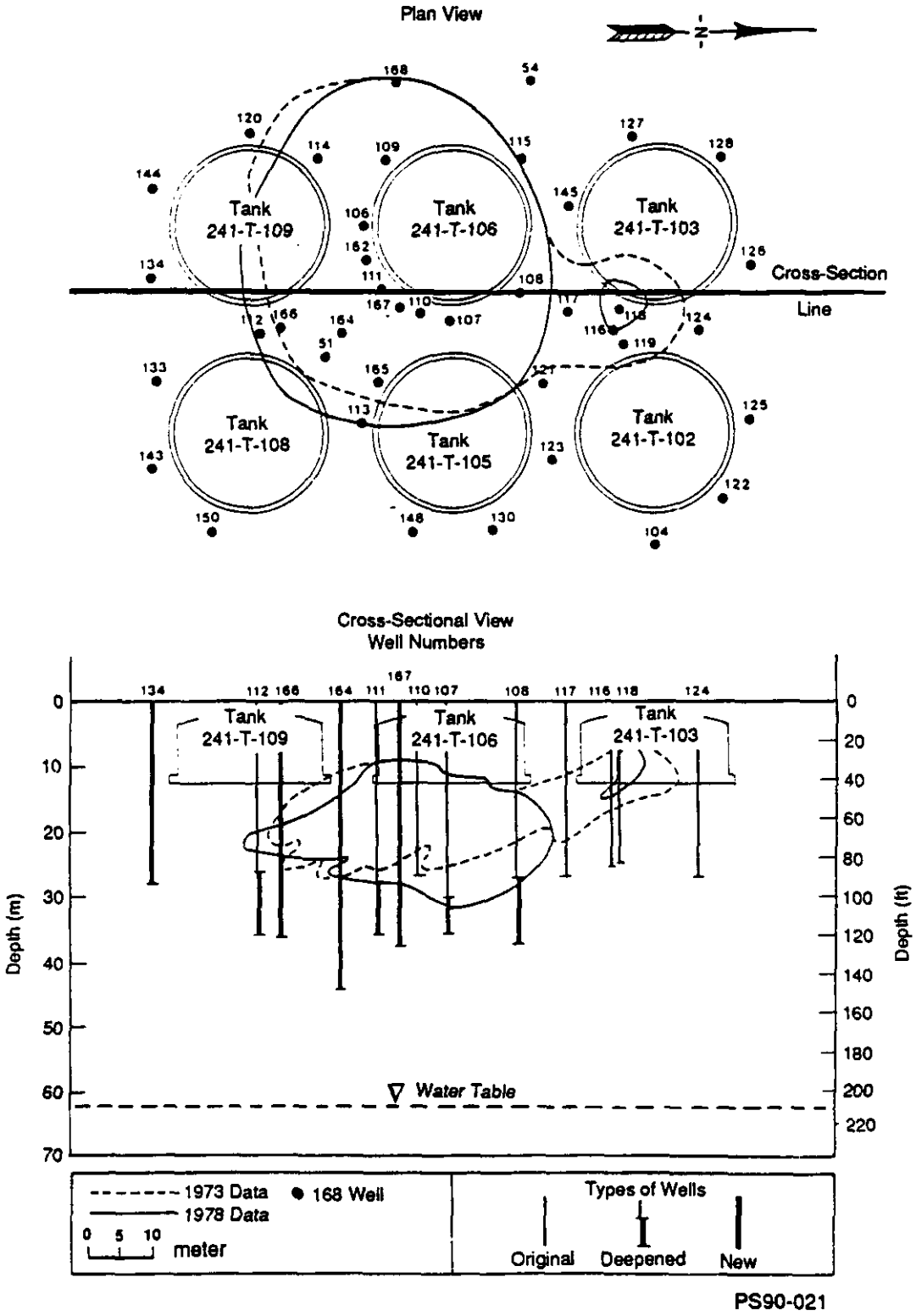

Figure 11. Plan and Vertical Cross-Sectional Views of the 1973 and 1978 ^{106}Ru (1 μCi/L) Volumetric Isopleths.

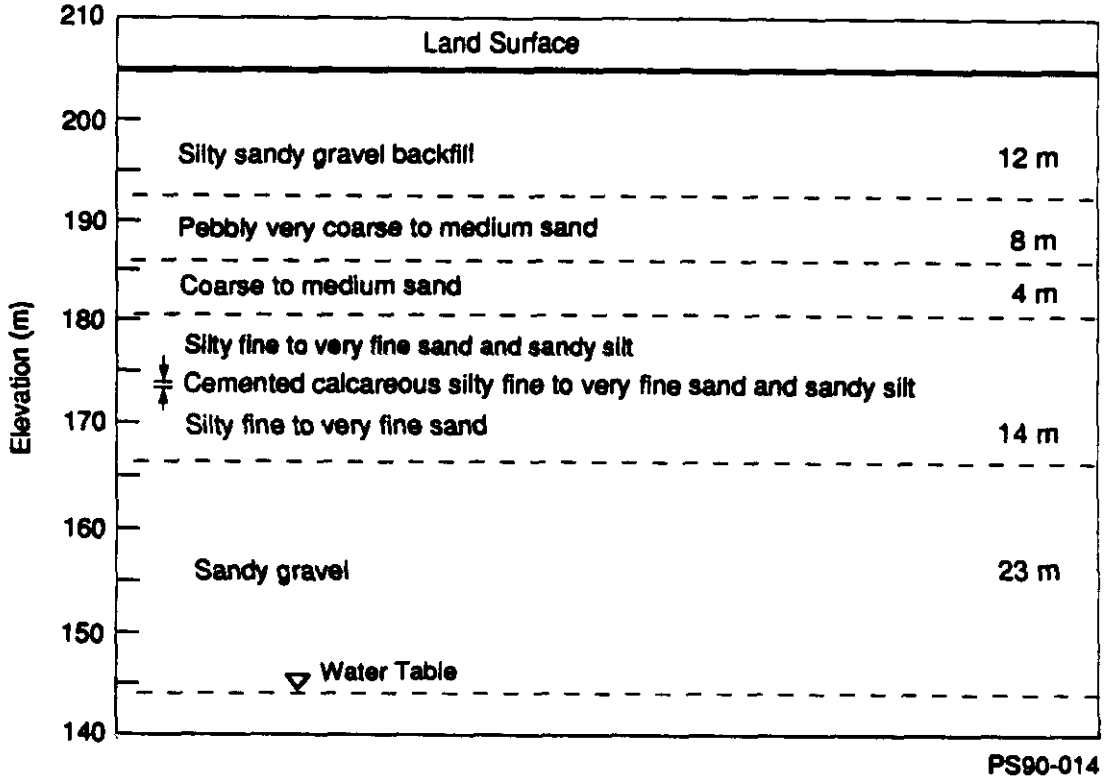

Figure 12. Textures and Thicknesses of the Five Stratigraphic Zones at the T Tank Farm.

itself is represented as an impervious block. This treatment allows the infiltrating water to be diverted around the tank. Thus, in a local zone around the perimeter of the tank, the volumetric flux may be significantly enhanced. As part of the simulation, water infiltration around the tank from 1960 to the 1973 leak was simulated to approximate the steady-state moisture conditions before the leak.

The three-dimensional domain is a region of 3.7×10^5 m^3, having dimensions of 88 x 68 x 80 m. This domain was discretized into a 24 x 15 x 36-m grid containing 12,960 cells. A variable grid spacing was used in all three dimensions. The smallest cells in the model are 2.0 x 2.0 x 0.5 m and are located beneath the tank in the leak zone.

Although directly measured sediment properties for the Tank 241-T-106 site are not currently available, several data catalogs are available (Sewart et al. 1987; see Appendix C). The textural descriptions for the five sediment samples analyzed during excavation of the 210-AP Tank Farm in the 200 East Area (Sewart et al. 1987) were matched to the descriptions of the five sediment layers identified at the T Tank Farm. The corresponding moisture retention curves and hydraulic properties for the samples were input to the PORFLO-3 model. The saturated hydraulic conductivity (K_{sat}) and the saturated, volumetric moisture content (θ_{sat}) of the samples are shown in Figure 13, as they are applied to the stratigraphic subdivisions identified in Figure 12.

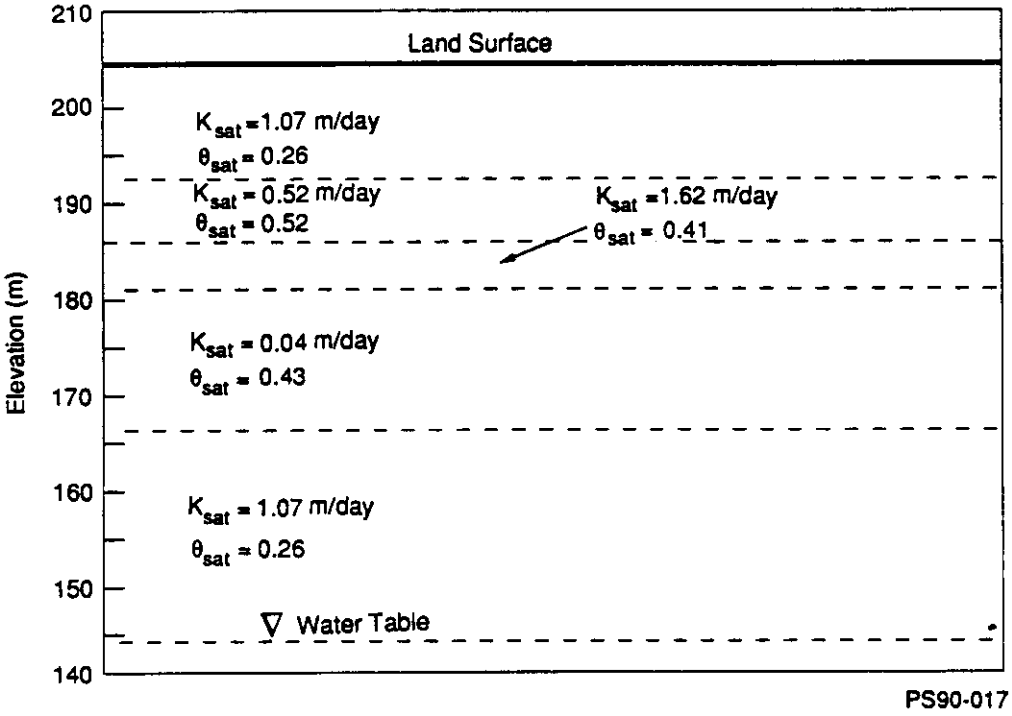

Figure 13. Saturated Hydraulic Conductivity and Saturated Moisture Content Values for the Five Stratigraphic Layers Identified at the T Tank Farm.

The vertical hydraulic conductivity used in the model was reduced by a factor of two from that given in the data catalog. Previous simulations with constant infiltration (Smoot and Sagar 1990) indicated that a small anisotropy produced the best calibration to the observed plume measurements. The absence of site-specific data, however, introduces uncertainty into the simulation results.

Transport coefficients were assumed for each of the five major soil horizons. For all horizons, the Fickian molecular diffusion coefficient (D) was held constant at 1×10^{-5} m^2/day and longitudinal and transverse dispersivity at 1.0 m and 0.1 m, respectively. For those model simulations that address retardation, a distribution coefficient of 5×10^{-7} m^3/g (0.5 mL/g) was used for ^{106}Ru and 1×10^{-4} m^3/g (100.0 mL/g) for ^{137}Cs. Continued work is needed to quantify contaminant transport properties of Hanford Site sediments; the values used in the simulation were only estimates.

3.2 CONTAMINANT PLUME SIMULATION RESULTS

The time period of simulation for the leak at Tank 241-T-106 began in 1960. Infiltration was simulated for the 13 yr before the leak in 1973. The annual recharge values listed in Table 3 were input to the model instead of an average value. The simulation began in 1960, to approximate the steady-state moisture conditions around the tank resulting from infiltration before the leak. The use of annually varying recharge values significantly

increases the computational effort needed for the simulations. The model is very sensitive to changes in mass flux; therefore, the model time steps must be small to accommodate the annual change in recharge, resulting in increased iterations per unit of time.

Relative saturation simulated for 1969 is shown in Figure 14. The figure shows relative saturation increasing in the sediments around the perimeter of the tank. Lobes of higher relative saturation have developed in the sediments below the sides of the tank and a generally symmetric pattern of moisture distribution is observed at depth. This significantly contrasts with the uniform, layered distribution of moisture content that would be observed for constant infiltration conditions imposed at the start of the leak.

Relative saturation simulated for the summer of 1974 is shown in Figure 15. The increase in saturation around the sides of the tank is still evident. The distribution of saturation at depth is more uniform than that observed in 1969. One explanation could be that the leaked fluid increased the moisture content in the sediments underneath the tank that were otherwise shielded from infiltration. Such an effect could tend to make the distribution of moisture content more uniform. Alternatively, the moisture distribution in 1969 might have been a transient phenomena, indicating that the model had not reached steady-state conditions. Relative saturations at later times were similar to the 1974 profile, which further supports this hypothesis. Simulation at earlier times may be necessary to approximate steady-state infiltration conditions before the leak.

3.2.1 Ruthenium-106 Movement

The simulated movement of the ^{106}Ru plume at selected time steps during the first year after the tank leak is shown in Figure 16. The contours represent the 1 μCi/L isopleth for ^{106}Ru. The simulations show both a greater horizontal and a greater vertical spread of the plume than that observed in 1973 (Figure 10).

The greater spread of the simulated plume is most likely the result of the infiltration values applied to the model. Related simulations of the Tank 241-T-106 (see Chapter 1.0) incorporated identical hydraulic properties. The major difference in those simulations was that the infiltration was held constant at 0.05 m/yr. This value contrasts with an average annual value of about 0.13 m/yr indicated by simulations of the UNSAT-H Version 2.0 simulations (Table 3). The results for the 0.05 m/yr simulation are shown in Figure 17 for comparison. The additional flux of moisture could produce the increased movement of the plume observed in the simulations shown in Figure 18.

The simulations for ^{106}Ru at later times are shown in Figure 10. The simulation results indicate that the 1 μCi/L isopleth for ^{106}Ru approaches, but does not reach, the water table in the early 1980's, about 7 yr after the leak. After that time, the simulated plume begins to recede. The shrinkage of the simulated plume appears to be primarily the result of radioactive decay.

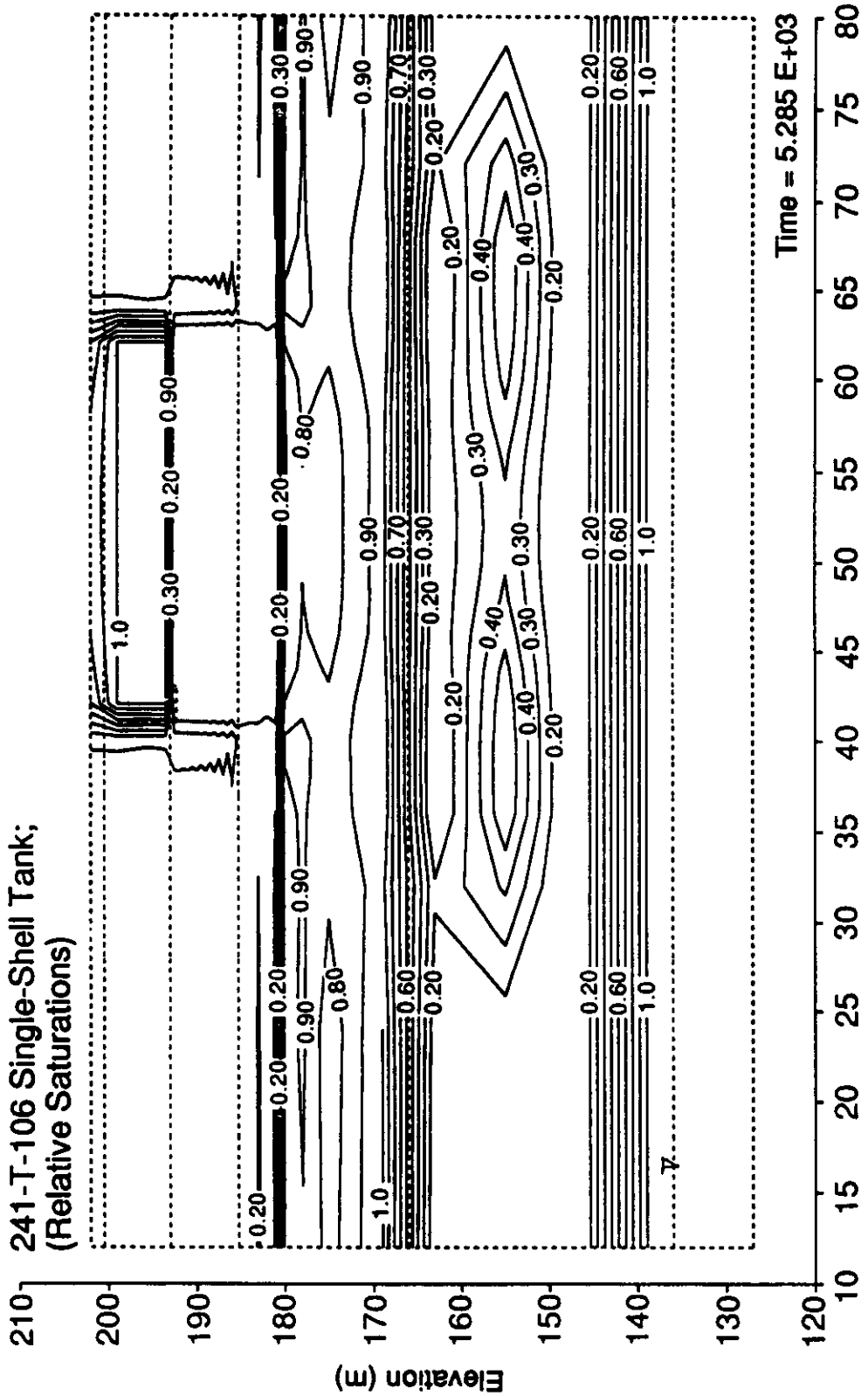

Figure 14. PORFLO-3 Simulation of Relative Saturation in 1969.

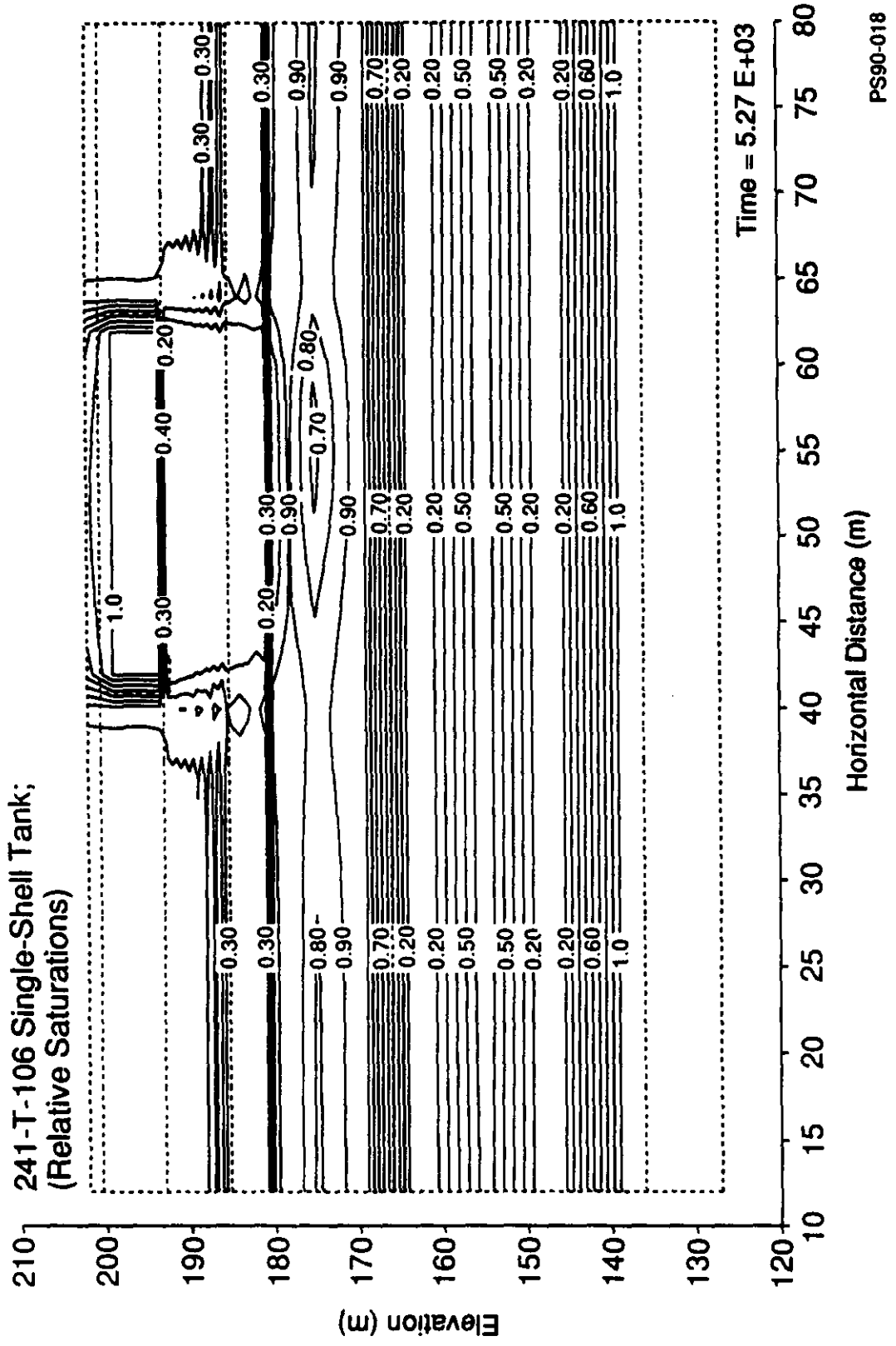

Figure 15. PORFLO-3 Simulation of Relative Saturation in 1974.

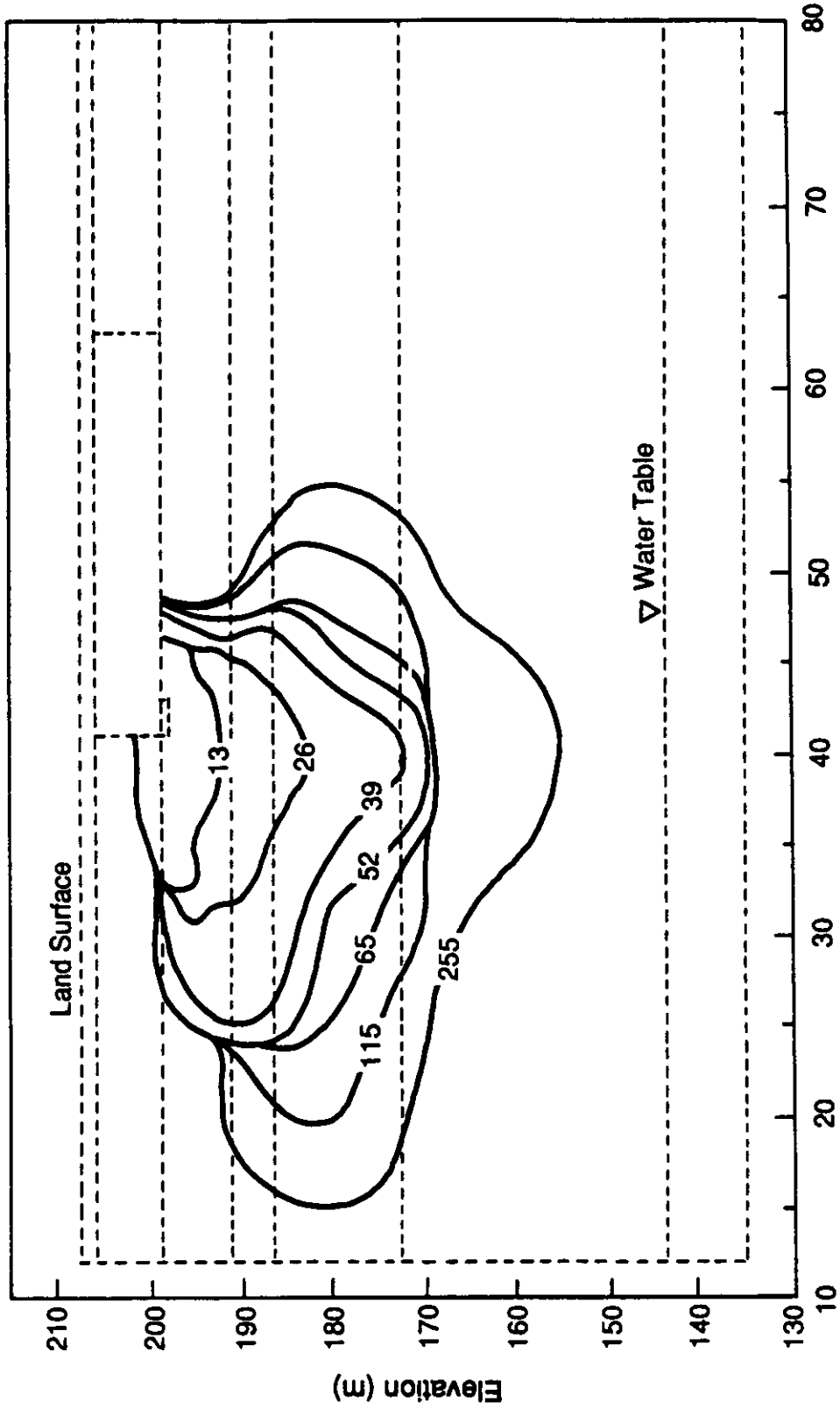

Figure 16. PORFLO-3 Simulation of the Vertical Extent of the ^{106}Ru (1 μCi/L) Volumetric Isopleth for Varying Infiltration Rates at Early Simulation Times.

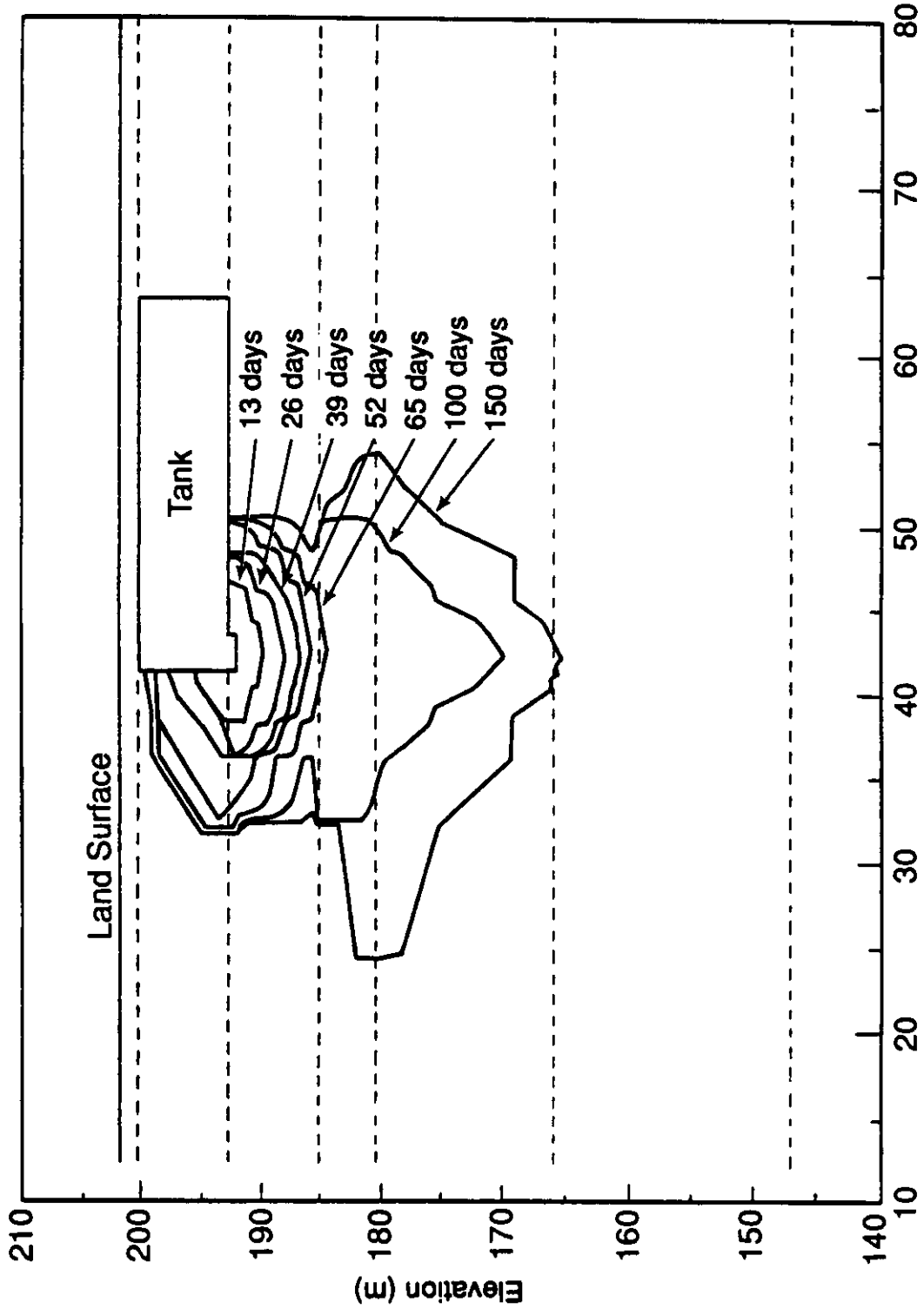

Figure 17. PORFLO-3 Simulation of the Vertical Extent of the ^{106}Ru (1 μCi/L) Volumetric Isopleth for a Constant 0.05 m/yr Infiltration Rates at Early Simulation Times (Days).

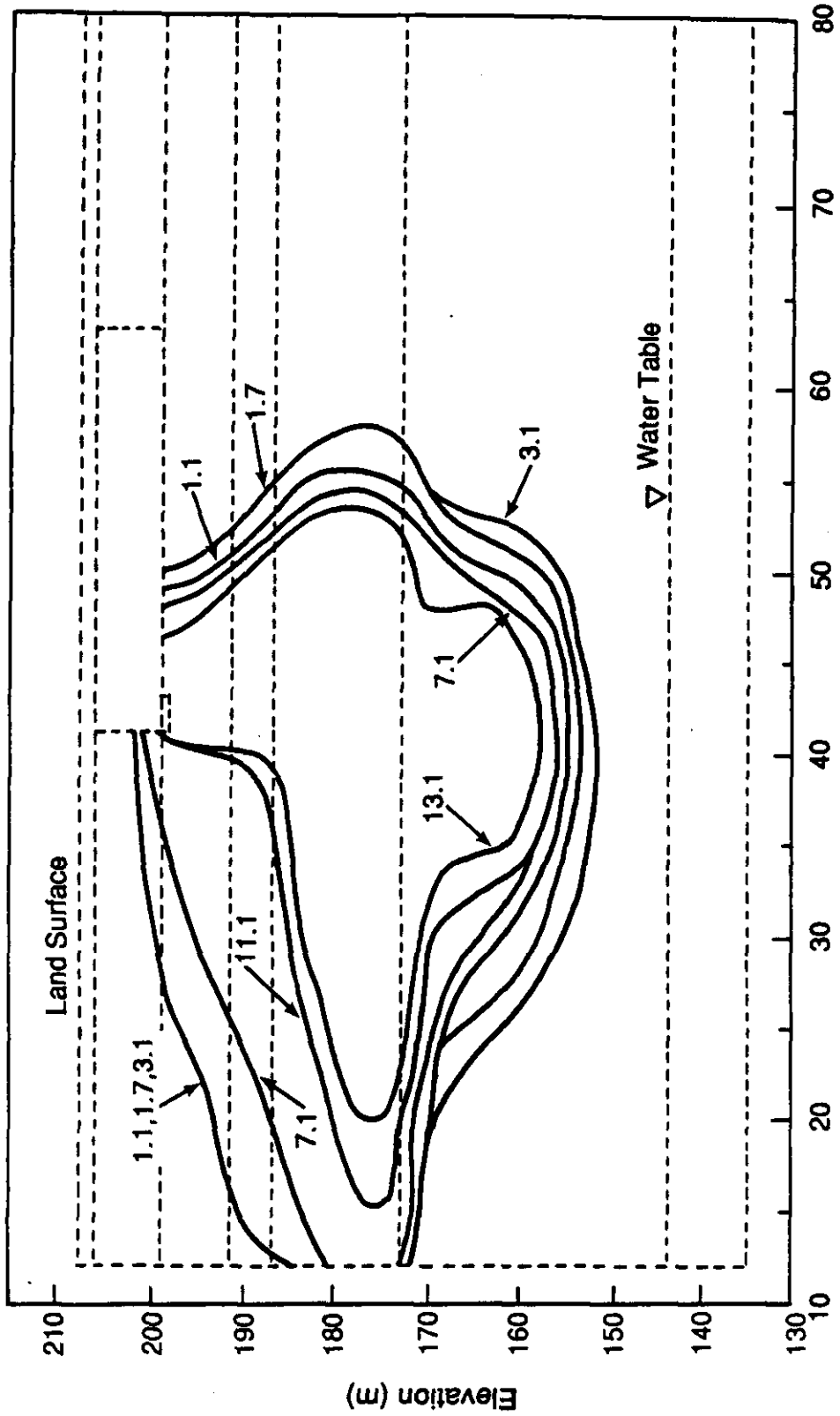

Figure 18. PORFLO-3 Simulation of the Vertical Extent of the ^{106}Ru (1 μCi/L) Volumetric Isopleth for Varying Infiltration Rates at Late Simulation Times (Years).

3.2.2 Cesium-137 Movement

Cesium-137 is highly sorbed by the minerals in the Hanford formation sediments underlying the tank. The simulated distribution of ^{137}Cs is shown in Figure 19. The simulated plume has a radius of several meters. After about 50 days, the extent of the plume becomes approximately stationary. This result is similar to that observed for related simulations (see Chapter 1.0) at lower infiltration rates. The ^{137}Cs sorption appears to be sufficiently high that the increased infiltration rate does not significantly increase the mobility of the simulated ^{137}Cs plume.

3.3 CONTAMINANT PLUME SIMULATION CONCLUSIONS

The UNSAT-H Version 2.0 (Fayer and Jones 1990) simulations suggest a higher average annual recharge rate than previously has been estimated for the 241-T-106 Tank Farm. The results of the PORFLO-3 Version 1.0 simulations indicate that the increased flushing of the soil column, resulting from higher infiltration, may increase the potential rate of movement of the ^{106}Ru plume. The simulated ^{106}Ru plume approached, but did not enter, the water table by the early 1980's; after that time, the simulated ^{106}Ru plume began to recede because of radioactive decay. The simulated ^{137}Cs plume is highly sorbed by minerals in the sediments beneath the tank and migrates much less than ^{106}Ru; the simulated ^{137}Cs plume becomes essentially stationary after about 50 days. These results are preliminary and no calibration of the ^{106}Ru plume to the higher infiltration rates was attempted. The annually varying recharge rate causes the problem to be computationally intensive because of the small time steps needed to accommodate the annual change in mass flux.

Future simulations of the leak at Tank 241-T-106 or similar tank leaks at the Hanford Site should include a more detailed study of the dynamics of the moisture conditions that develop in the surrounding soil column after the burial of a solid object such as a single-shell tank. Further simulations are warranted to investigate the implications of the higher infiltration rates suggested by the UNSAT-H Version 2.0 simulations. The preliminary simulations of Tank 241-T-106 using PORFLO-3 Version 1.0, as described in this report, indicate that the higher infiltration rates imply increased mobility of the contaminant plume; conversely, the PORFLO-3 simulations (Smoot and Sagar 1990) also indicate that remedial action in the form of an infiltration barrier could be an effective means to inhibit the movement of the plume.

No unsaturated zone data are presently available to define plumes for hazardous wastes that may also have contributed to the Tank 241-T-106 leak. Conservative species such as chloride are known to have been present in the tank. The migration of such species may be significantly more extensive than either ^{106}Ru or ^{137}Cs because of the absence of retardation and radioactive decay. The extent of migration of conservative species such as chloride should be investigated further.

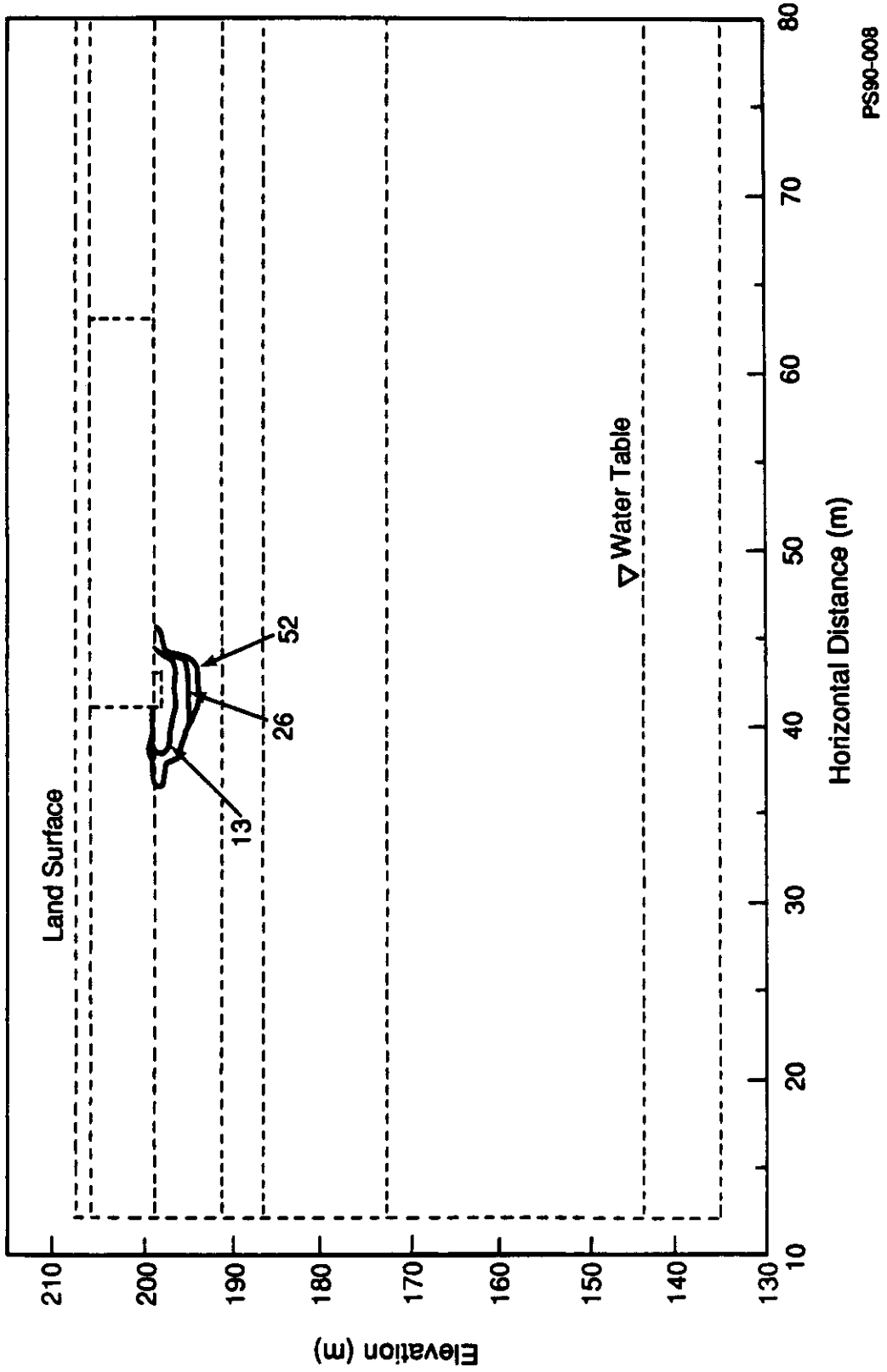

Figure 19. PORFLO-3 Simulation of the Vertical Extent of the ^{137}Cs (1 μCi/L) Volumetric Isopleth for Varying Infiltration Rates (Days).

In general, infiltration control may be a viable means of reducing the impact of years of defense waste accumulation at the Hanford Site. The simulation results are promising, but are based to a large extent on nonsite-specific flow and transport properties. More site-specific investigation is needed to characterize the hydrogeologic and chemical properties of sediments in the vicinity of the Tank 241-T-106.

4.0 REFERENCES

ARHCO, 1973, *Tank 241-T-106 Leak Investigation*, ARH-2874, Atlantic Richfield Hanford Company, Richland, Washington.

AEC, 1973, *Report on the Investigation of the 106-T Tank Leak at the Hanford Reservation, Richland, Washington*, TID 26431, U.S. Atomic Energy Commission, Richland, Washington.

Bird, R. B., W. E. Stewart, and E. N. Lightfoot, 1960, *Transport Phenomena*, Wiley, New York.

Brown, D. J., R. C. Routson, W. H. Price, and K. R. Fecht, 1979, *Status of Liquid Waste Leaked from the 241-T-106 Tank*, RHO-ST-1, Rockwell Hanford Operations, Richland, Washington.

Doorenbos, J. and W. O. Pruitt, 1977, *Guidelines for Predicting Crop Water Requirements*, FAO Irrigation and Drainage Paper No. 24, 2nd ed., Food and Agriculture Organization of the United Nations, Rome, Italy.

Ecology, EPA, and DOE, 1989, *Hanford Federal Facility Agreement and Consent Order*, Washington State Department of Ecology, U.S. Environmental Protection Agency, and U.S. Department of Energy, Olympia, Washington.

Fayer, M. J. and T. L. Jones, 1990, *UNSAT-H Version 2.0: Unsaturated Soil and Heat Flow Code*, PNL-6779, Pacific Northwest Laboratory, Richland, Washington.

Fayer, M. J., G. W. Gee, and T. L. Jones, 1986, *UNSAT-H Version 1.0: Unsaturated Flow Code Documentation and Applications for the Hanford Site*, PNL-5899, Pacific Northwest Laboratory, Richland, Washington.

GAO, 1989, *DOE's Management of Single-Shell Tanks at Hanford, Washington*, GAO/RCED-89-157, U.S. General Accounting Office, Washington, D.C.

Gee, G. W., 1987, *Recharge at the Hanford Site: Status Report*, PNL-6403, Pacific Northwest Laboratory, Richland, Washington.

Gee, G. W. and R. R. Kirkham, 1984, *Arid Site Water Balance: Evapotranspiration Modeling and Measurements*, PNL-5177, Pacific Northwest Laboratory, Richland, Washington.

Last, G. V., B. N. Bjornstad, M. P. Bergeron, D. W. Wallace, D. R. Newcomer, J. A. Schramke, M. A. Chamness, C. S. Cline, S. P. Airhart, and J. S. Wilbur, 1989, *Hydrogeology of the 200 Areas Low-Level Burial Grounds - An Interim Report*, PNL-6820, Vol. 1, Pacific Northwest Laboratory, Richland, Washington.

Price, W. H. and K. R. Fecht, 1976, *Geology of the 241-T Tank Farm*, ARH-LD-135, Atlantic Richfield Hanford Company, Richland, Washington.

Richardson, C. W., 1981, "Stochastic Simulation of Daily Precipitation, Temperature, and Solar Radiation," *Water Resour. Res.* 17(1):182-190.

Routson, R. C., W. H. Price, D. J. Brown, and K. R. Fecht, 1979, *High-Level Waste Leakage from the 241-T-106 Tank at Hanford*, RHO-ST-14, Rockwell Hanford Operations, Richland, Washington.

Runchal, A. K. and B. Sagar, 1989, *PORFLO-3: A Mathematical Model for Fluid Flow, Heat, and Mass Transport in Variably Saturated Geologic Media, Users Manual, Version 1.0*, WHC-EP-0041, Westinghouse Hanford Company, Richland, Washington.

Sagar, B. and A. K. Runchal, 1990, *PORFLO-3: A Mathematical Model for Fluid Flow, Heat, and Mass Transport in Variably Saturated Geologic Media - Theory and Numerical Methods, Version 1.0*, WHC-EP-0042, Westinghouse Hanford Company, Richland, Washington.

Sewart, G. H., W. T. Farris, D. G. Huizenga, A. H. McMakin, G. P. Streile, and R. L. Treat, 1987, *Long-Term Performance Assessment of Grouted Phosphate/Sulfate Waste From N Reactor Operations*, PNL-6152, Pacific Northwest Laboratory, Richland, Washington.

Smoot, J. L. and B. Sagar, 1990, *Three-Dimensional, Contaminant Plume Dynamics in the Vadose Zone: Simulation of the 241-T-106 Single-Shell Tank Leak at Hanford*, PNL-7221, Pacific Northwest Laboratory, Richland, Washington.

Stone, W. A., J. M. Thorp, O. P. Gifford, and D. J. Hoitink, 1983, *Climatological Summary for the Hanford Area*, PNL-4622, Pacific Northwest Laboratory, Richland, Washington.

van Genuchten, M. Th., 1980, "A Closed-Form Equation for Predicting the Hydraulic Conductivity of Unsaturated Soils," *Soil Sci. Soc. Am. J.* 44:892-898.

Walker, F. W., D. G. Miller, and F. Feiner, 1984, *Chart of the Nuclides*, General Electric Company, San Jose, California.

This page intentionally left blank.

APPENDIX A

HYDRAULIC PROPERTY CHARACTERIZATION OF THE GROUT SITE

This page intentionally left blank.

September 1, 1987

To: RWNelson

From: MJFayer Mike

Subject: Grout Site Hydraulic Properties

Bill, attached is a report which documents representative hydraulic properties for the major soil materials beneath the grout site, the backfill material around the vaults, the clay cap, the gravel cocoon, the concrete, and the grout. These properties were assembled to allow the model testing to proceed; they are not intended for use in the final performance assessment unless laboratory testing indicates that they are acceptable.

In conversations with MChamness, Westinghouse is working on a draft of a Grout Site Characterization Report. I believe PNL should look into officially obtaining a copy.

I have learned that undisturbed core samples from a well within the Grout Site have been arriving in the PNL lab. Please consider my comments in the attached appendix when you proceed with lab measurements.

Hydraulic Property Characterization of the Grout Site

by MJFayer and SOudziak

The purpose of this report is to provide soil hydraulic properties for the major soil layers located beneath the grout site, the backfill to be used around the vaults, the clay cap, the gravel cocoon, the concrete walls of the vaults, and the grout itself. These properties will be used in the tests designed to provide data for making a decision as to which computer code is most appropriate to use for Grout Performance Assessment. Westinghouse is currently working on a draft version of a grout site characterization report, but we do not expect it to be available for several months, perhaps by November 1987.

The two sources of data that were used for soils characterization beneath the grout site are listed below.

1. AP Tank Farm: Andy Reisenauer took samples from distinct soil layers that were exposed when the AP tank farm site was excavated. The maximum sample depth was only 50'. Characterization included particle size, water retention, and saturated conductivity. The latter two properties were determined on samples from which all gravel was removed.

2. Wells E25-25,26,27: The E-Well samples are cores obtained in 5' increments down to the water table. No attempt was made to separate samples based on material from each distinct layer that was encountered. Each sample is a mixture of whatever was obtained from a 5'-long core. Maximum sampling depth was >250'. Characterization included particle size, water retention, and saturated conductivity for selected samples. The latter two properties were determined on samples from which all gravel was removed.

Suzanne Dudziak used the E-well logs to draw up a generalized discretization of the soil layers beneath the grout site. Note that the layering scheme she generated differs from that shown in Sewart et al. (1987). Sewart et al. estimated the soil layering beneath the grout site by interpolating soil profile data from beneath the 216-A-8 and 216-A-37 cribs, which are located near the grout site. In all likelihood, as more direct data from the grout site becomes available, our description of the layering sequence will probably change. The attached Appendix contains a discussion of the current data set. We are proceeding with the layering sequence outlined here because this information is sufficient for model testing; it is likely to be insufficient for the actual grout site performance assessment.

Because the E-well samples are mixtures of layers, their measured soil hydraulic properties are less useful than the properties measured for the AP-samples (see the Appendix). Together, Suzanne and I have assigned AP soil types to the generalized soil layers as shown in Table 1.

Table 1. Generalized Soil Layering Beneath the Grout Site

Depth Interval (ft)	Soil Type No.	E-well General Soil Layer Description	AP Sample Number	Gravel Content (%)
0-10	1	VF-C Sand	AP-2	0
10-40	2	Sl.Grav. M-VC Sand	AP-4g	10
40-60	3	M-C Sand	AP-3	0
60-80	2	Sl.Grav. M-VC Sand	AP-4g	10
80-140	1	VF-C Sand	AP-2	0
140-170	3	M-C Sand	AP-3	0
170-265	4	Sandy Gravel	AP-1g	38

The available water retention data were used to generate parameters for the van Genuchten functions for representing soil hydraulic properties. The generated parameters for samples AP-1 through AP-4 are listed in Table 2. All of the lab data were used. Samples AP-1 and AP-4 had their gravel content removed before the lab tests. To correct the soil hydraulic properties for gravel, we used the technique of Bouwer and Rice (1983). The modified parameters are listed in Table 2 under samples AP-1g and AP-4g. Note that sample AP-4g is listed as containing 10% gravel. The AP-4 sample actually had 32% gravel, which was sieved out before analysis. According to the E-well logs, the layer we are trying to represent is a slightly-gravelly sand. Therefore, we chose to reduce the gravel content from 32 to 10%.

The material selected to surround the grout vaults can be determined by the site operator. The current understanding for material surrounding the vaults is that coarser-textured material is preferable to finer-textured material. Because 50% of the to-be-excavated material is coarse-textured, we assume that the backfill can be this material (AP-4g from Table 1). Note that less material will be needed to backfill the excavation and therefore the fine-textured soil layers can be screened out before backfilling.

At the moment, the grout vault design specifies that there will be a sloped 1'-thick layer of clay above each vault. Because no specific clay has been identified for the grout site, we have chosen to approximate the clay with a material that can be found near, if not within, the grout site. This material, sample AP-5, is texturally classified as a silt loam soil but should be sufficient for the modeling tests. The parameters for soil AP-5 are listed in Table 2.

Immediately surrounding the vaults may be a 3'-thick blanket of gravel. A specific gravel size has not been identified as yet. Therefore, we used the estimated gravel hydraulic properties from Fayer et al. (1985). The van Genuchten functions were fit to the gravel data; the fitted parameters are listed in Table 2.

Table 2. Soil Hydraulic Property Parameters for the van Genuchten Functions (m=1-1/n)

Material Descriptor	θ_s (-)	θ_r (-)	α (1/cm)	n (-)	K_s (cm/hr)	Gravel Content (%)
AP-1	0.417	0.0322	0.1008	2.9224	9.18	0
AP-1g	0.2585	0.0200	0.1008	2.9224	4.46	38
AP-2	0.521	0.0958	0.0309	3.1071	2.15	0
AP-3	0.436	0.0552	0.0494	3.2863	2.92	0
AP-4	0.454	0.0419	0.0666	2.6751	8.10	0
AP-4g	0.4086	0.0377	0.0666	2.6751	6.73	10
AP-5	0.428	0.0133	0.0118	1.3945	0.178	0
Gravel	0.419	0.0308	4.6947	2.5721	1261.0	100
Concrete (CL-40d)	0.237	0.0000	5.250E-6	1.4365	1.79E-6	0
Grout (82-030b)	0.383	0.0665	1.487E-6	1.6592	3.42E-6	0

Data for the concrete and grout formulation to be used at Hanford are not available. There are concrete and grout data available, however, from work done by Paula Heller for Sandia. We have taken data for a specific sample of each material and fit the hydraulic property functions; the fitted parameters are listed in Table 2.

Plots of all the following materials listed in Table 2 are attached after the Appendix: AP-1, AP-2, AP-3, AP-4, AP-5, gravel, concrete, and grout. Some of the plots are partially outside the axes scales but no attempt was made to correct this problem (it would involve modifying code). The plots are provided for comparative purposes (note that all axes are the same).

References

Bouwer, H. and R. C. Rice. 1983. "Effect of Stones on Hydraulic Properties of Vadose Zones" in Proceedings of the Characterization and Monitoring of Vadose (Unsaturated) Zone, National Water Well Association, Worthington, Ohio.

Fayer, M. J., W. Conbere, R. R. Heller, and G. W. Gee. 1985. Model Assessment of Protective Barrier Designs. PNL-5604, Pacific Northwest Laboratory, Richland, Washington.

Sewart, G. H., W. T. Farris, D. G. Huizenga, A. H. McMakin, G. P. Streile, and R. L. Treat. 1987. Long-Term Performance Assessment of Grouted Phosphate/Sulfate Waste From N Reactor Operations. PNL-6152, Pacific Northwest Laboratory, Richland, Washington.

APPENDIX

Review of Soil Hydraulic Property Characterization of the Grout Site

by MJFayer

In my attempt to characterize the soil layering beneath the grout site, I have worked with two sets of the data - the AP Tank Farm samples and the samples from the E25-25,26,27 wells. Besides sampling location and depth, the only major difference between the two sets is that the AP samples were taken from discrete soil layers while the E-well samples were composites of 5'-long cores (there is a possibility that the samples are only subsamples of the 5' cores). This brings up a fundamental question concerning site characterization, which is, what level of characterization is adequate? For example, can thin lenses of silt, perhaps 2-cm thick, be ignored when modeling the site for performance assessment? Is it acceptable to mix the silt layer into the bulk material and treat it as a uniform mixture? Should the silt layer be documented (depth below surface, thickness) and explicitly modeled, knowing full well that to model the site with the lens will require quite detailed node spacing in the vicinity of the lens? Keep in mind that the E-well logs describe numerous lenses of various materials, ranging in texture from silt to gravel. For the most part, these lenses appear to have a limited extent and it is likely that some of the lenses, together with some of the major material layers, may be sloped, thus increasing the importance of the 3-dimensional aspect to the flow problem.

After pulling out all of our hair, what do we do next? One possibility is to proceed in stages of progressively more-complex characterization. By that, I mean that we begin with a base modeling case in which only the major soil layers are represented (the base case could even be a homogeneous profile). The flow and transport solution to this problem serves as our reference. We then refine the soil layering characterization to include some of the thinner layers ignored previously. We solve the problem and compare the new solution with the old. Refine the layering some more, resolve the problem, and obtain a third solution. What is happening to our solution compared to each preceding solution? Beyond what level of detail does the solution change immeasurably? This technique is the old "refine the grid until the solution doesn't change" trick, except that here it means refine the soil layering description and grid.

So how does this all fit in with soil hydraulic property characterization? To use the "refine the layering" technique, one needs data on a scale equal to or smaller than the finest model layering sequence. The data from the E-Wells provides only a coarse approximation of the layering sequences. This is understandable because the wells were not drilled for the purpose we have outlined. To obtain the level of detail necessary will require that cores from a future well be sampled according to soil type and not depth. Locations and thicknesses of all recognizable layers should be noted and samples taken.

Concerning the E-well data, there are several observations that I would like to make.

1. There were no in-situ bulk density measurements. These data are important for packing of samples for water retention and conductivity experiments.

2. There were no particle density measurements. This parameter, together with bulk density, can be used to calculate the porosity (i.e., saturated water content).

3. For particle size analysis, it was a very good idea to sieve and report the gravel fraction. This practice should continue.

4. For water retention, only a single sample from each material was run for the hanging water column experiment. Duplicates, such as used for the pressure plate experiments, would be much better.

5. For the hanging water column experiments, there was no consistency in the degree of saturation achieved when the samples were presumed to be saturated. Of the 20 samples, only 4 had a degree of saturation (S) near 100%. The remaining 16 samples had S values that ranged from 60 to 140%. A similar problem, although to a lesser extent, occurred with the AP samples. This inability to achieve close to 100% saturation affects both the measured water retention and the saturated hydraulic conductivity. In the future, a procedure should be implemented to more effectively saturate the samples.

6. In the process of drilling, I would think that the larger gravels (large cobbles and boulders) are less likely to end up in the sample. Core barrel sizes may range from 12" dia at the surface to 6" dia near the water table. As the diameter of the core is decreased, the larger gravels may be either pushed aside or, more likely, broken up by the driller in order to proceed deeper. How this affects our characterization of such zones will have to be explored. One possibility is that such layers, if they have large lateral extent, may be accesible elsewhere. Thus, they could be definitively characterized by sampling the exposed section rather than relying solely on the drilled sample for characterization.

7. To date, soil hydraulic property tests have been performed on the size fraction <2 mm in dia. There is a technique (Bouwer and Rice 1983) to correct the properties for the gravel content, but do we want to depend on this technique without testing it? Bouwer and Rice performed their tests with two gravel sizes, 1.5 and 15 cm in diameter. The E-well gravels are certainly less uniform in size distribution and most of the particles are less than 1.5 cm in diameter. My suggestion is to first run tandem tests for selected samples, one set without the gravel, one set with the gravel component, to assure ourselves that we can use the relationship developed by Bouwer and Rice or to develop a relationship specific to Hanford. Note that running samples with the gravel will require a larger sample size. To be comparable, the samples without the gravel should be the same size.

8. The initial water contents reported by PNL are for the bulk samples. For those regions in which significant layering occurred, it is unclear what use a bulk water content value would serve. If the water contents could be referred to specific soil types, they would be more useful. Using the E-well logs, I believe the more or less homogeneous zones could be identified. The reported in situ water contents for these identified zones would have value in the characterization effort.

References

Bouwer, H. and R. C. Rice. 1983. "Effect of Stones on Hydraulic Properties of Vadose Zones" in Proceedings of the Characterization and Monitoring of Vadose (Unsaturated) Zone, National Water Well Association, Worthington, Ohio.

241-AP-1

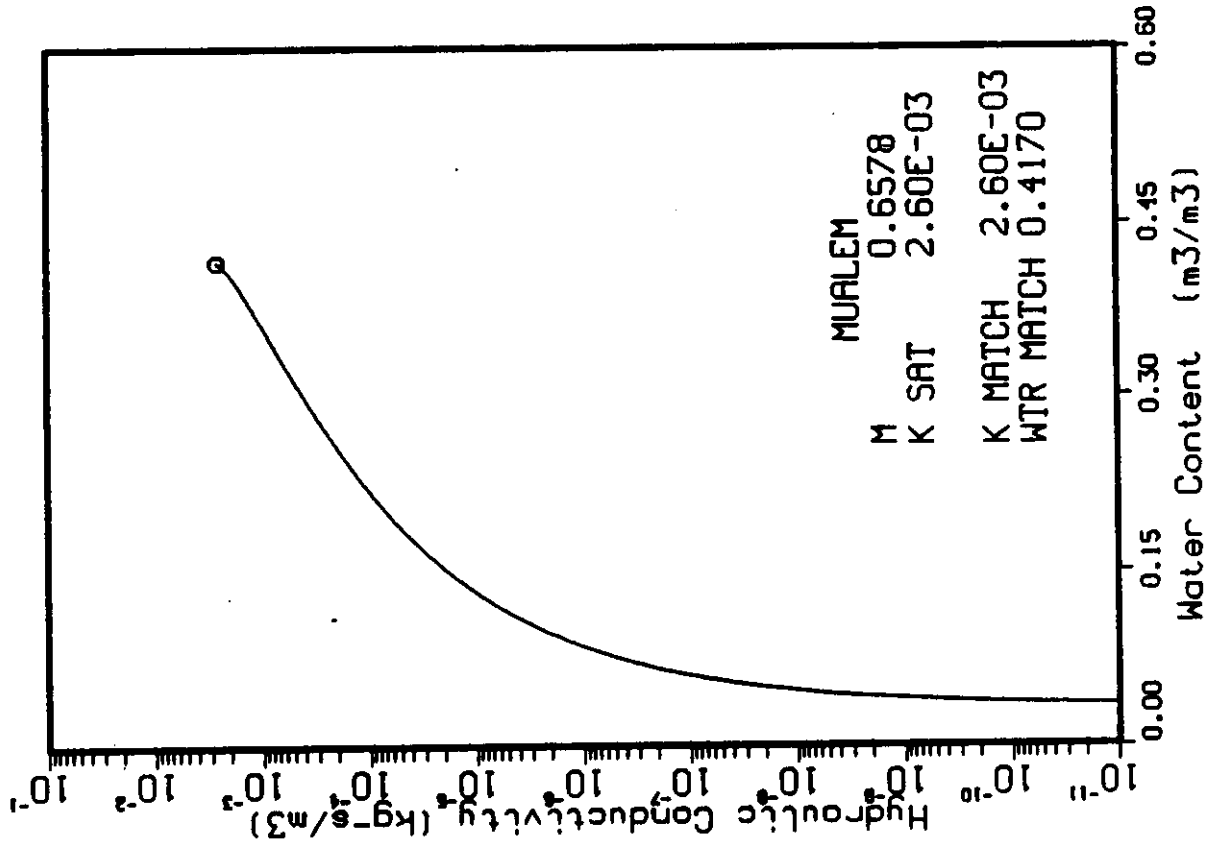

241-AP-1

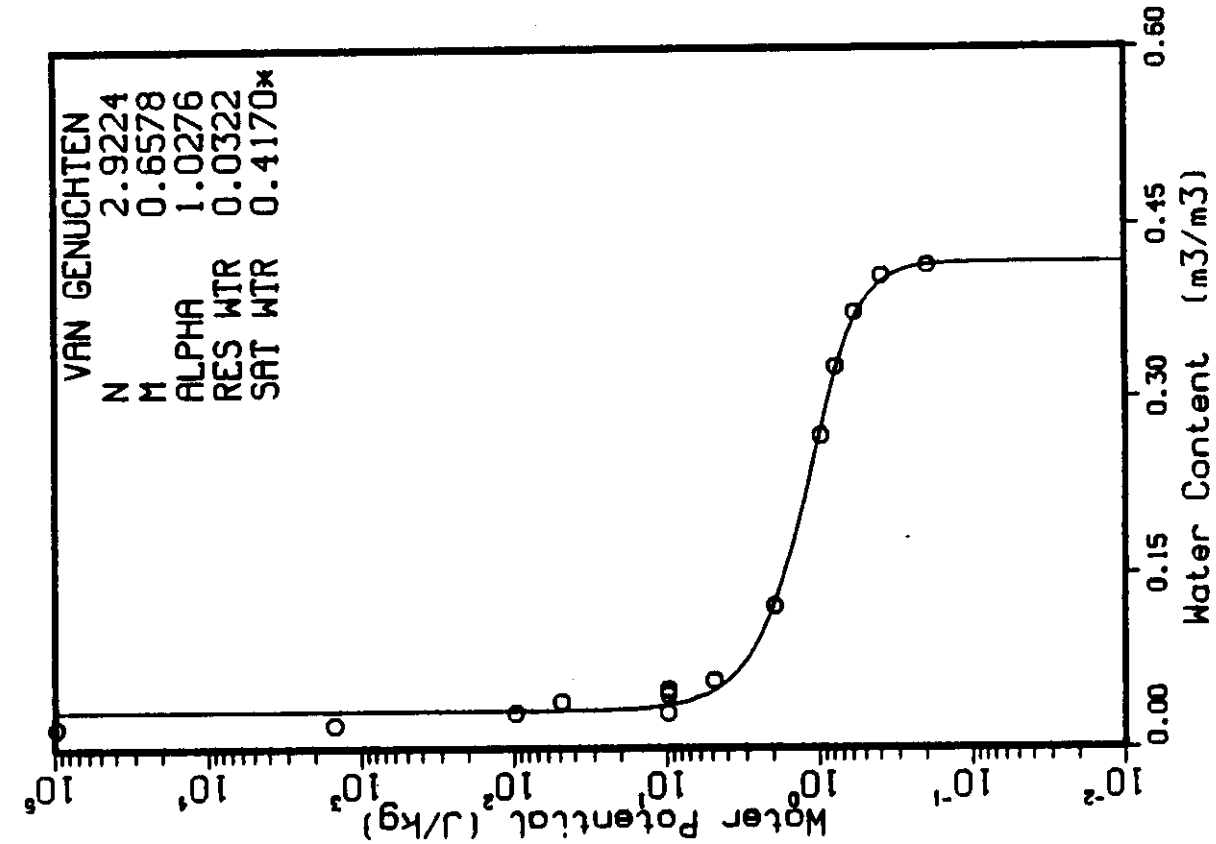

241-AP-2

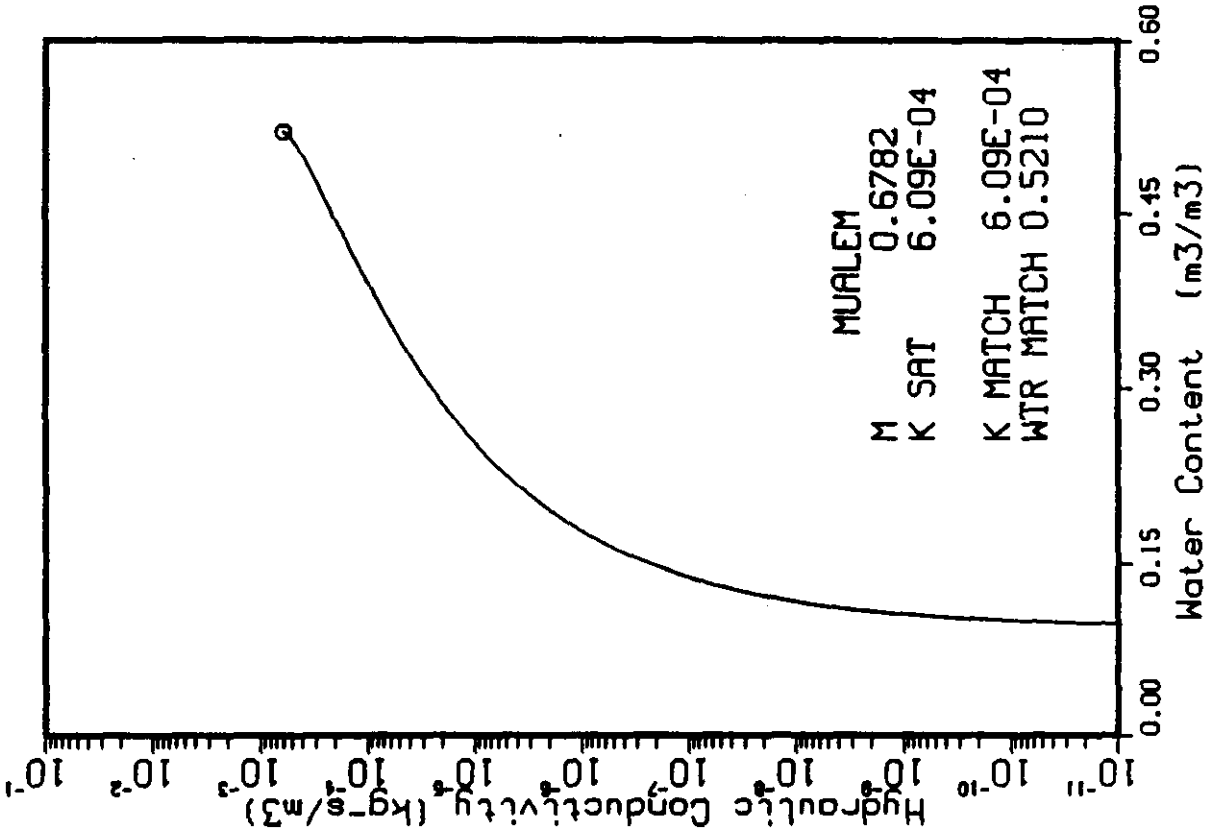

241-AP-2

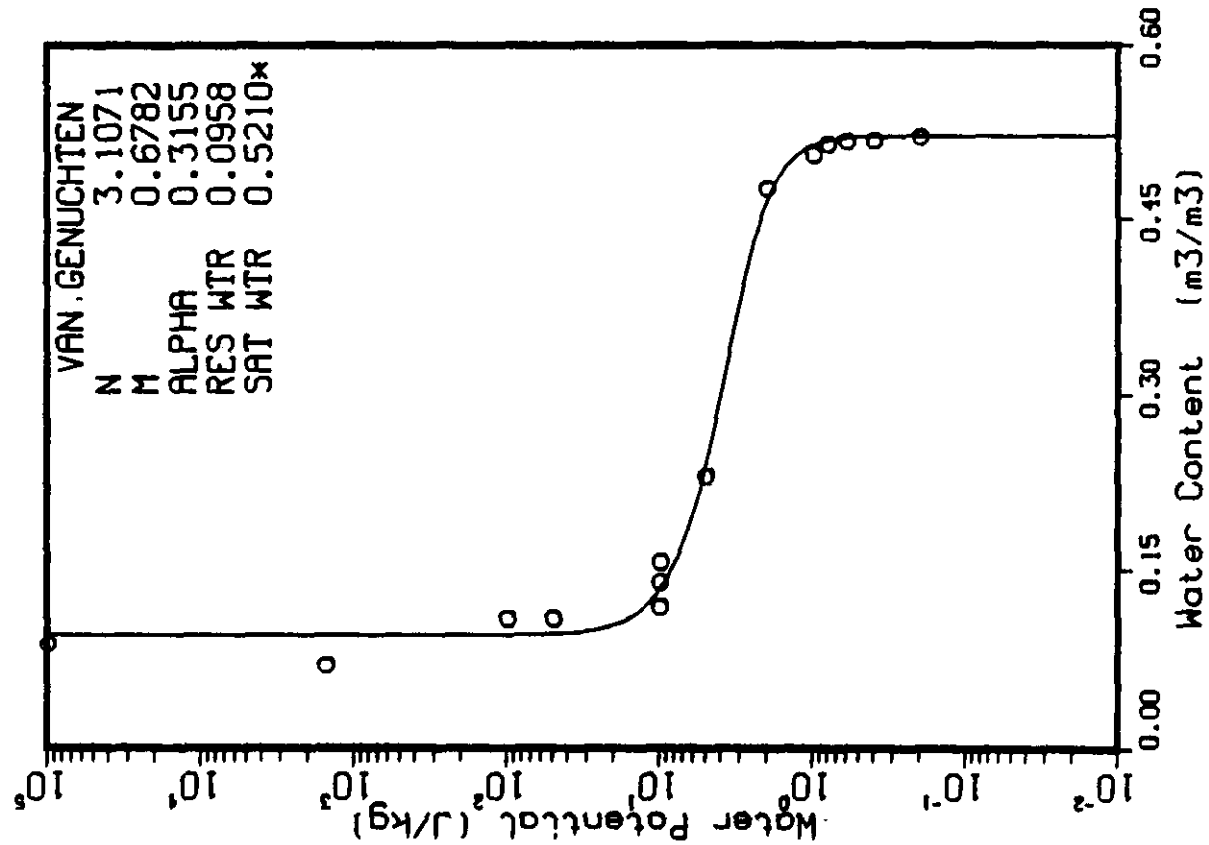

241-AP-3

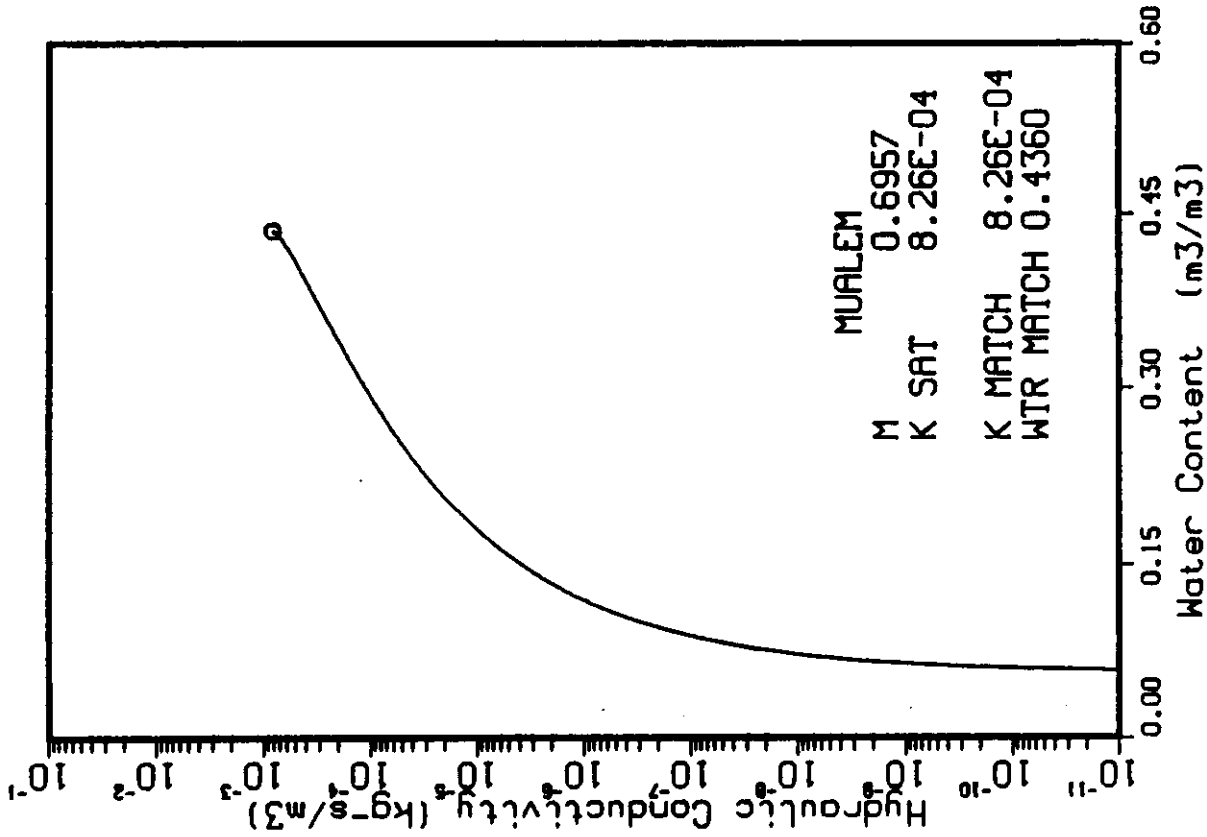

241-AP-3

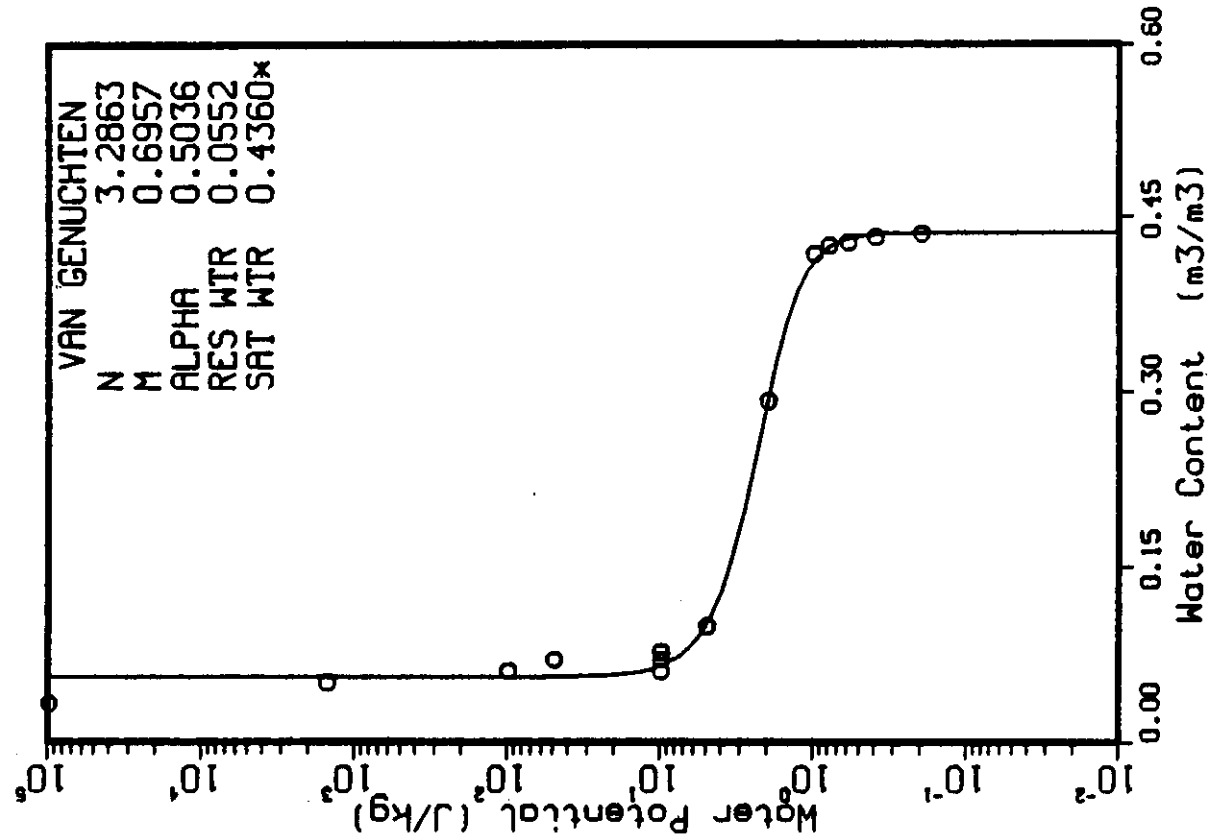

241-AP-4

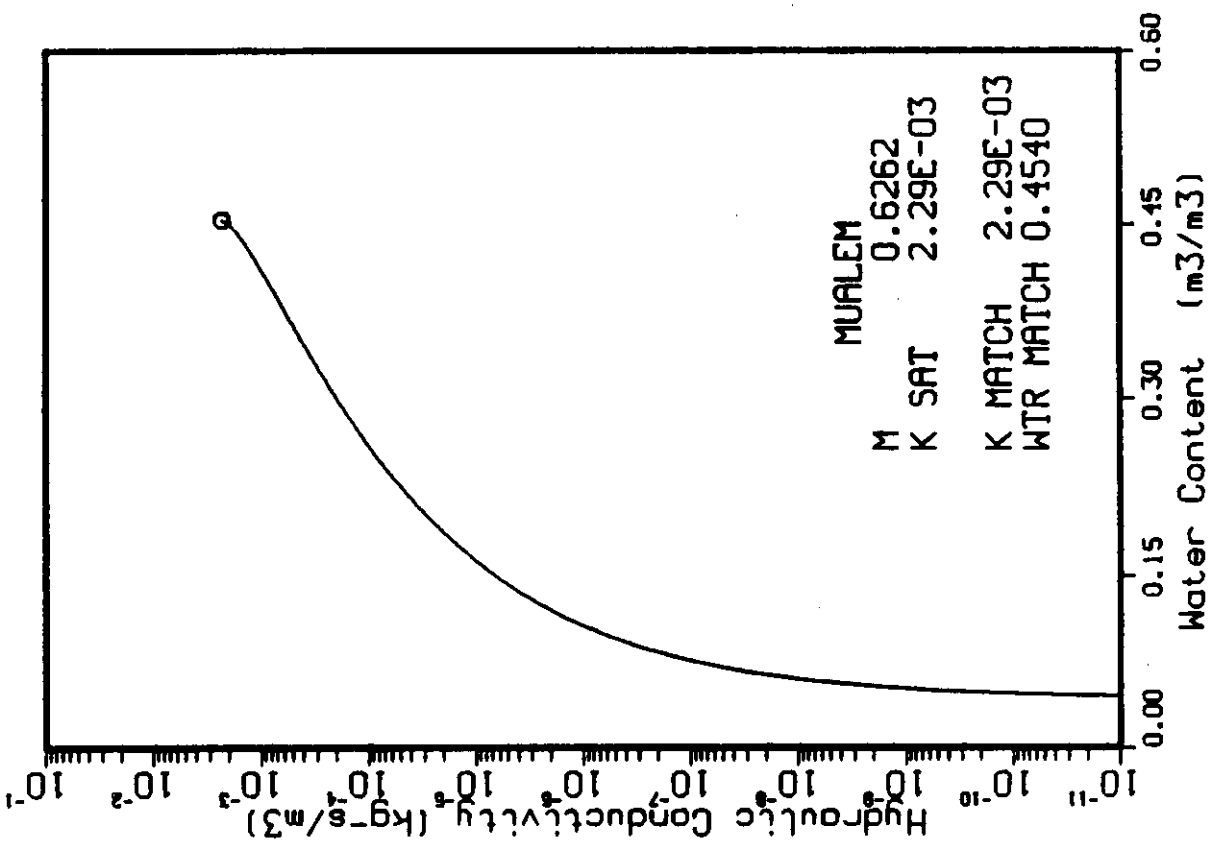

241-AP-4

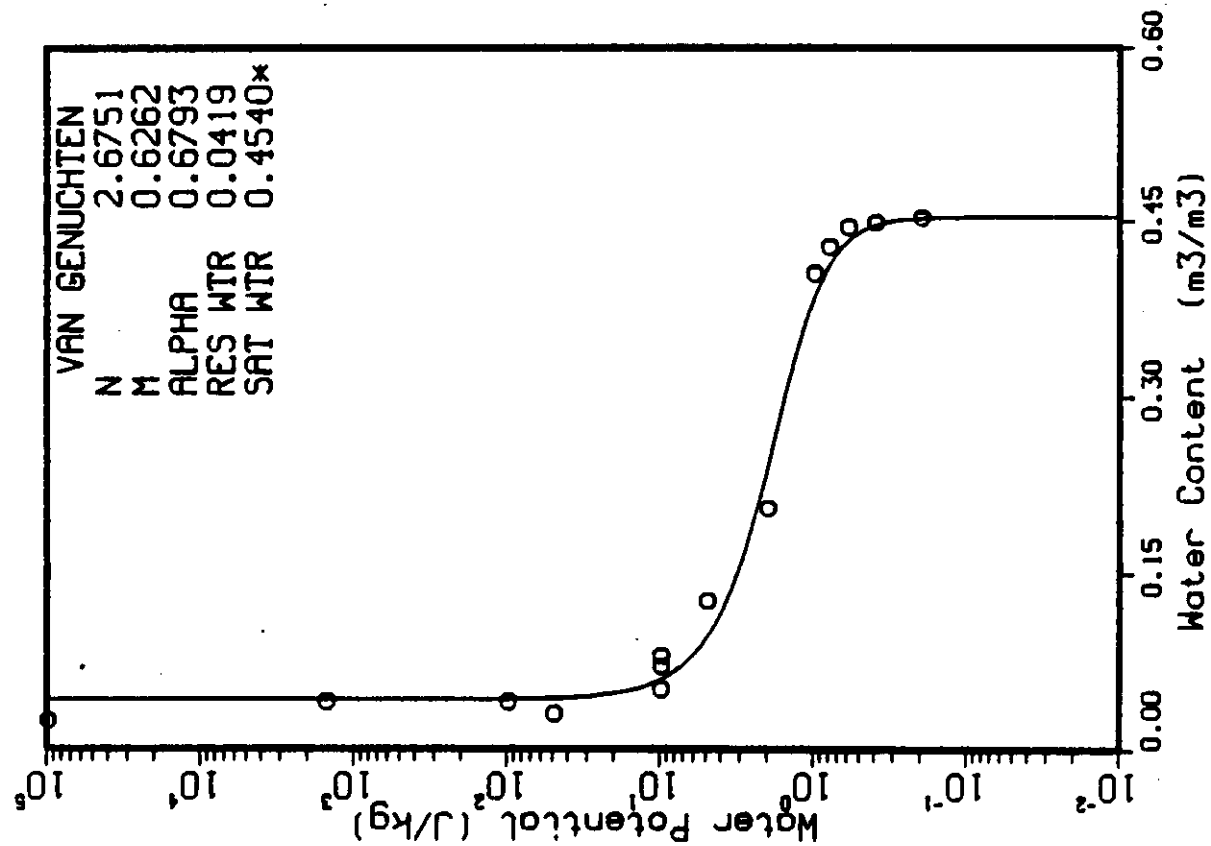

241-AP-5

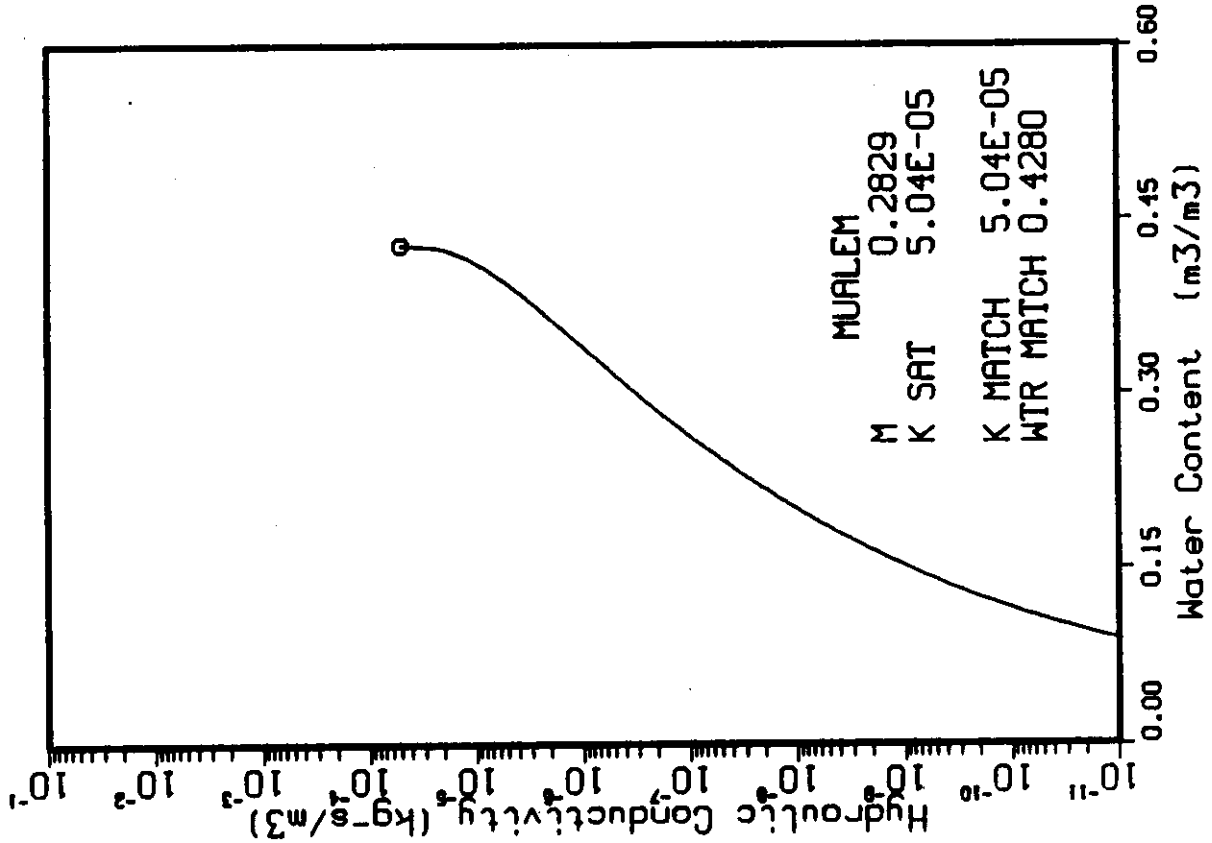

241-AP-5

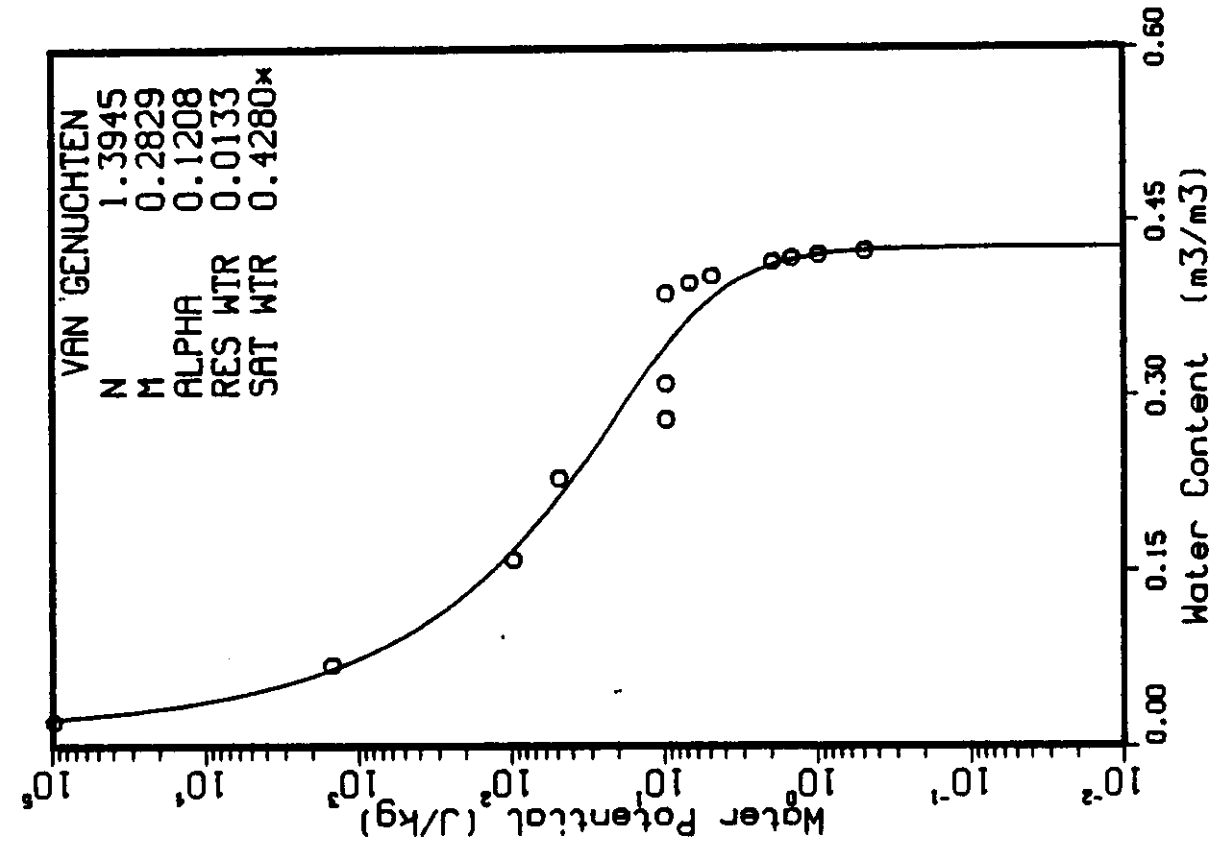

Gravel from PNL-5604

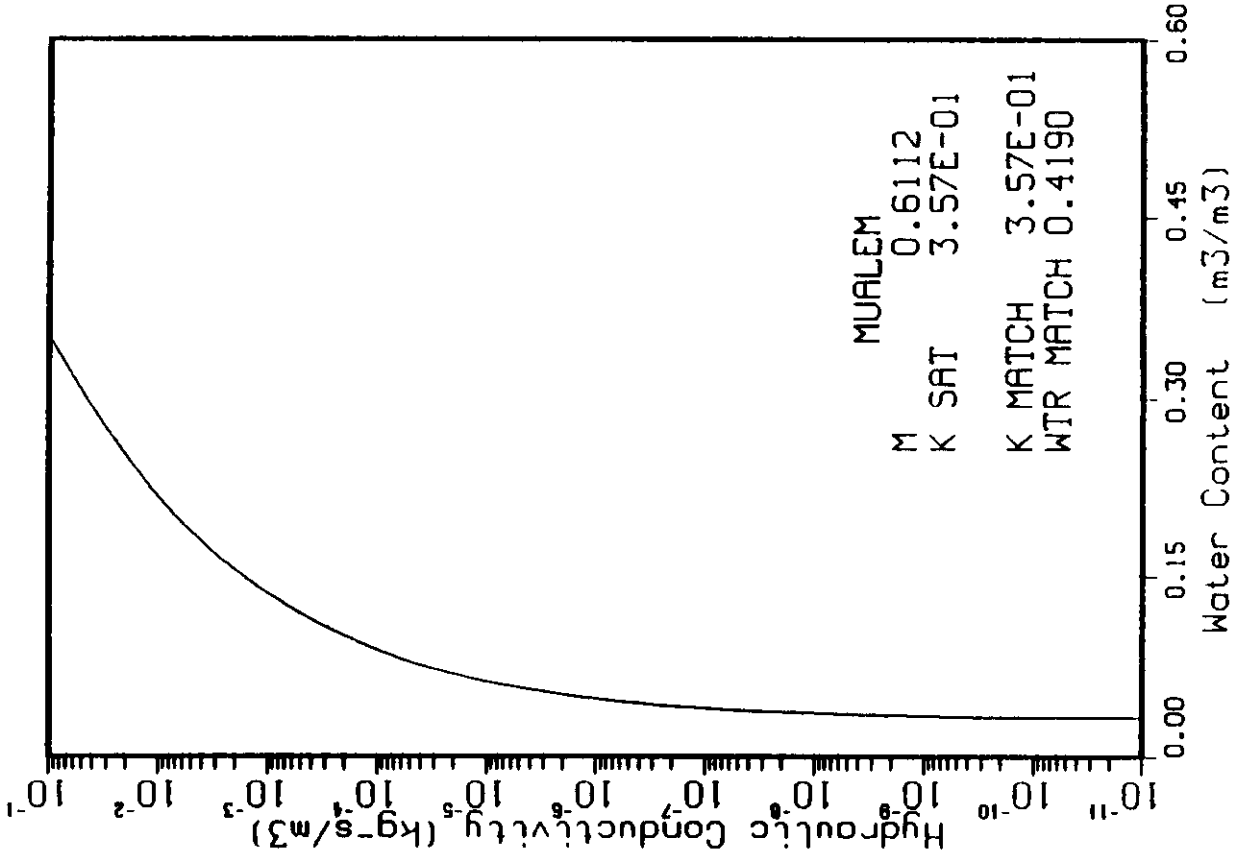

Gravel from PNL-5604

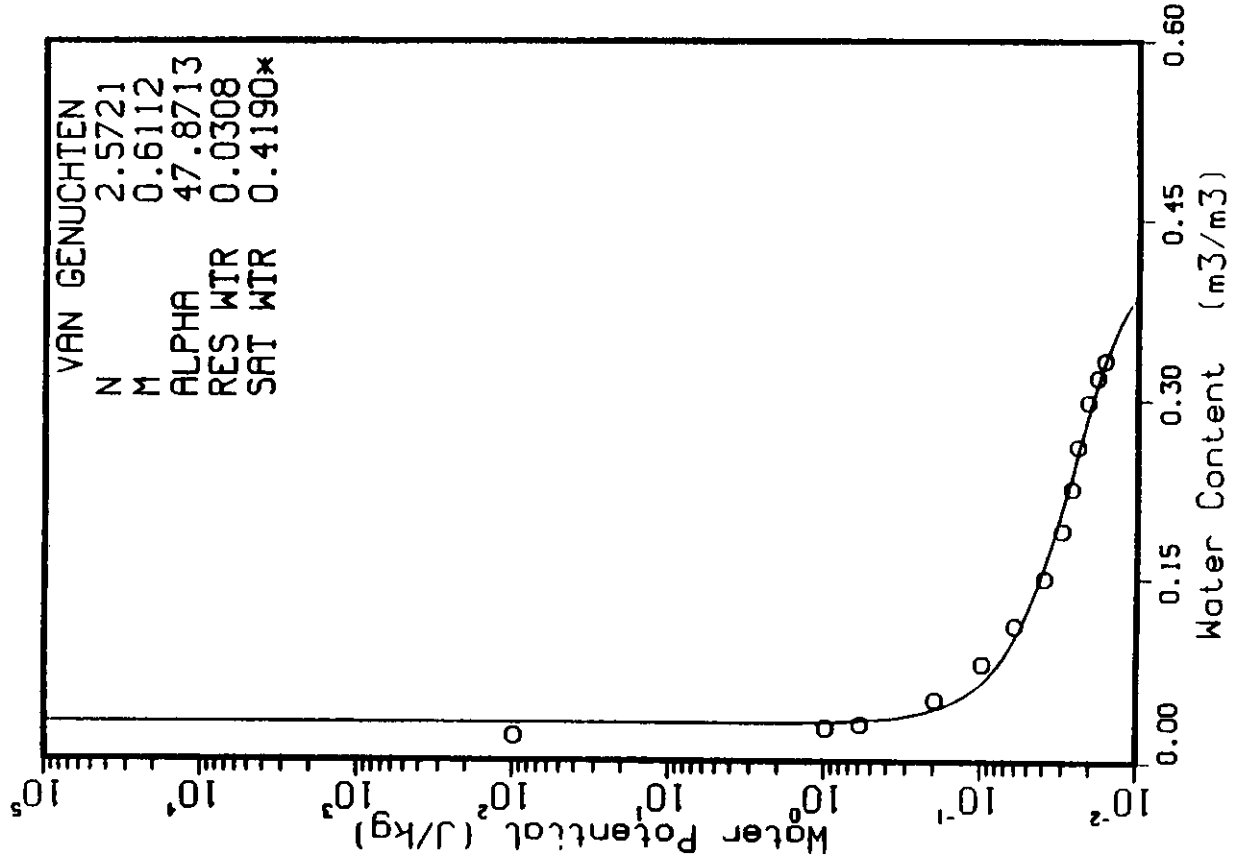

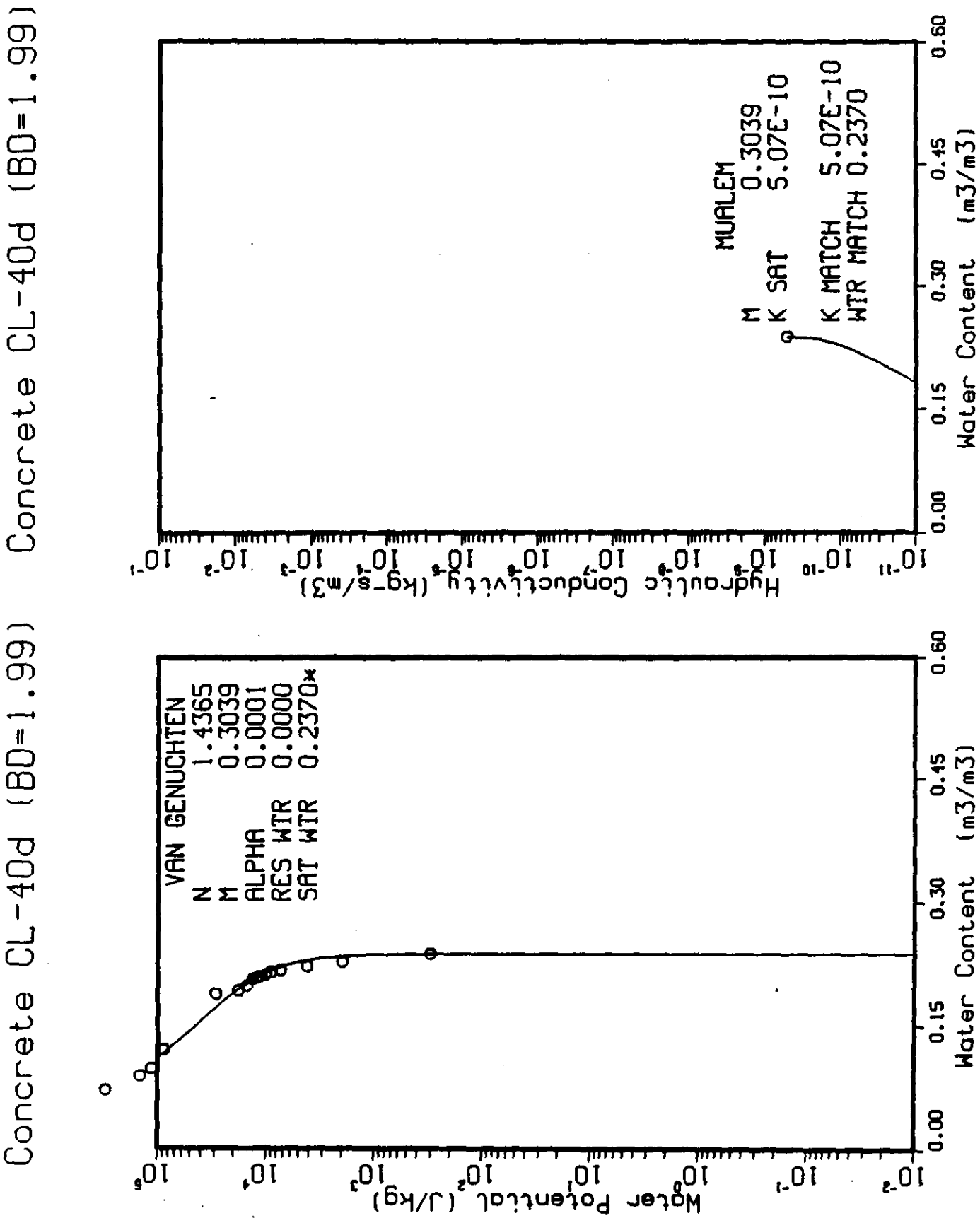
Concrete CL-40d (BD=1.99)
Concrete CL-40d (BD=1.99)
Hydraulic Conductivity (kg-s/m3)
Water Content (m3/m3)
MUALEM
M 0.3039
K SAT 5.07E-10
K MATCH 5.07E-10
WTR MATCH 0.2370
Water Potential (J/kg)
Water Content (m3/m3)
VAN GENUCHTEN
N 1.4365
M 0.3039
ALPHA 0.0001
RES WTR 0.0000
SAT WTR 0.2370*

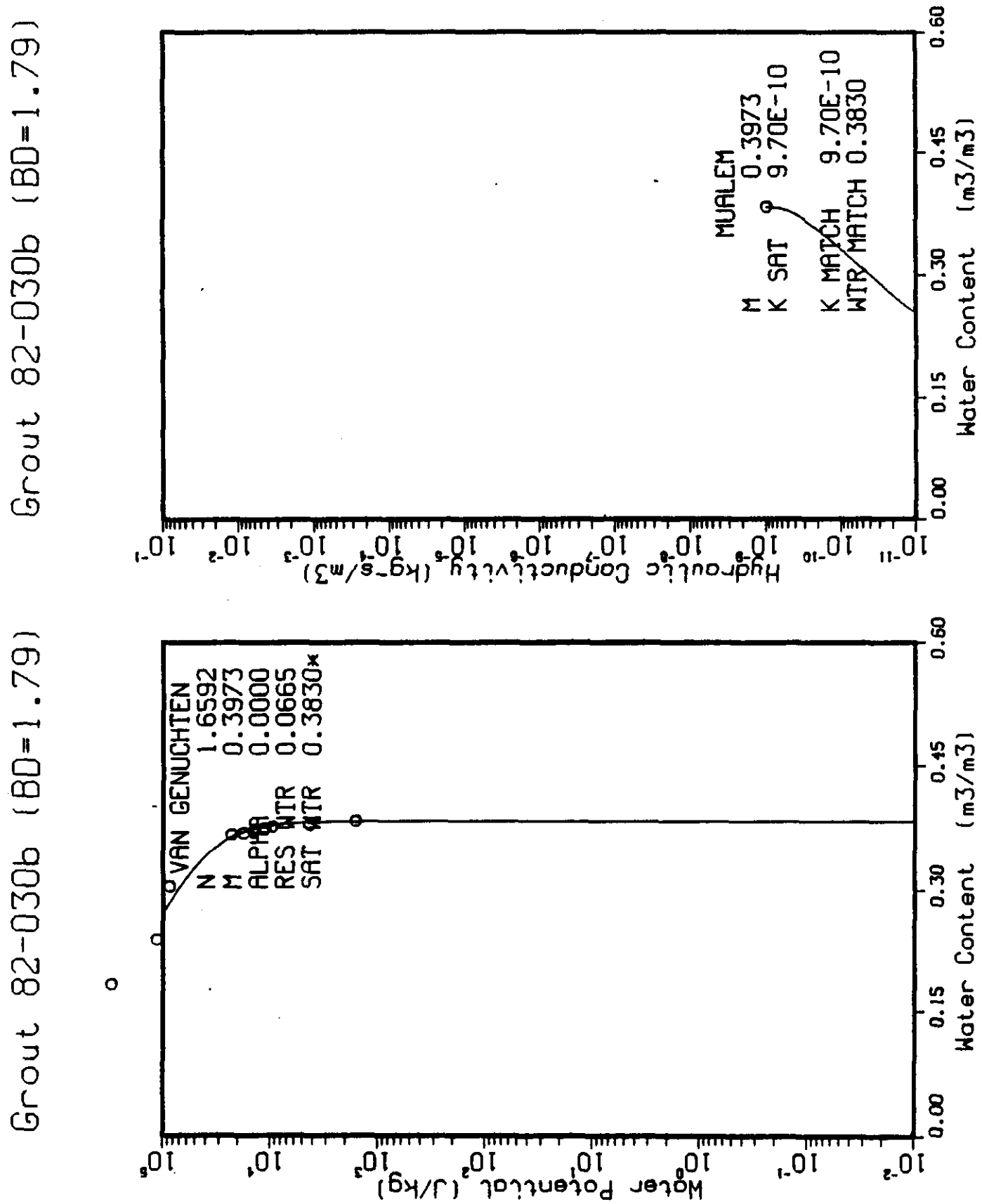
Grout 82-030b (BD=1.79)
Hydraulic Conductivity (kg-s/m3)
Water Content (m3/m3)
MUALEM
M 0.3973
K SAT 9.70E-10
K MATCH 9.70E-10
WTR MATCH 0.3830
Grout 82-030b (BD=1.79)
Water Potential (J/kg)
Water Content (m3/m3)
VAN GENUCHTEN
N 1.6592
M 0.3973
ALPHA 0.0000
RES WTR 0.0665
SAT WTR 0.3830*

APPENDIX B

PHYSICAL ANALYSIS FOR GROUT STUDY

This page intentionally left blank.

Battelle
Pacific Northwest Laboratories

Project Number

Internal Distribution

GW Gee
MJ Graham
GV Last
LL Wendell
Project File
File/LB

Date May 3, 1984

To A. E. Reisenauer

From P. R. Heller PRH

Subject Physical Analysis for Grout Study

The following is a brief report of the characterization work done on 6 samples in March 1984

Soil Materials and Sampling

Table 1 lists the materials characterized in this study:

TABLE 1. Materials Characterized

Log Number	Elevation Feet	Elevation Meter
241-AP-1	630	192
241-AP-2	638	194
241-AP-3	644	196
241-AP-4	655	200
241-AP-5	658	201
241-AP-6	665	203

These samples were taken at the various levels listed in Table 1 by digging in the east wall of the excavation for 241 AP Tank farms. These samples were all analyzed for hydraulic conductivity, particle size and water retention.

Methods of Analysis

Particle Size

Particle size was determined on two separate bases. The particles larger than 2 mm were determined by dry sieve analysis using sieve sizes of 3 in., 2 in., 1 in., 3/4 in., 1/2 in., No. 4 and No. 10 mesh (Tyler numbers). For all samples, sand, silt and clay distribution was determined based on only the less than 2-mm-sized particles from each large sample. The samples were analyzed for a complete distribution curve, except for dispersion of the sample, by ASTM procedure D 422. Sample dispersion was done using an ultrasonic homogenizer for more complete dispersion of the particles. Table 2 presents the results of the particle size analysis.

54-1900-001 (3-71)

TABLE 2. Particle Size Analysis

Sample	Hydrometer Analysis (based on 2 mm size) % Sand	% Silt	% Clay
241-AP-1	98	2	0
241-AP-2	91	6	3
241-AP-3	97	2	1
241-AP-4	98	2	0
241-AP-5	27	64	9
241-AP-6	66	27	7

Dry Sieve Analysis

Percentage Less Than

Sample	3 in.	2 in.	1 in.	3/4 in.	1/2 in.	4.75 mm	2.0 mm
241-AP-1	100	100	98.98	97.55	96.18	90.89	62.37
241-AP-2	100	100	100	100	100	100	99.99
241-AP-3	100	100	100	100	100	99.89	99.32
241-AP-4	100	100	94.06	90.96	87.31	80.26	67.92
241-AP-5	100	100	100	100	99.92	99.92	99.92
241-AP-6	100	100	100	100	97.49	99.23	98.62

Hydraulic Conductivity

Hydraulic conductivity of each of the samples was determined using a falling water head method of analysis (Klute 1965). In this method, the sample is placed in a container and enclosed with lids having an inflow valve at one end and an outflow value at the other end. The inflow valve is connected to a standpipe of a known cross-sectional area and height. The sample is saturated before any test runs are done. An initial head in the standpipe is recorded and water is allowed to flow from the standpipe through the sample for a given length of time. The ending head level in the standpipe is recorded. The hydraulic conductivity is determined using the following equation

$$K = (a/L/At)\ln(H1/H2)$$

where a = cross-sectional area of the standpipe
L = length of the sample
A = cross-sectional area of the sample
t = time for the hydraulic head difference to decrease from H1 to H2.

The hydraulic conductivity values were determined on an average of five falling head runs over a period of several minutes or several hours, depending on the flow rate, and at room temperature (22 ± 2 C). Table 3 lists the hydraulic conductivities.

TABLE 3. Hydraulic Conductivity

Sample	Hydraulic Conductivity cm/sec
241-AP-1	2.55 E-03
241-AP-2	5.97 E-04
241-AP-3	8.10 E-04
241-AP-4	2.25 E-03
241-AP-5	4.94 E-05
241-AP-6	8.61 E-05

Water Retention

Water retention characteristics were measured using three different techniques depending on the applied pressure. For pressures in the very wet range, 0 cm to 100 cm, hanging water columns were used. For the 100 cm to 500 cm pressure range Tempe cells (Soil Moisture Equipment Corporation, Santa Barbara, California) were used and for the drier range, 100 cm to 15,300 cm pressure, pressure plate extractors (Soil Moisture Equipment Corporation, Santa Barbara, California) were used.

For the hanging water columns the sample was packed to a predetermined density in a buchner funnel which was connected to an outflow tube. A graduated cylinder was used for measuring the outflow. The samples were allowed to remain saturated 48 hours before the excess water was drained at 0 cm pressure. The pressure head was increased slowly until it reached 100 cm, see Table 4. After reaching equilibrium at 100 cm pressure, the samples were weighed and oven dried to determine moisture content.

Tempe cells were used to determine the water retention characteristics at 100 cm and 500 cm pressure head. The samples were packed into cells 3 cm x 5.4 cm (height x diameter) and placed over a porous ceramic plate. Each cell was individually sealed with end cups. Pressure was applied across the top of the cell, first at 100 cm pressure, then 500 cm pressure. At the end of the run the samples were weighed and oven dried to determine moisture content.

Water retention characteristics were measured at 100 cm, 1000 cm, and 15,300 cm pressure using a pressure plate extractor. Equilibrium water contents were

obtained by packing the samples in containing rings on a porous ceramic plate where they were saturated and pressure drained in the extractor. Water contents were determined in the same manner as the other methods.

Each sample in each of the three methods was packed to the same density to allow comparison of the volumetric water content. The 100 cm values for each method was averaged to determine that point (100 cm) on the drainage curve.

PRH:pd

TABLE 4. Water Retention Characteristics as Measured by Various Methods

Sample	Pressure Plate (Volumetric H_2O Content) vol/vol			Tempe Cells	
	100 cm	1,,000 cm	15,300 cm	100 cm	500 cm
241-AP-1	0.03	0.03	0.02	0.05	0.04
241-AP-2	0.12	0.11	0.07	0.14	0.11
241-AP-3	0.06	0.06	0.05	0.07	0.07
241-AP-4	0.05	0.04	0.04	0.07	0.03
241-AP-5	0.31	0.16	0.07	0.28	0.23
241-AP-6	0.24	0.12	0.08	0.34	0.21

Sample	Sat	Hanging H_2O Columns 2 cm	4 cm	5 cm	6 cm	8 cm	10 cm	15 cm	20 cm	50 cm	70 cm	100 cm
241-AP-1	0.417	0.414	0.405		0.373	0.326	0.268		0.122	0.058		0.046
241-AP-2	0.521	0.520	0.517		0.516	0.514	0.505		0.477	0.231		0.157
241-AP-3	0.436	0.435	0.432		0.428	0.425	0.418		0.292	0.099		0.077
241-AP-4	0.454	0.453	0.449		0.445	0.428	0.405		0.206	0.127		0.079
241-AP-5	0.428			0.425			0.422	0.419	0.416	0.403	0.397	0.388
241-AP-6	0.417			0.414			0.410	0.409	0.406	0.388	0.375	0.374

241-AP-1

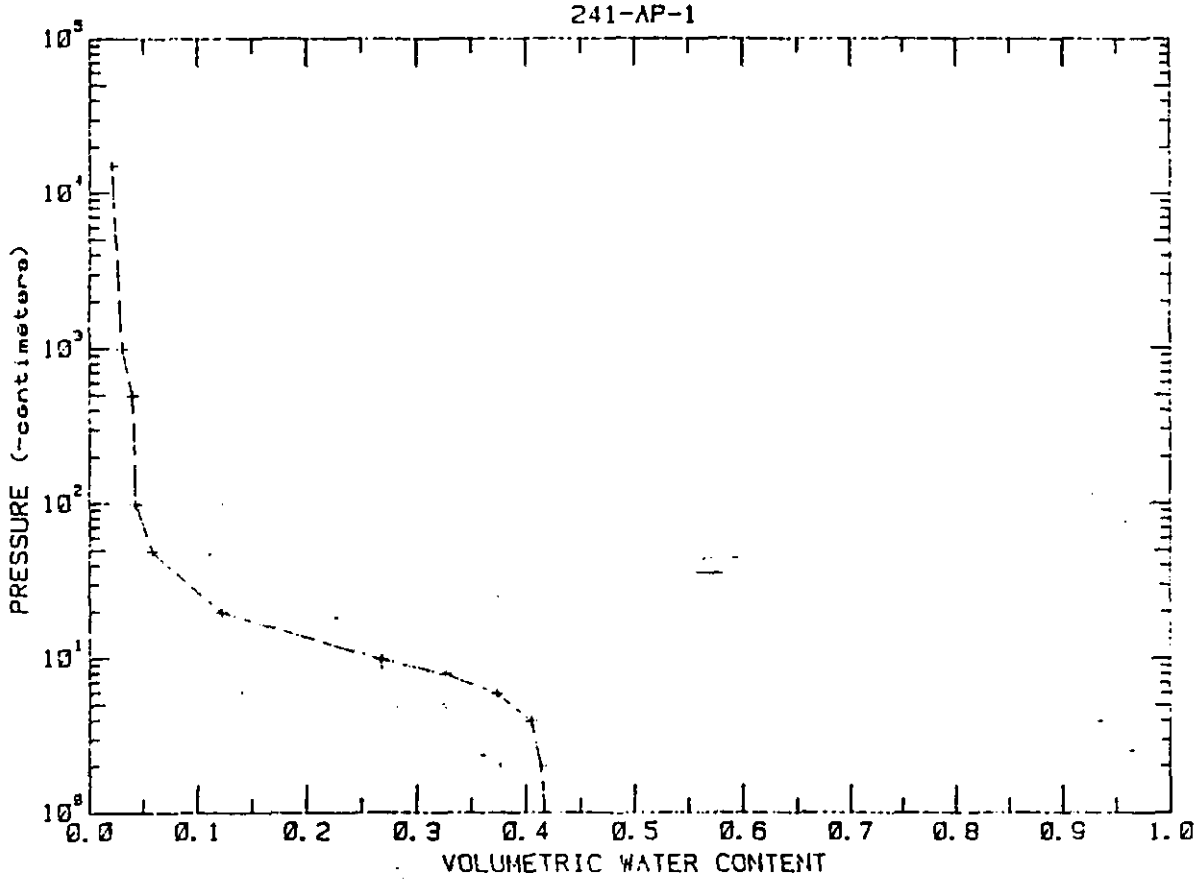

241-AP-2

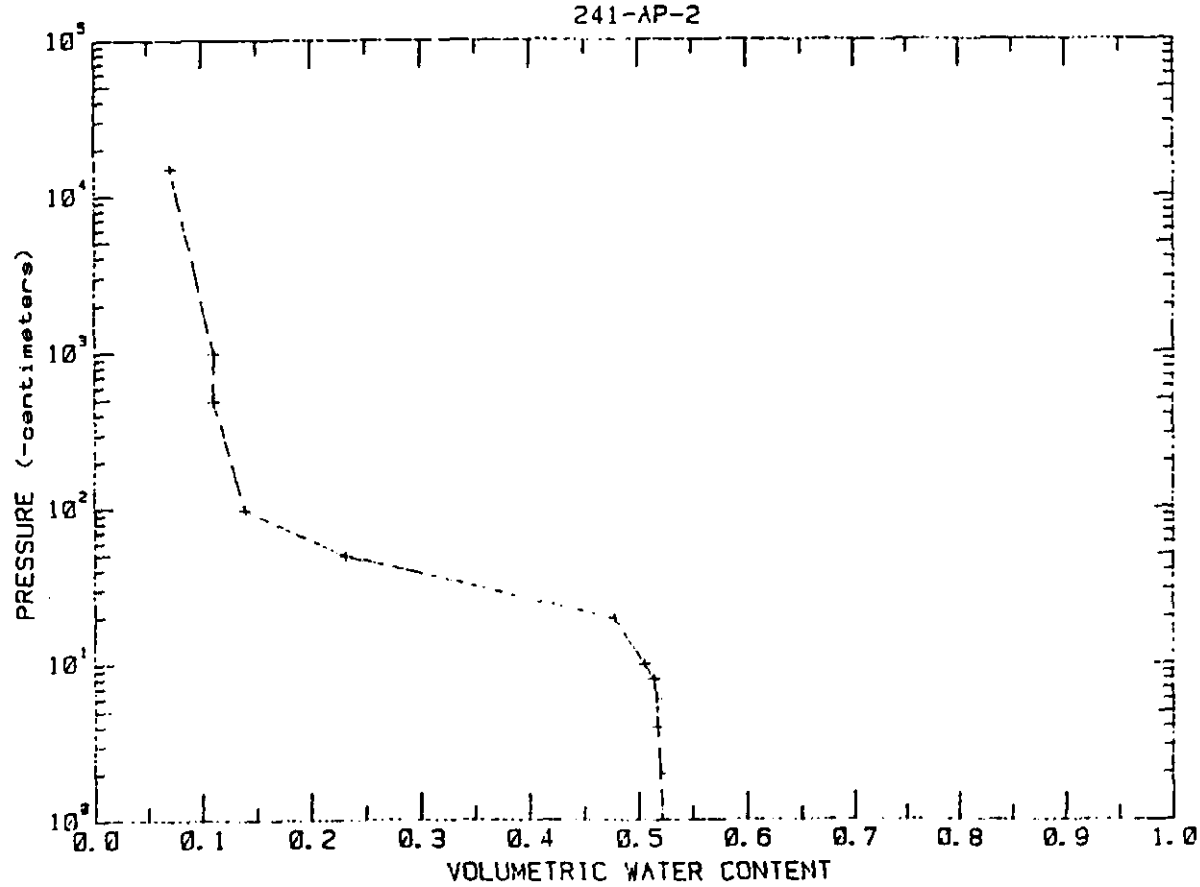

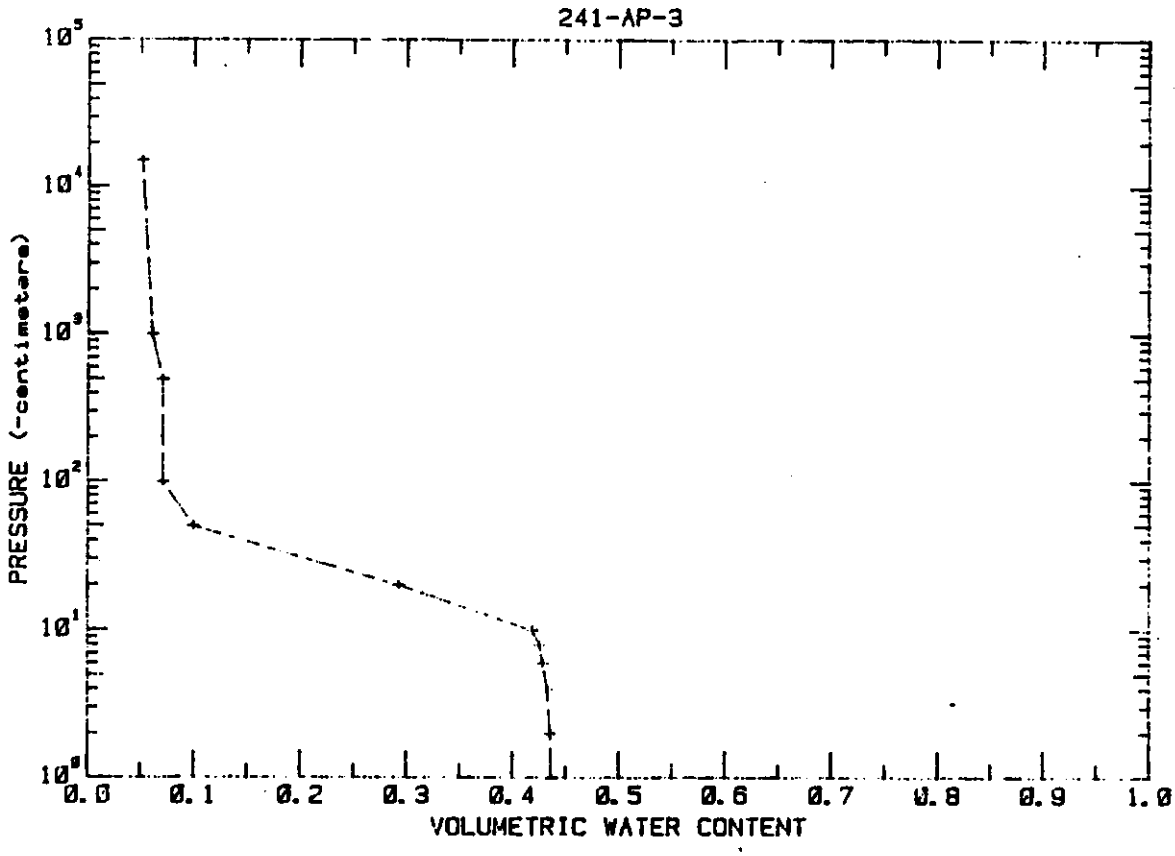
241-AP-3
PRESSURE (-centimeters)
VOLUMETRIC WATER CONTENT

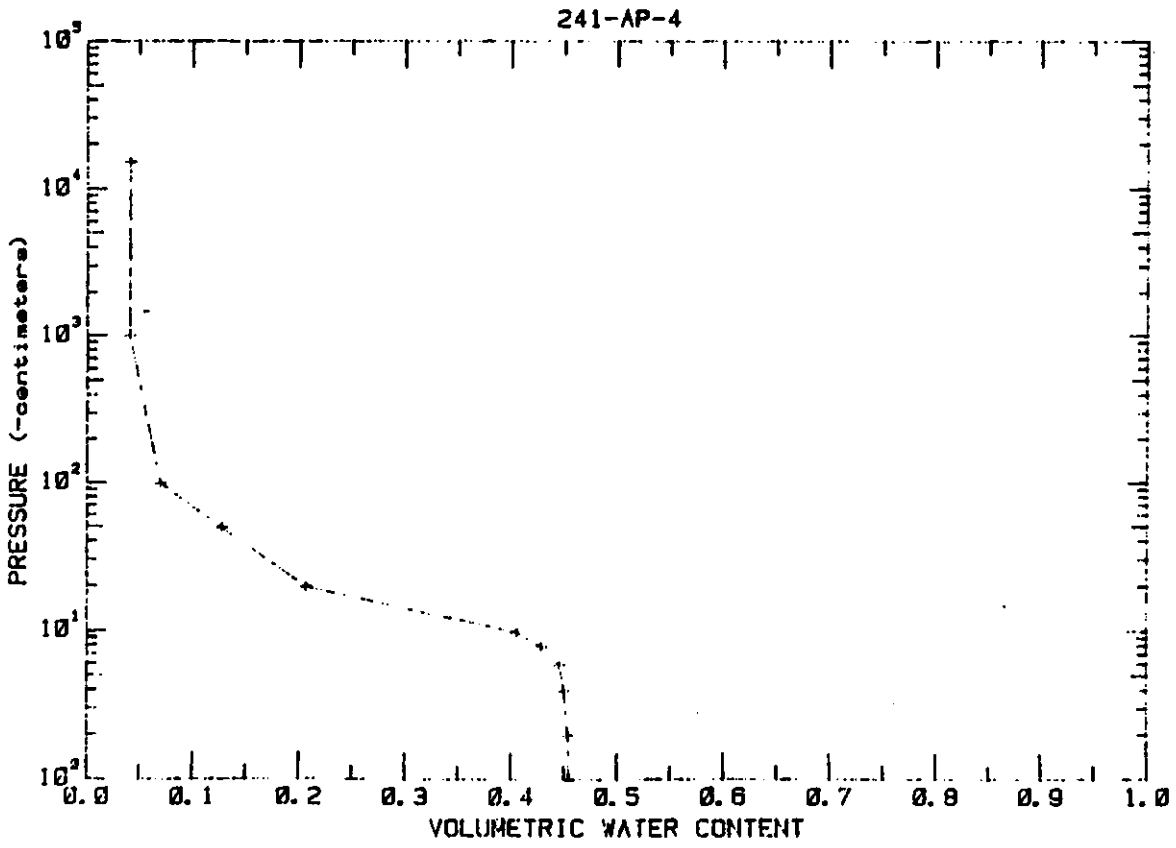
241-AP-4
PRESSURE (-centimeters)
VOLUMETRIC WATER CONTENT

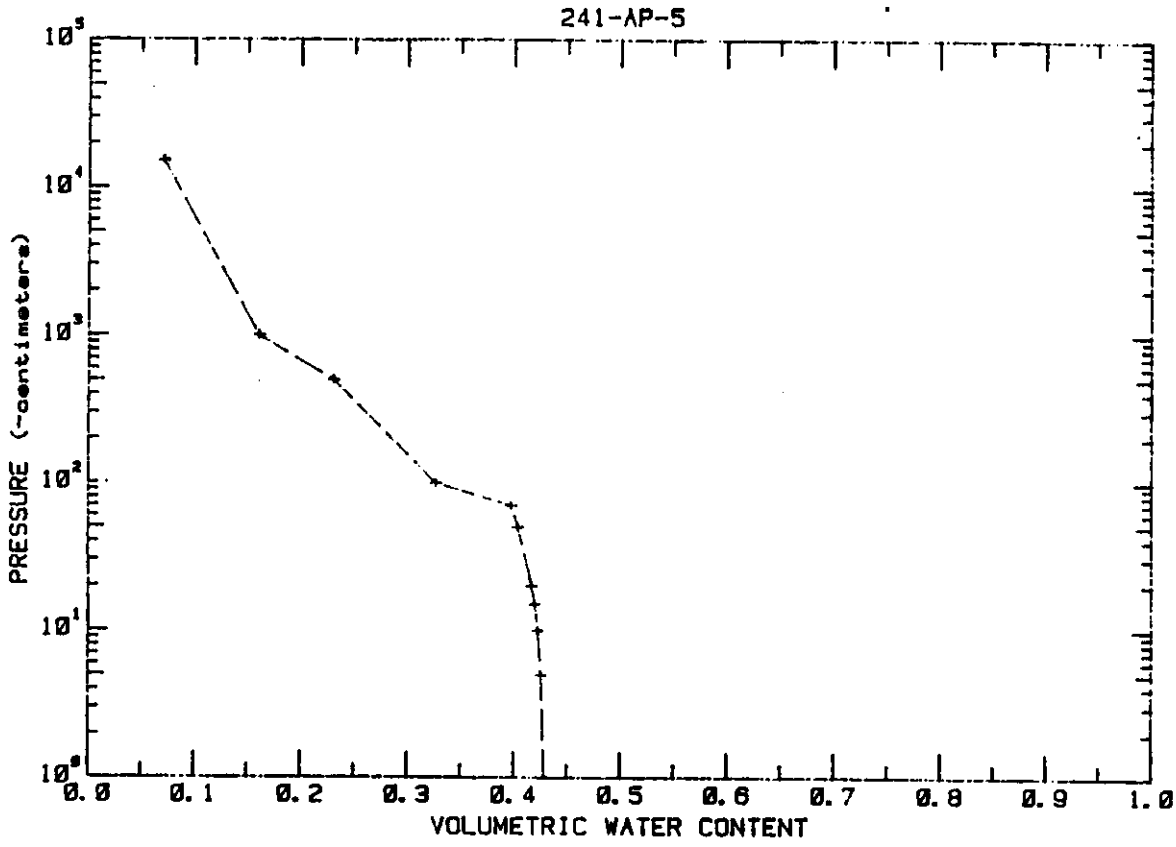
241-AP-5
PRESSURE (-centimeters)
VOLUMETRIC WATER CONTENT

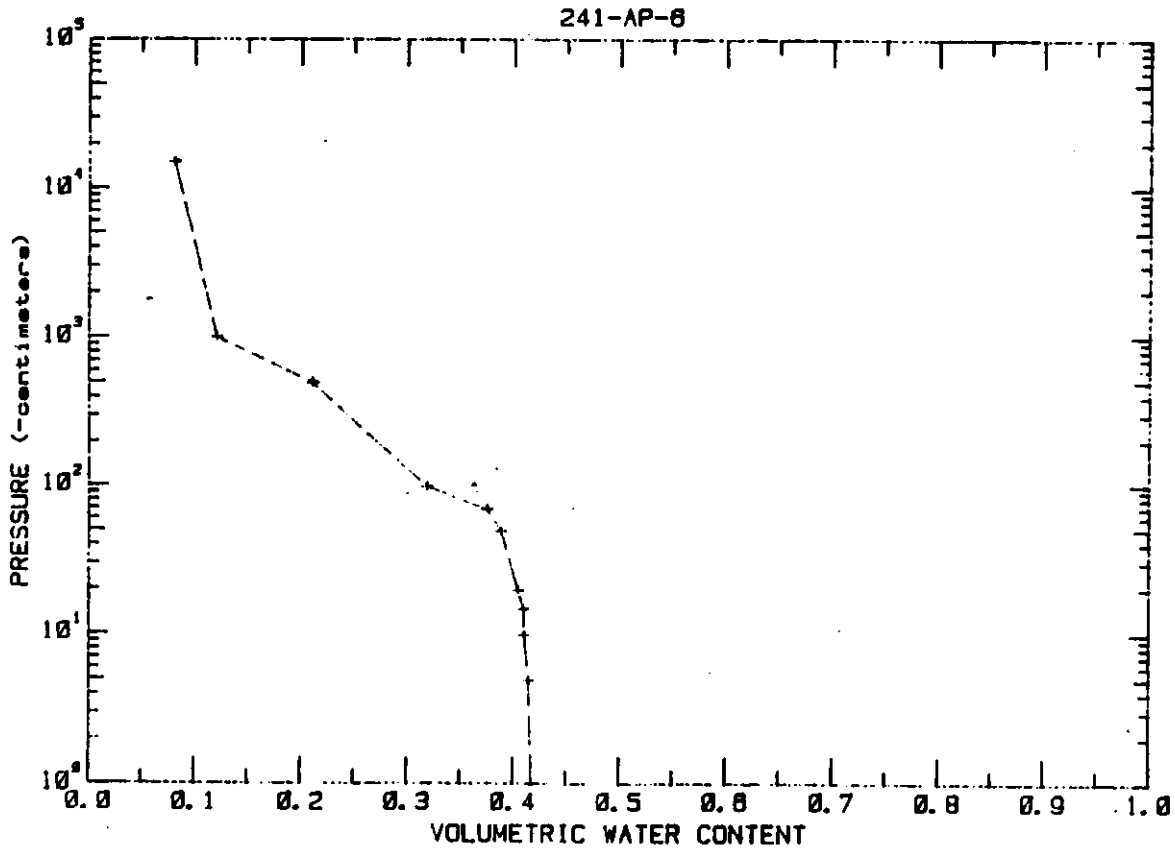
241-AP-6
PRESSURE (-centimeters)
VOLUMETRIC WATER CONTENT

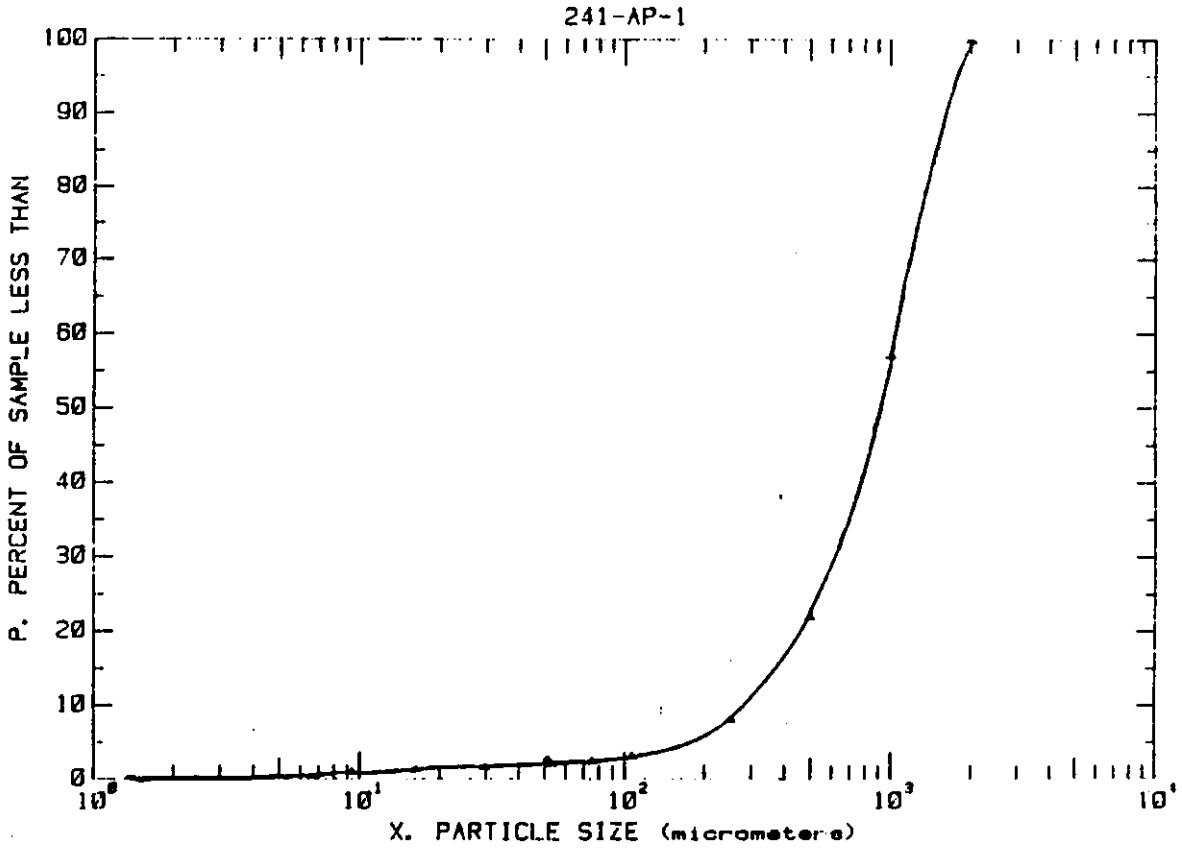
241-AP-1
P. PERCENT OF SAMPLE LESS THAN
X. PARTICLE SIZE (micrometers)

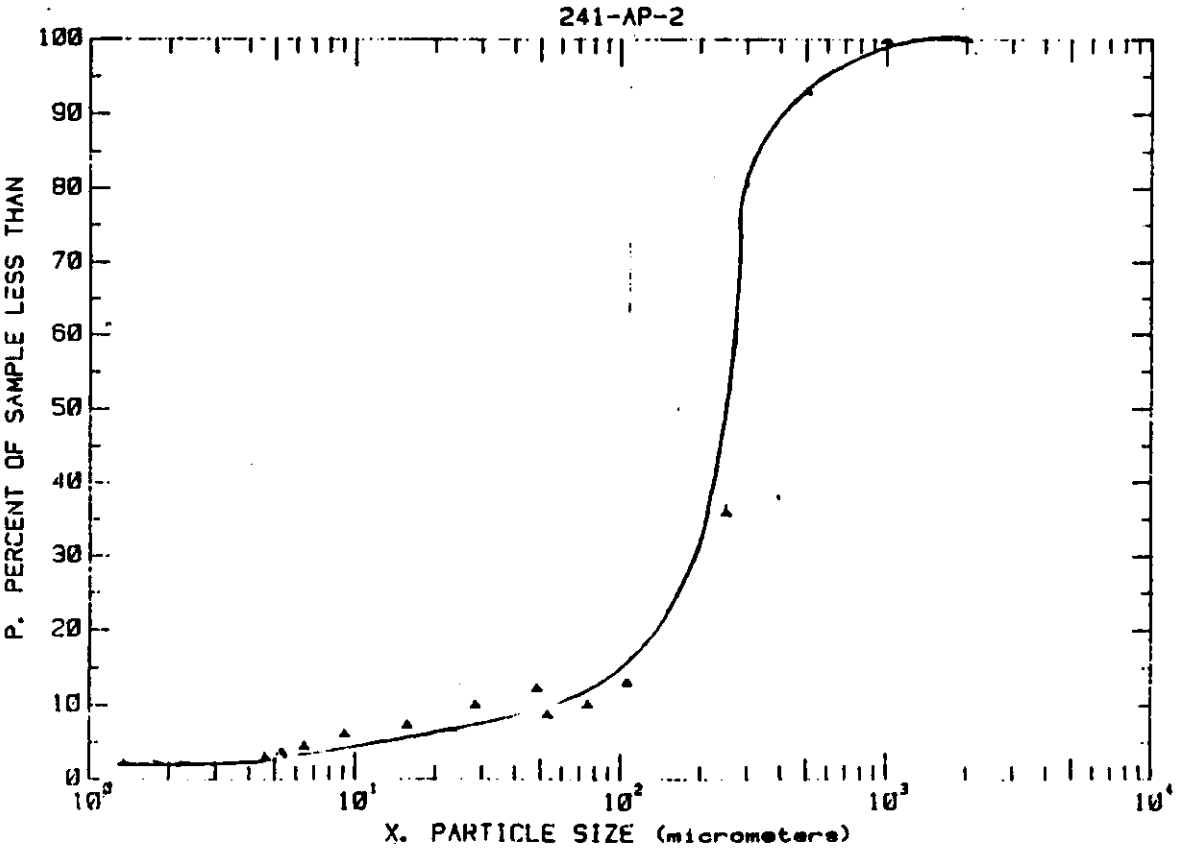
241-AP-2
P. PERCENT OF SAMPLE LESS THAN
X. PARTICLE SIZE (micrometers)

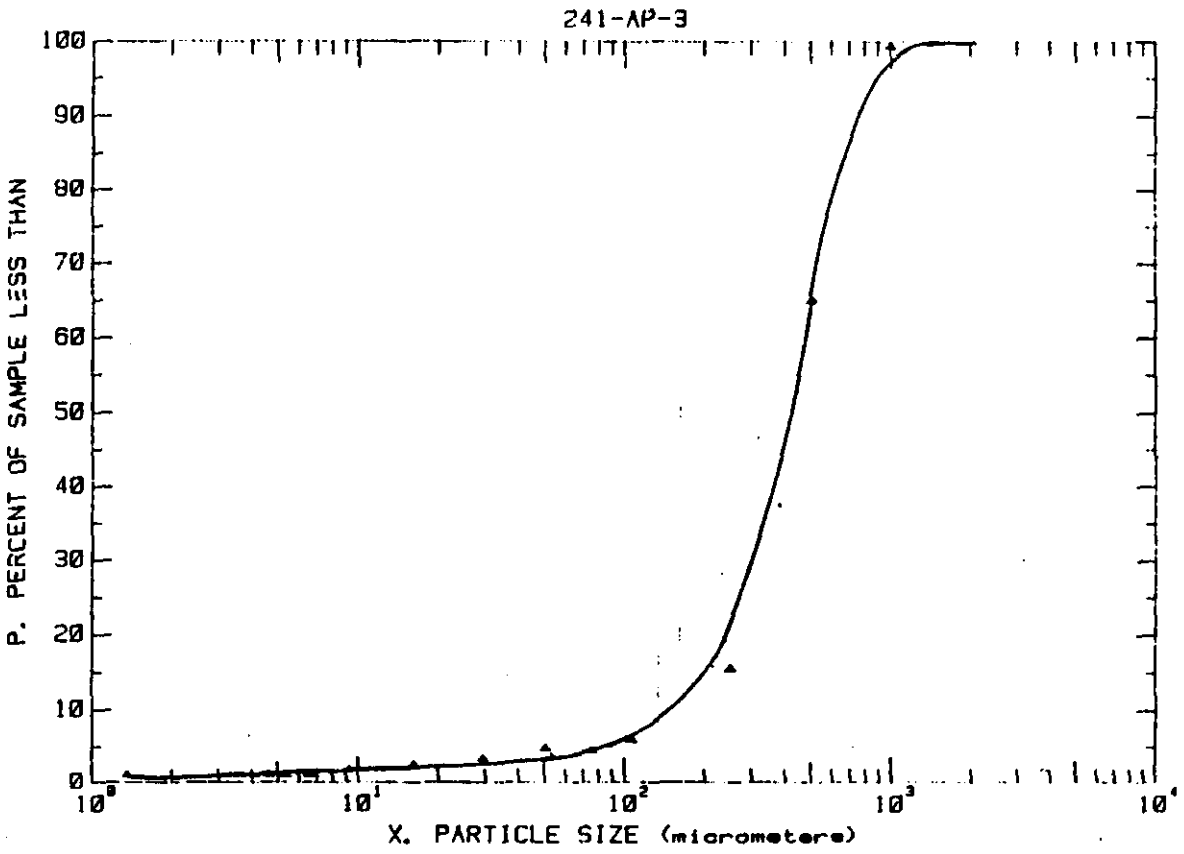
241-AP-3
P. PERCENT OF SAMPLE LESS THAN
X. PARTICLE SIZE (micrometers)

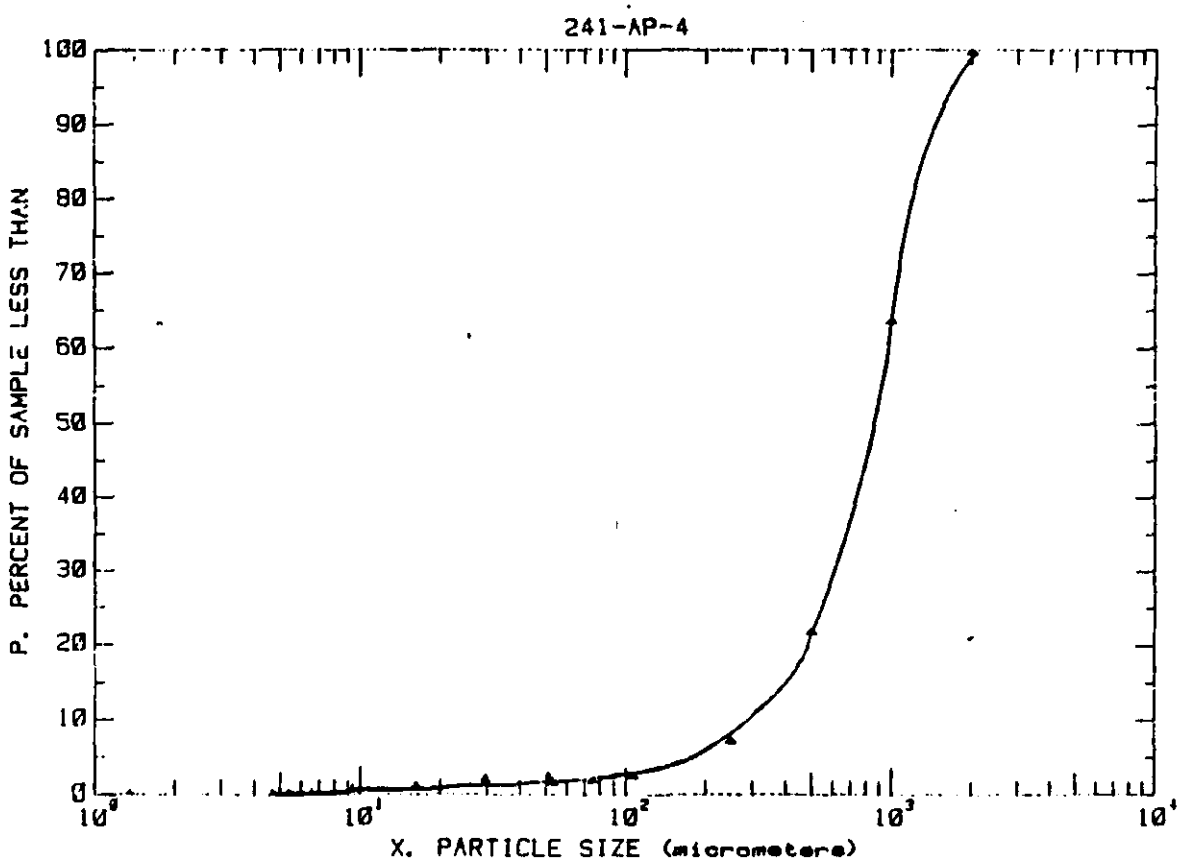
241-AP-4
P. PERCENT OF SAMPLE LESS THAN
X. PARTICLE SIZE (micrometers)

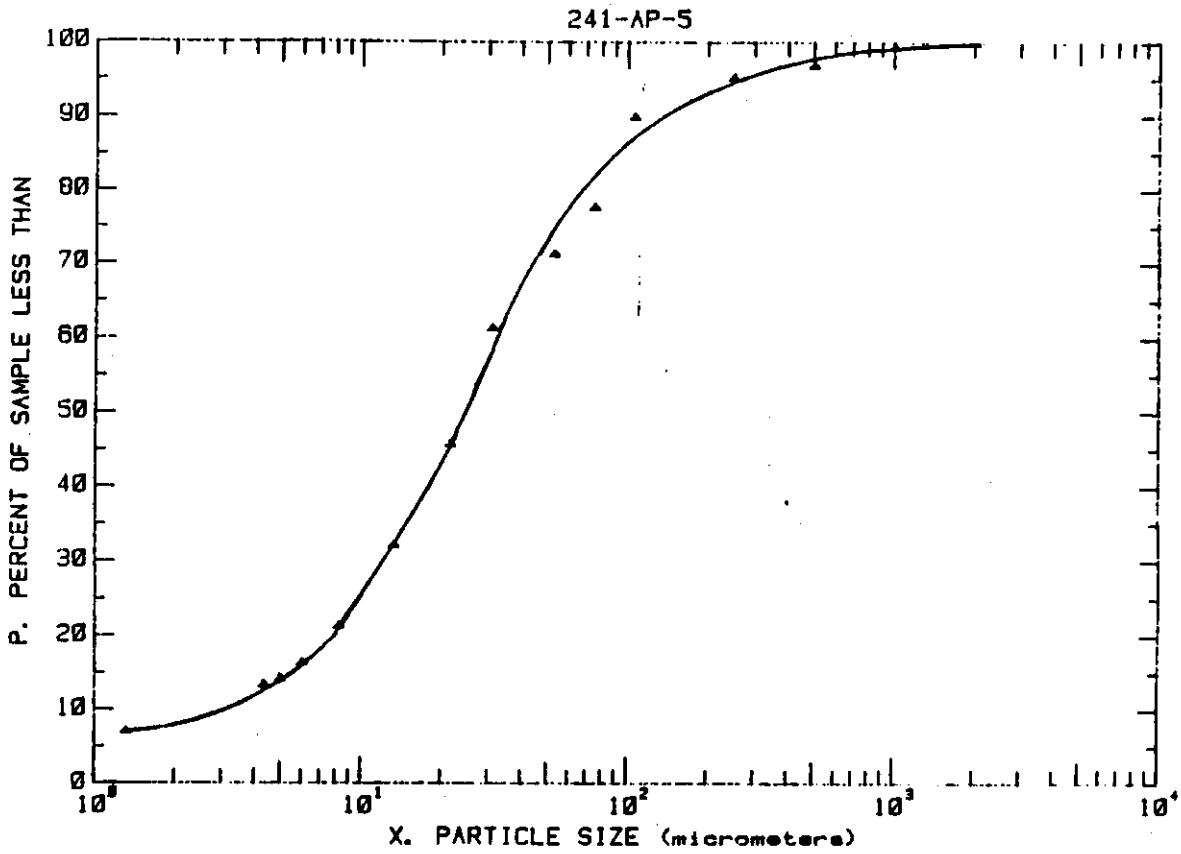
241-AP-5
P. PERCENT OF SAMPLE LESS THAN
100
90
80
70
60
50
40
30
20
10
0
10^0
10^1
10^2
10^3
10^4
X. PARTICLE SIZE (micrometers)

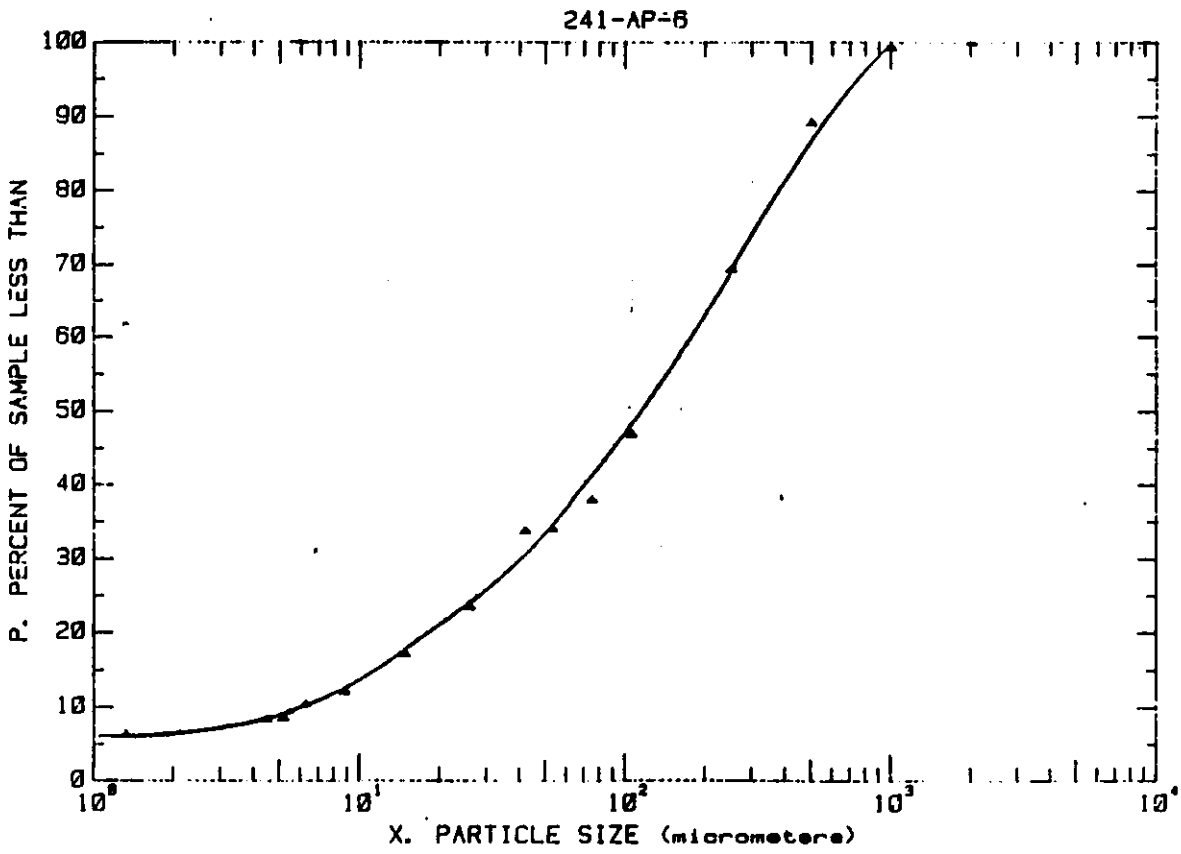
241-AP-6
P. PERCENT OF SAMPLE LESS THAN
100
90
80
70
60
50
40
30
20
10
0
10^0
10^1
10^2
10^3
10^4
X. PARTICLE SIZE (micrometers)

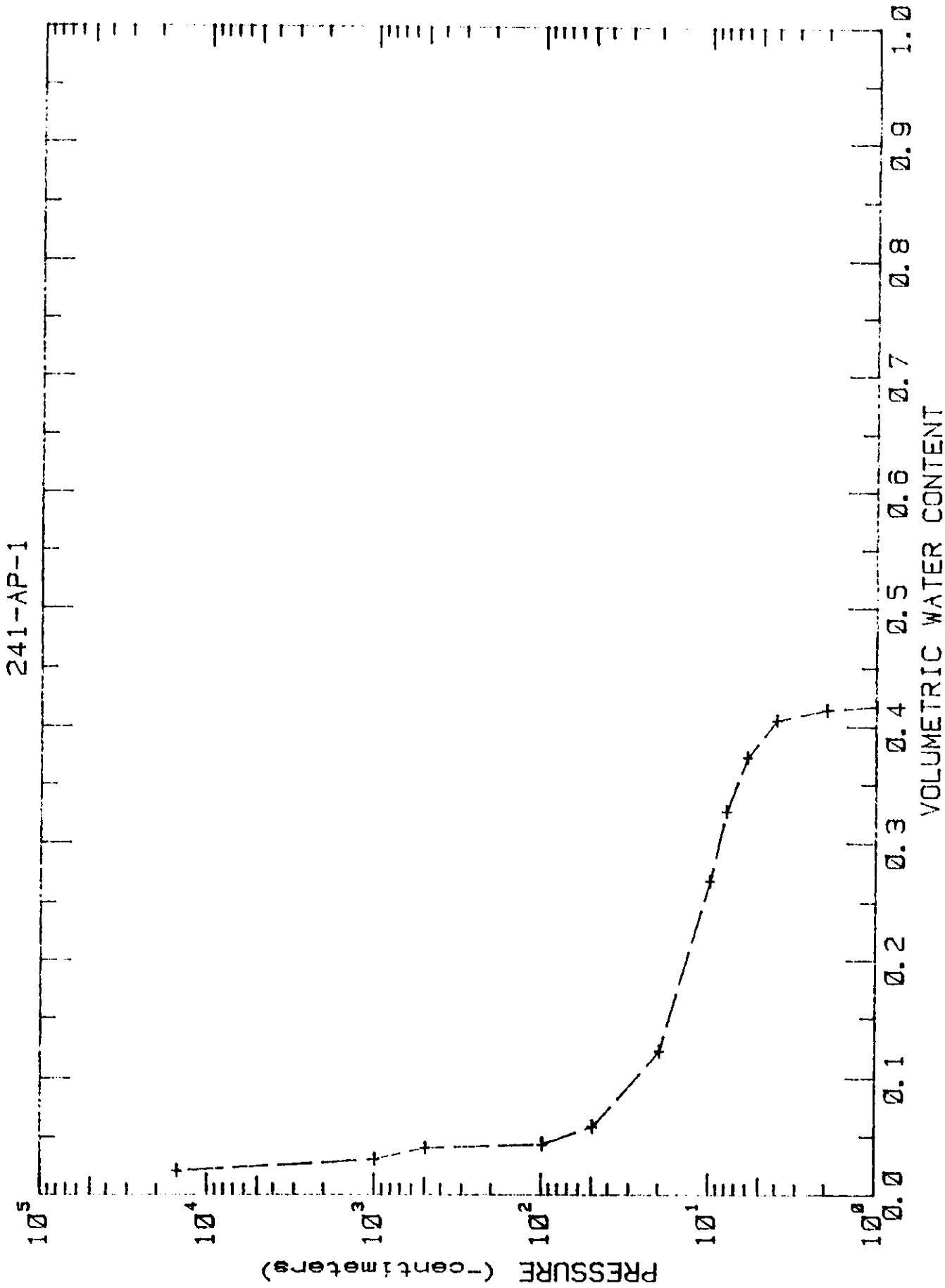
241-AP-1
VOLUMETRIC WATER CONTENT
0.0
0.1
0.2
0.3
0.4
0.5
0.6
0.7
0.8
0.9
1.0
PRESSURE (-centimeters)
10^0
10^1
10^2
10^3
10^4
10^5

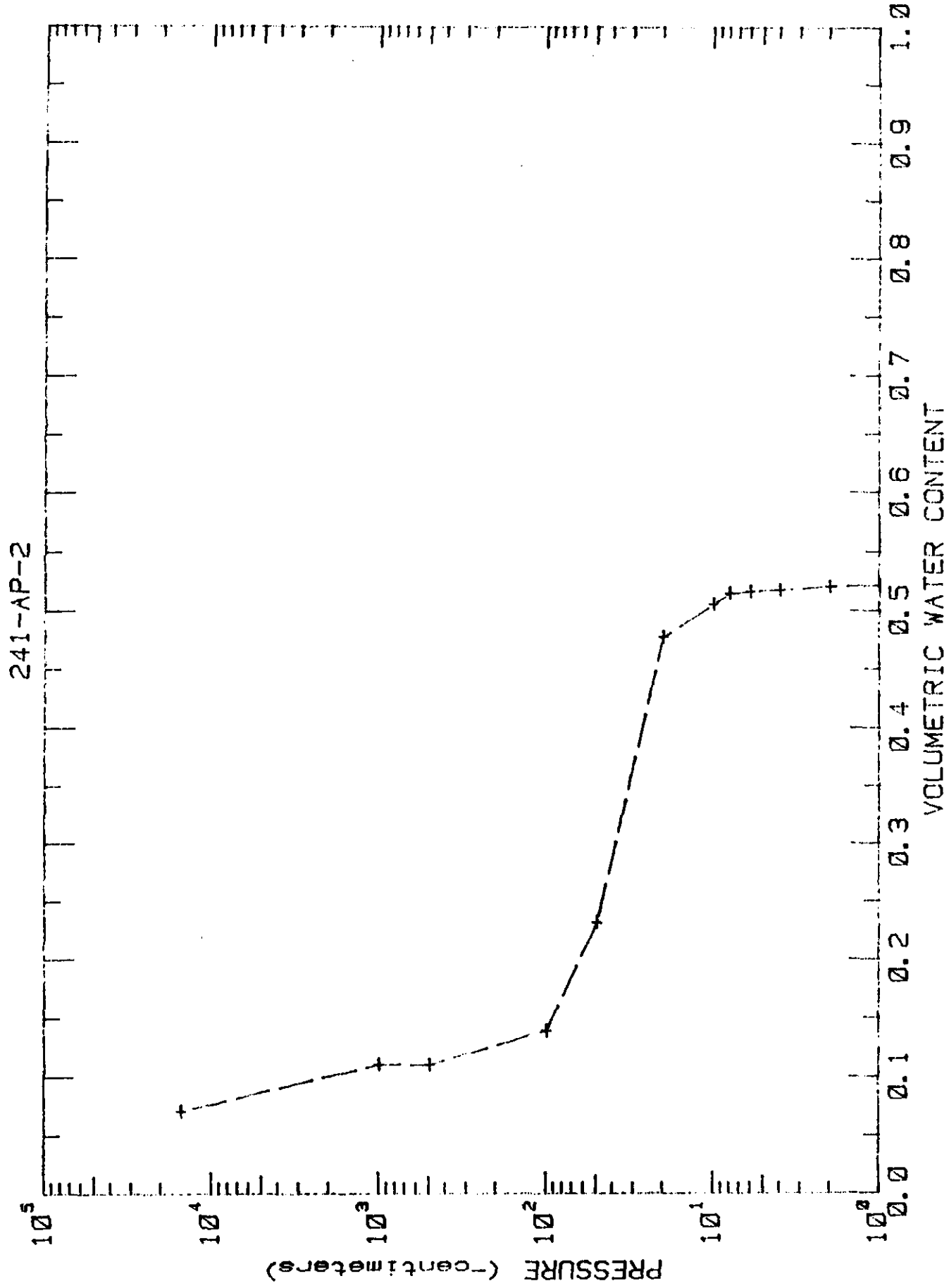
241-AP-2
VOLUMETRIC WATER CONTENT
0.0
0.1
0.2
0.3
0.4
0.5
0.6
0.7
0.8
0.9
1.0
PRESSURE (centimeters)
10^5
10^4
10^3
10^2
10^1
10^0

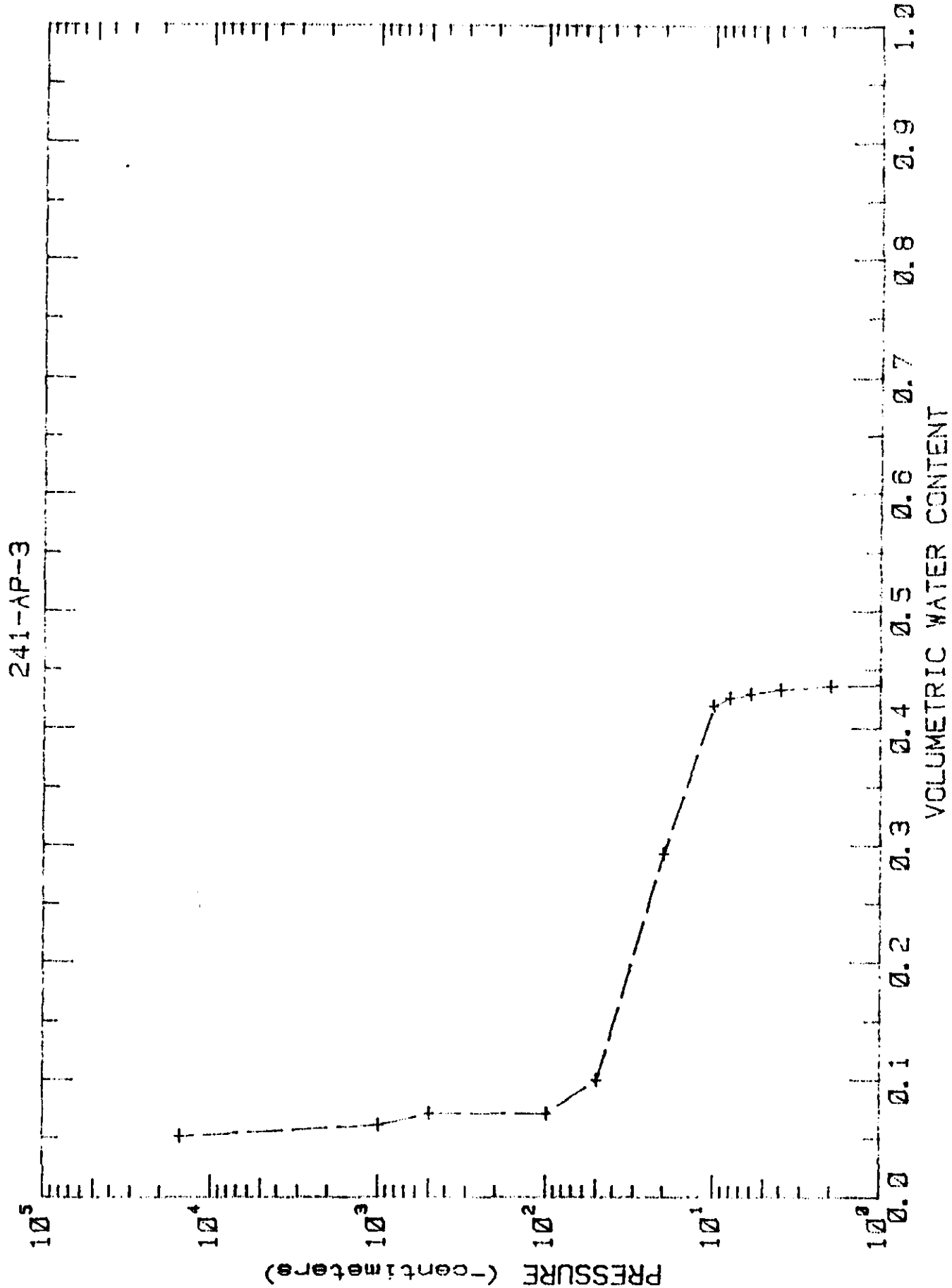
241-AP-3
VOLUMETRIC WATER CONTENT
0.0
0.1
0.2
0.3
0.4
0.5
0.6
0.7
0.8
0.9
1.0
PRESSURE (centimeters)
10^5
10^4
10^3
10^2
10^1
10^0

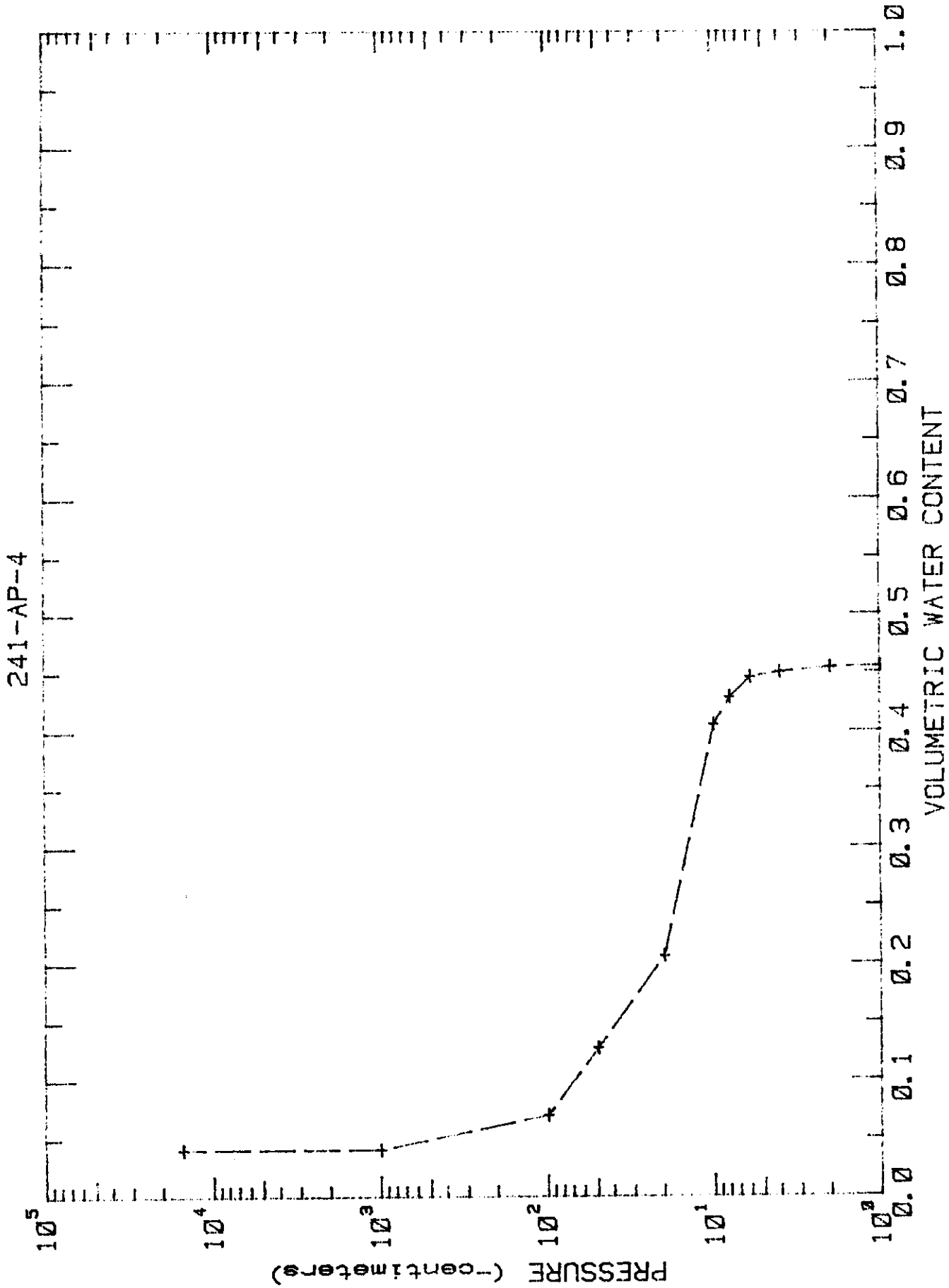
241-AP-4
VOLUMETRIC WATER CONTENT
0.0
0.1
0.2
0.3
0.4
0.5
0.6
0.7
0.8
0.9
1.0
PRESSURE (-centimeters)
10^5
10^4
10^3
10^2
10^1
10^0

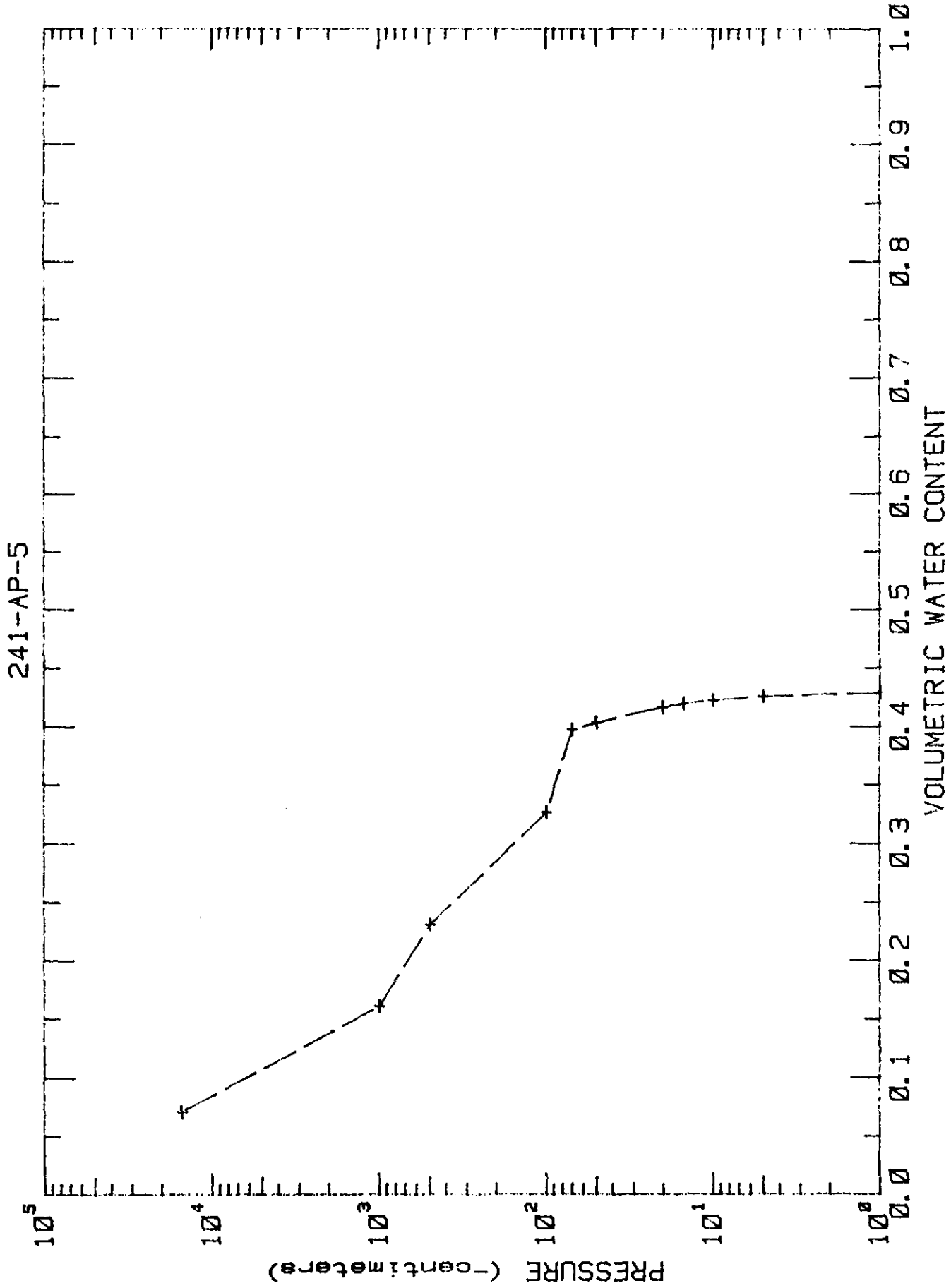
241-AP-5
VOLUMETRIC WATER CONTENT
0.0
0.1
0.2
0.3
0.4
0.5
0.6
0.7
0.8
0.9
1.0
PRESSURE (-centimeters)
10^5
10^4
10^3
10^2
10^1
10^0

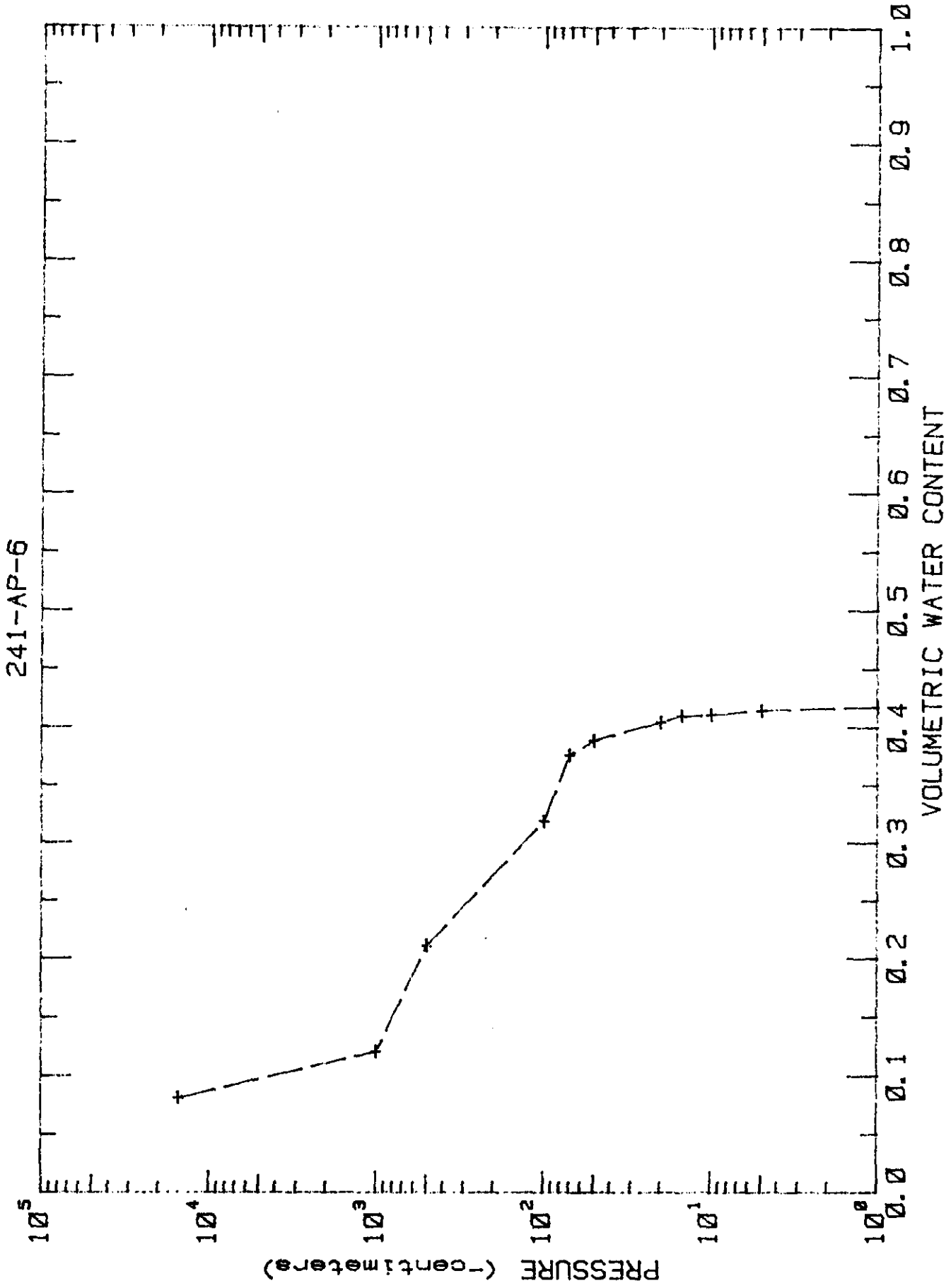
241-AP-6
VOLUMETRIC WATER CONTENT
0.0
0.1
0.2
0.3
0.4
0.5
0.6
0.7
0.8
0.9
1.0
PRESSURE (-centimeters)
10^5
10^4
10^3
10^2
10^1
10^0

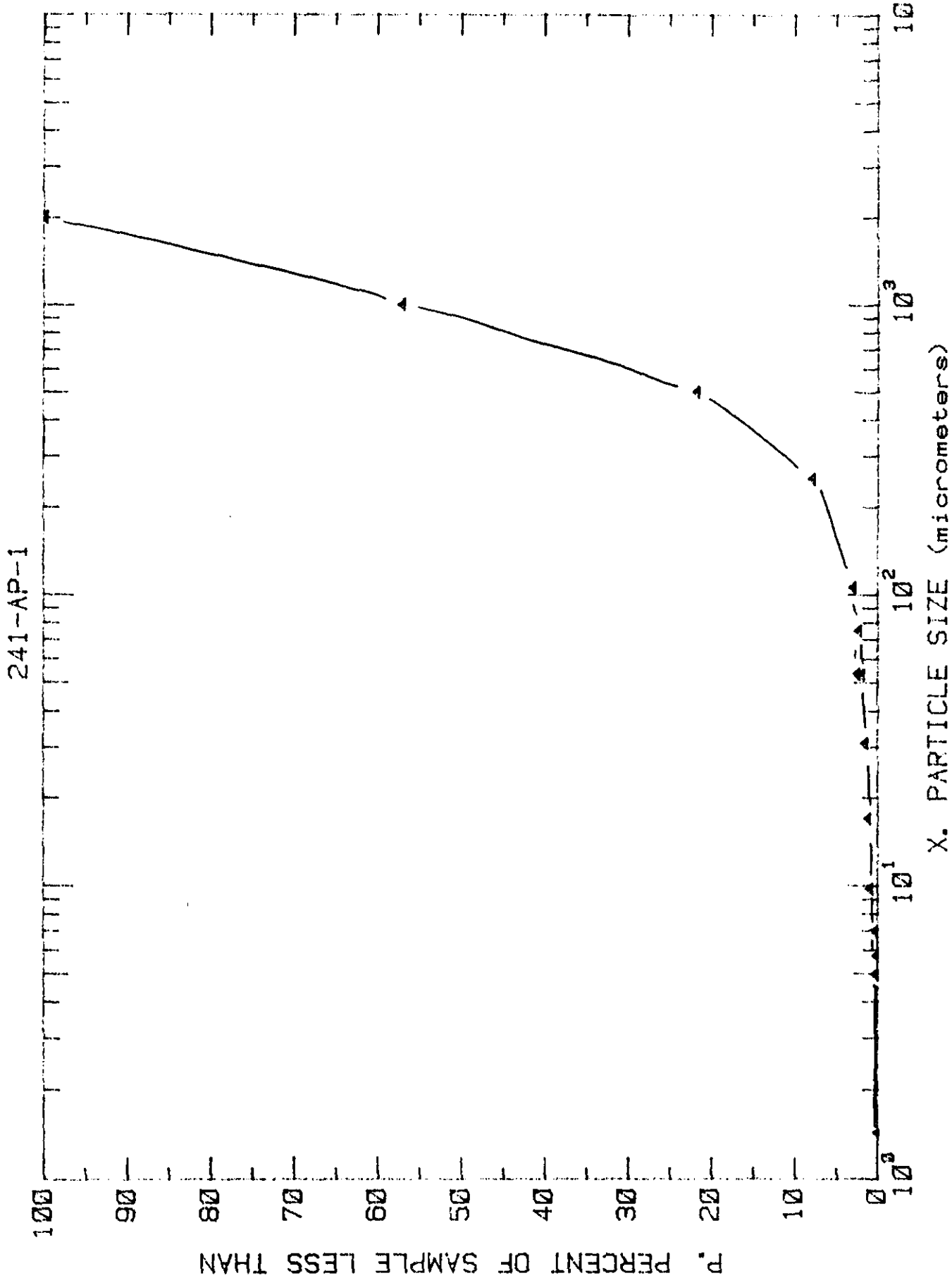
241-AP-1
P, PERCENT OF SAMPLE LESS THAN
100
90
80
70
60
50
40
30
20
10
0
X, PARTICLE SIZE (micrometers)
10^0
10^1
10^2
10^3
10^4

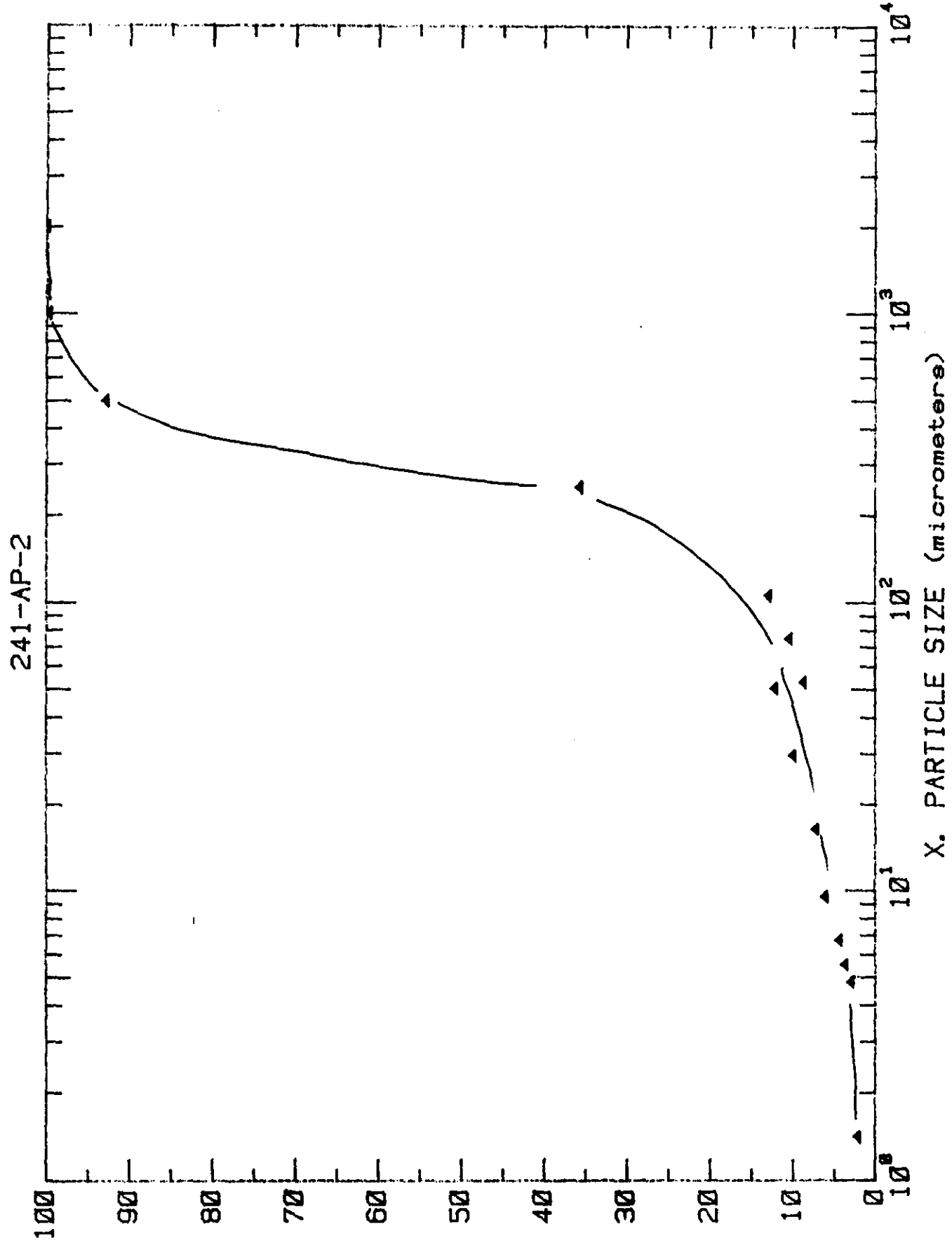
241-AP-2
P, PERCENT OF SAMPLE LESS THAN
100
90
80
70
60
50
40
30
20
10
0
X, PARTICLE SIZE (micrometers)
10^0
10^1
10^2
10^3
10^4

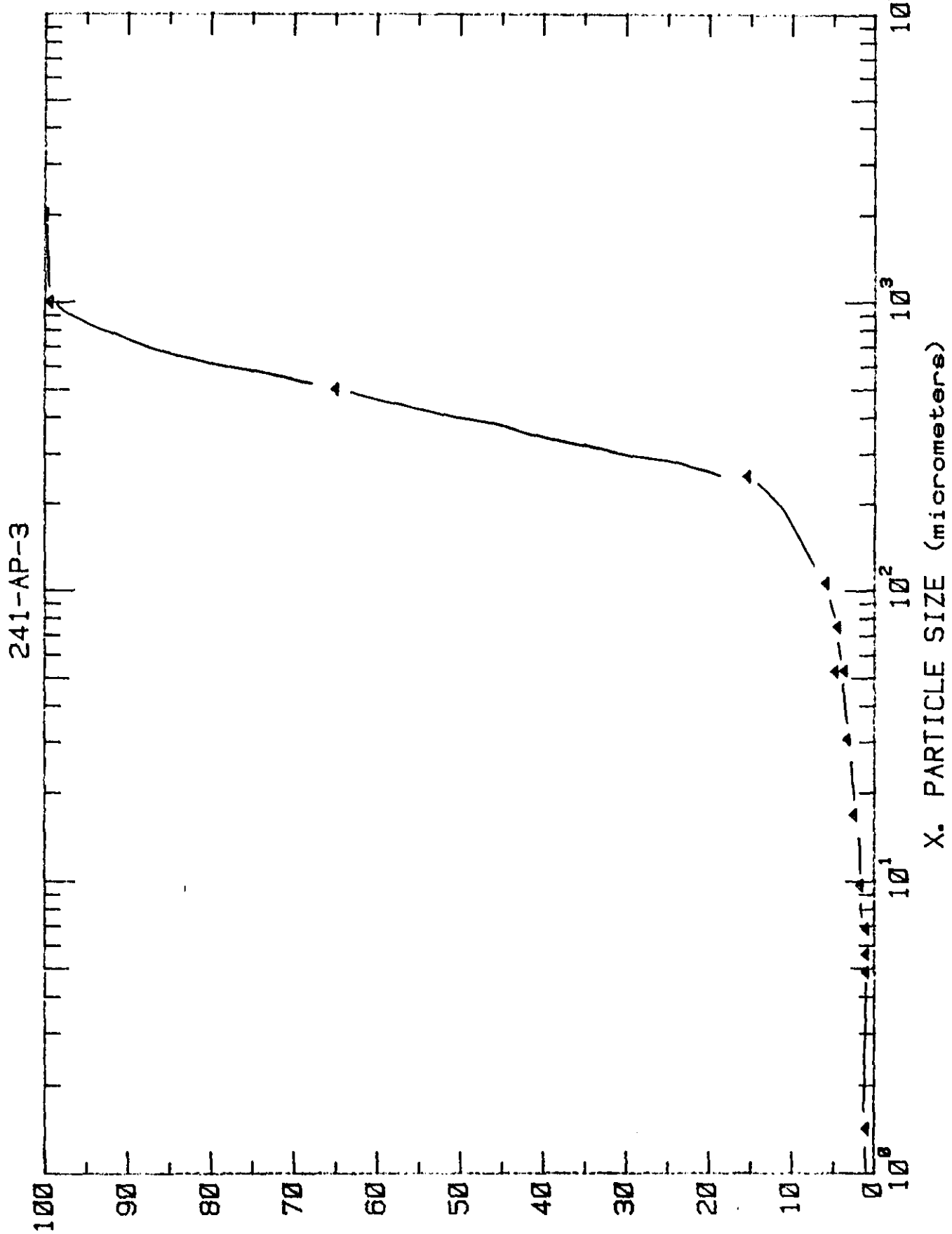
241-AP-3
P, PERCENT OF SAMPLE LESS THAN
100
90
80
70
60
50
40
30
20
10
0
X, PARTICLE SIZE (micrometers)
10^0
10^1
10^2
10^3
10^4

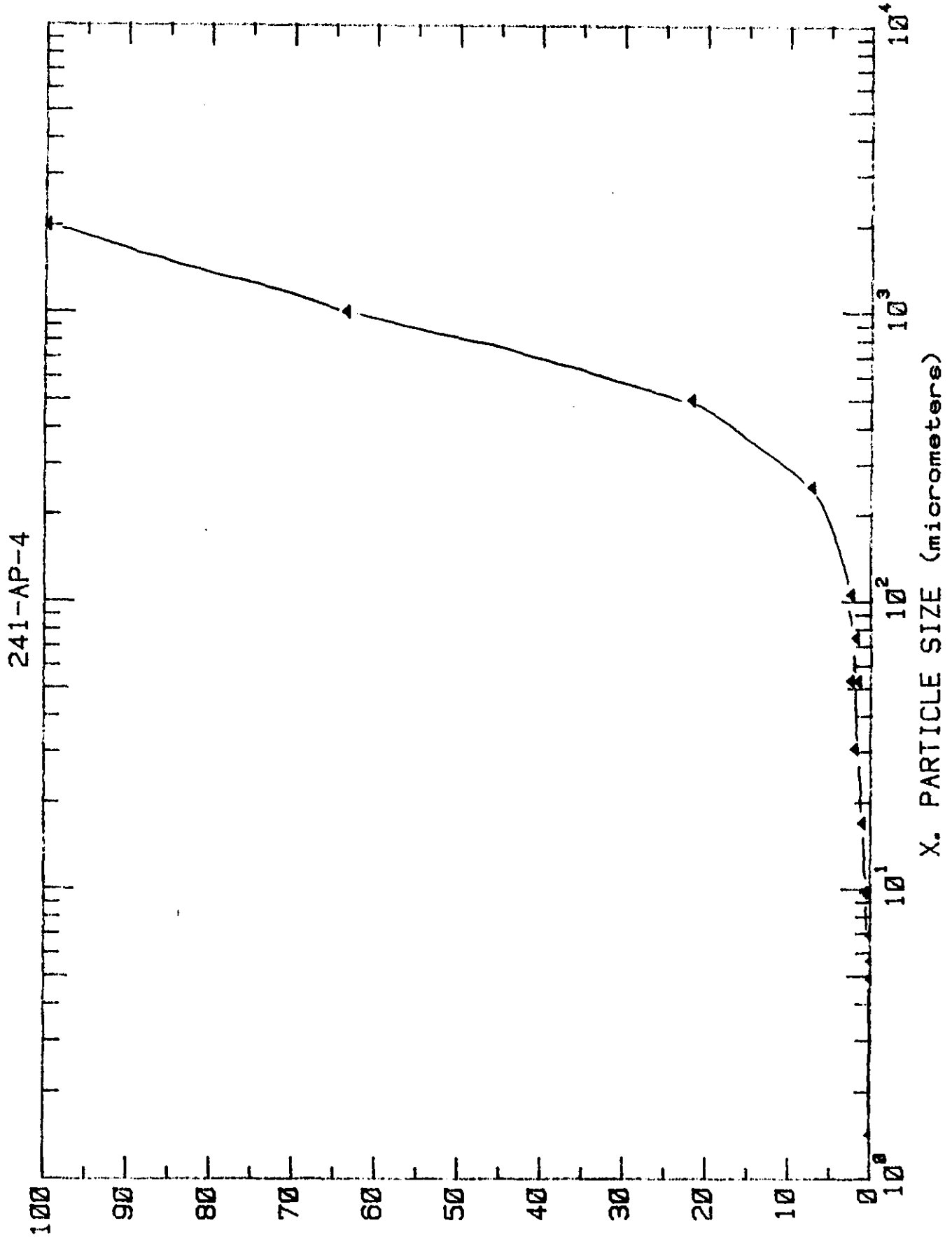
241-AP-4
P, PERCENT OF SAMPLE LESS THAN
100
90
80
70
60
50
40
30
20
10
0
X, PARTICLE SIZE (micrometers)
10^0
10^1
10^2
10^3
10^4

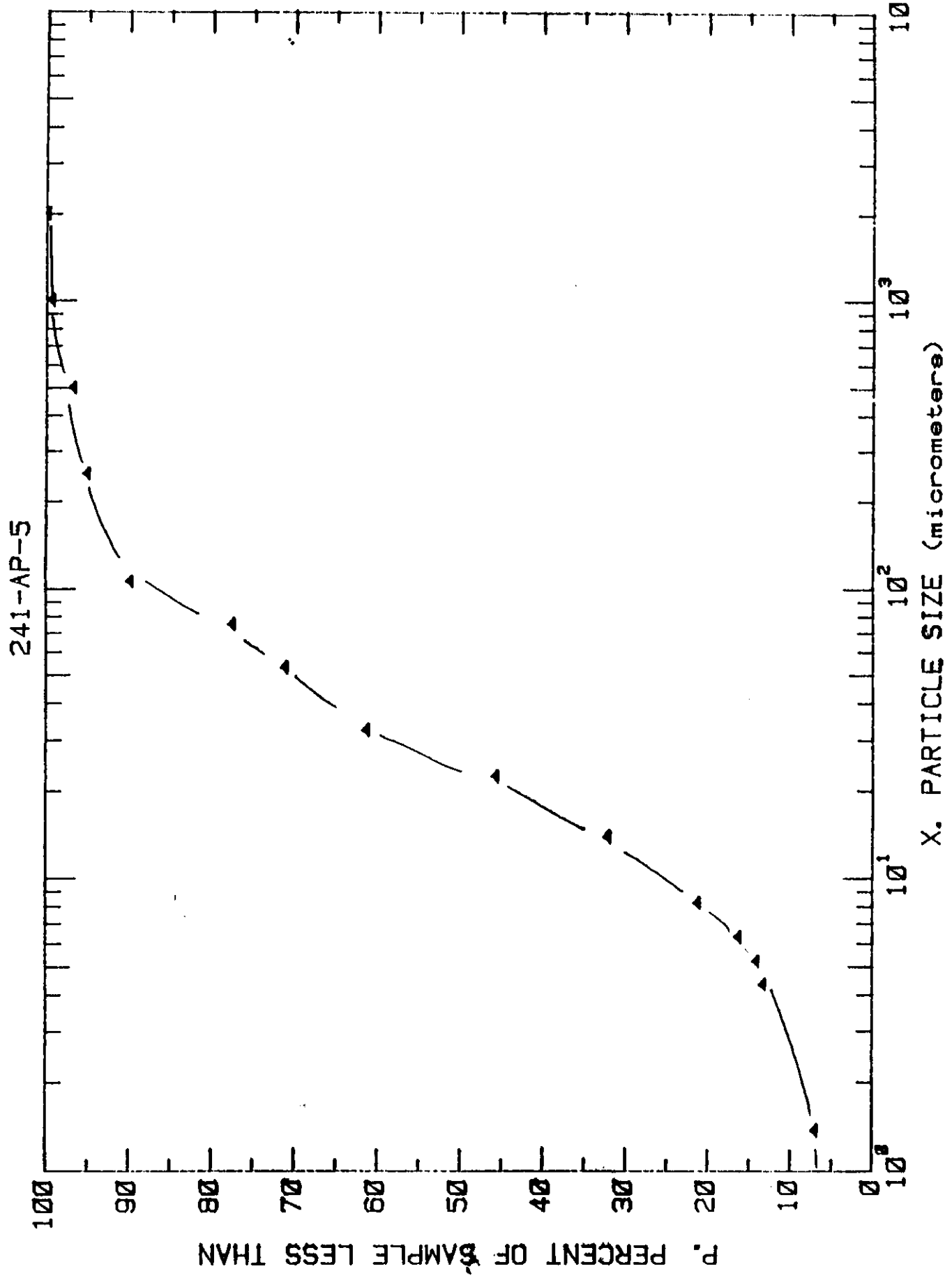
241-AP-5
P, PERCENT OF SAMPLE LESS THAN
100
90
80
70
60
50
40
30
20
10
0
X, PARTICLE SIZE (micrometers)
10^0
10^1
10^2
10^3
10^4

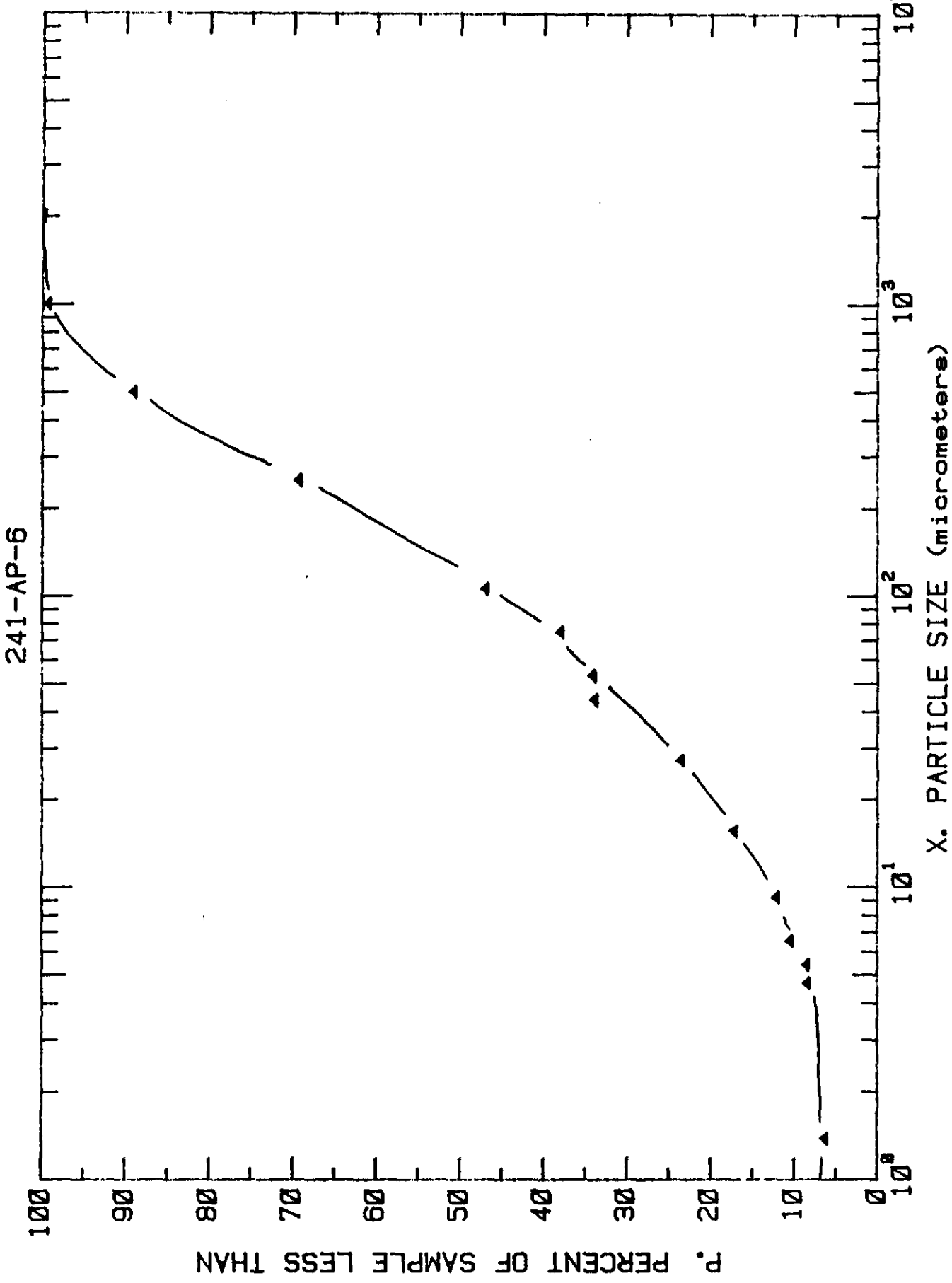
241-AP-6
P. PERCENT OF SAMPLE LESS THAN
100
90
80
70
60
50
40
30
20
10
0
X. PARTICLE SIZE (micrometers)
10^0
10^1
10^2
10^3
10^4

This page intentionally left blank.

APPENDIX C

GROUT SITE SEDIMENT SAMPLE ANALYSES

This page intentionally left blank.

Battelle
Pacific Northwest Laboratories

Project Number 13917

Internal Distribution

Date May 12, 1988

To K. A. Higley

From M. J. Fayer Mike

Subject Grout Site Sediment Sample Analyses

JS Depner
GW Gee
PR Heller
DA Lamar
DH Mitchell
RW Nelson
ML Rockhold
GP Streile
File/LB

Attached are the results of water retention tests conducted on the sediment samples from well E25-234 located within the Grout Site. The data indicate that a large degree of variability exists in the hydraulic properties of the sediments beneath the Grout Site and the variability is evident at the smallest scale of measurement.

Given that a large degree of variability exists at the Grout Site and that time and funding are limited, the best approach for hydraulic property characterization may be two-fold. First, utilize the information available from the large number of wells drilled in the area. The sediments from many of these wells were sampled for particle size distribution. These data can be used to predict water retention properties using methods such as that of Arya and Paris (1981). Although the predictions will be more uncertain than actual measurements, we expect that the larger number of samples will reduce the uncertainty in areal variations. Second, the data from a few well-placed wells from which undisturbed samples are removed for detailed analyses can serve as a check on the other wells.

Based on questions which arose during the laboratory analyses, we recommend that a consensus be reached by the end users of these data as to the level of detail that they require. In addition, we recommend that the field sampling and laboratory procedures be revised for any future testing to allow for the test results to be more closely correlated. This revision will depend partly on the nature of the consensus reached.

GROUT SITE SEDIMENT SAMPLE ANALYSES

by M. J. Fayer, M. L. Rockhold, and P. R. Heller

This report outlines the general procedures and results of water retention analyses performed on undisturbed sediment samples from Grout Well No. 299-E25-234, Coordinates N 40547.2, W 45618.5. The report also includes hydraulic conductivity predictions for the sediments based on the van Genuchten (1978) and Mualem (1976) models. For details on well location, sampling procedure, and previous testing, consult the memo from M. Fayer to D. Lamar dated 1 March 1988.

SAMPLING PROCEDURE

Two types of samples were required for water retention testing. The first type was an undisturbed core for hanging water column experiments. The second type was disturbed sample material for pressure-plate and vapor equilibrium tests. The procedures for all tests can be found in Klute (1986) and the CX-1 Operator's Manual (1987).

The undisturbed cores were obtained by coring the upper surface of the saturated conductivity core with a bulk density sampler. This sampler allowed for the removal of two cores, one vertically below the other, separated by 1 cm of soil. The volume of these small cores was 67.8 cm^3 which represents about 2.6% of the volume of the conductivity core. The conductivity cores from two depths (126' and 133'10") contained too much gravel to allow subsampling. Therefore, these cores were broken apart, mixed, and repacked in small cylinders with a volume of 150.5 cm^3. Each small core was then used in a hanging water column experiment. After the test, the water content and bulk density of each core were determined. This test covered the matric potential range from 5 to 150 cm (0.0005 to 0.015 MPa).

The disturbed samples for the pressure-plate tests came from material located near the conductivity core when the conductivity core was cut from the original sample. The pressure-plate samples were packed in rings to a bulk density of 1.6 g/cm^3 before testing. Two repetitions of this test were conducted at matric potentials of 510, 1020, and 3060 cm (0.05, 0.1, and 0.3 MPa). The values reported in Table 1 are averages of three replicates (there was little variation among replicates).

The disturbed samples for the vapor equilibrium tests came from the upper end of the conductivity core after the test was completed. Because vapor adsorption is relatively independent of bulk density, no attempt was made to pack these samples to a specific density. The gravimetric water contents from this test were converted to volumetric values using the average bulk density from the hanging water column cores. The vapor adsorption test covers the matric potential range above 1.5 MPa.

CURVE FITTING PROCEDURE

Water retention data are usually fitted with a continuous function because 1) functions are more efficient to use in model simulations than are tabular values and 2) functions can be easily used to predict unsaturated hydraulic conductivity. For the samples reported here, the van Genuchten

retention function (van Genuchten 1978) was fit the the retention data. The function is

$$\theta = \theta_r + (\theta_s-\theta_r)\ [1+(\alpha h)^n]^{-m}$$

where θ is water content, θ_s is saturated water content, θ_r is residual water content, and α, n, and m are curve fitting parameters, with the restriction that m=1-1/n. When fitting the retention function for each depth, θ_s, α, and n were fitted while θ_r was fixed at the lowest measured value. For describing unsaturated conductivity, the van Genuchten retention function yields

$$K = K_s \frac{\{1-(\alpha h)^{n-1}[1+(\alpha h)^n]^{-m}\}^2}{[1+(\alpha h)^n]^{m/2}}$$

using the Mualem conductivity model (Mualem 1976).

DISCUSSION

The results of all three experiments are reported in Table 1. The van Genuchten function was fit to all of the retention data listed in Table 1 for each depth and the resulting curve-fitting parameters are listed in Table 2. Both the measured retention data and the van Genuchten functions are displayed for all depths in Figures 1-14. The results indicate that the data were collected at a sufficient number of matric potential values to cover the range of water content. Of the three tests, the hanging water column test took the longest amount of time (about 2 months) to complete. This time could be reduced by decreasing the number of matric potential values at which the test is conducted.

Judging from the figures, nine of the depths exhibited well-behaved retention properties, where well-behaved means that the two hanging water column tests gave similar results and the data from all three tests (hanging water column, pressure plate, and vapor adsorption) were consistent. In contrast, four depths (19'4", 25'9", 69'8", and 117'6") exhibited a large degree of variability. For one of those depths (25'9"), a second set of hanging water column tests was conducted to see if the first set was an anomaly. The results, included in Table 1, indicate that a significant variation in properties exists within sample 25'9" over a distance of 4 cm. Although the data for all four tests are used in Figure 3 to represent sample 25'9", the hanging water column samples could be divided into two separate and distinct sediment types (a-b' and a'-b). To illustate this point, we had Samples a' and b' analyzed for particle size using the wet seiving technique and the results are listed in Table 3. Both samples contain at least 90% sand and would thus be classified as sands. Using classification alone would lead to the conclusion that these samples were identical. However, the samples are different in their distribution of sand sizes. By weight, 52% of Sample a' passed through the 250μ-diameter sieve versus only 18% of Sample b'. Sample a' also has 10% silt and clay versus only 3% for Sample b'. These differences in particle size distribution are sufficient to yield different retention properties for the two samples.

The water retention curves for all depths are plotted in Figure 15. A discernible grouping of depths is not apparent and the range of variation is large. At a matric potential of -100 cm, the water content varies from 0.07 to 0.32 cm^3/cm^3. Of the curve-fitting parameters in Table 2, θ_r and n show some consistency among depths while θ_s, α, and K_{ls} vary considerably with no apparent correlation.

The predicted conductivity functions for every depth are displayed in Figure 16 and there are obvious differences. In general, the values of conductivity range over 3 orders-of-magnitude (OM) near the wet end and more than 10 OM near the dry end. Keep in mind that the conductivity functions were generated using a single matching point, the saturated conductivity. Partly for that reason, as the dry end is approached, the predicted conductivity values have greater uncertainty.

A discrepancy was observed between conductivity-core and hanging-water-column-core bulk densities. Table 4 contains both values for all depths. Note that the mean bulk density value of the conductivity core is 0.15 g/cm^3, or 10%, greater than the hanging water column cores. The difference is either the result of the subsampling technique or the indirect method used to calculate the bulk density of the conductivity core. In the future, the indirect method can be replaced by direct measurement, thus eliminating this possible source of error.

The original undisturbed cores were subsampled to provide material to conduct the tests reported here. As noted in the previous memo, "The lined cores did not allow for visual examination. Thus, lenses and stratifications noted in the drillers log could not be observed in the samples, even though those features may have been there. One of the consequences of this lack of observation is that the tests conducted on subsamples of the core are being used to represent the entire core." Based on the laboratory results, heterogeneity on the scale of the conductivity cores evidently exists. This observation leads to the general question of what is the correct scale of measurement. The pressure-plate and particle and bulk density tests were conducted on independent subsamples of the original core. The hanging water column and vapor adsorption tests were conducted with material from within the conductivity cores, but the volume of material used represented only 5% or less of the conductivity core volume.

One potential solution is to choose some measurement scale, such as the conductivity core, as the minimum scale of characterization. Take the core, determine its conductivity, water content, and bulk density, then homogenize the material in the core. Using the resulting mix, repack the core to the original density, determine its conductivity and water content, then sample the mixture for the remaining tests. A second potential solution is to use plastic liners during the drilling operation. Layering and stratifications in the sample could be observed and recorded. Each distinct layer could then be treated as described in the previous solution.

Given that a large degree of variability exists at the Grout Site and that time and funding are limited, the best approach for hydraulic property characterization may be two-fold. First, utilize the information available from the large number of wells drilled in the area. The sediments from many of these wells were sampled for particle size distribution. These data can

be used to predict water retention properties using methods such as that of Arya and Paris (1981). Although the predictions will be more uncertain than actual measurements, we expect that the larger number of samples will reduce the uncertainty in areal variations. Second, the data from a few well-placed wells from which undisturbed samples are removed for detailed analyses can serve as a check on the other wells.

Table 1. Water Retention Data. Water contents reported at 0.1 cm are the saturated values calculated from the respective bulk and particle densities, between 5 and 150 cm from hanging water columns, 510 to 3060 from pressure plates, and above 3060 cm from vapor adsorption.

Matric Potential (-cm)	Water Content (cm^3/cm^3)		Matric Potential (-cm)	Water Content (cm^3/cm^3)	
	Sample 5'6"			Sample 19'6"	
	(a)	(b)		(a)	(b)
0.1	0.427	0.380	0.1	0.478	0.510
5	0.345	0.330	5	0.399	0.329
10	0.319	0.313	10	0.372	0.302
15	0.305	0.306	15	0.348	0.278
20	0.290	0.296	20	0.331	0.260
30	0.264	0.284	30	0.266	0.196
40	0.246	0.279	40	0.215	0.144
50	0.238	0.270	50	0.207	0.136
70	0.215	0.254	70	0.187	0.116
100	0.201	0.227	100	0.173	0.102
150	0.191	0.212	150	0.168	0.097
510	0.096		510	0.232	
1020	0.080		1020	0.201	
3060	0.064		3060	0.138	
14.9 MPa	0.061		8.3 MPa	0.070	
234.3 MPa	0.025		231.6 MPa	0.022	

	Sample 25'9"				Sample 29'	
	(a)	(b)	(a')	(b')	(a)	(b)
0.1	0.498	0.519	0.509	0.520	0.436	0.445
5	0.380	0.551	0.499	0.404	0.366	0.406
10	0.372	0.539	0.481	0.397	0.343	0.379
15	0.370	0.535	0.472	0.387	0.327	0.359
20	0.358	0.519	0.463	0.376	0.309	0.348
30	0.306	0.427	0.445	0.253	0.288	0.335
40	0.209	0.392	0.417	0.209	0.270	0.307
50	0.176	0.361	0.389	0.193	0.254	0.296
70	0.146	0.321	0.347	0.179	0.238	0.271
100	0.129	0.307	0.343	0.158	0.231	0.263
150	0.116	0.256	0.343	0.157	0.221	0.256
510	0.205				0.176	
1020	0.163				0.156	
3060	0.116				0.110	
7.8 MPa	0.081				0.056	
225.2 MPa	0.028				0.023	

Table 1. (contd)

Matric Potential (-cm)	Water Content (cm^3/cm^3)		Matric Potential (-cm)	Water Content (cm^3/cm^3)		Matric Potential (-cm)	Water Content (cm^3/cm^3)	
	Sample 37'3"			Sample 46'4"			Sample 54'9"	
	(a)	(b)		(a)	(b)		(a)	(b)
0.1	0.518	0.513	0.1	0.465	0.400	0.1	0.452	0.470
5	0.466	0.500	5	0.316	0.325	5	0.363	0.352
10	0.457	0.483	10	0.296	0.312	10	0.351	0.336
15	0.457	0.477	15	0.279	0.308	15	0.338	0.327
20	0.442	0.451	20	0.251	0.294	20	0.316	0.314
30	0.393	0.321	30	0.202	0.249	30	0.233	0.248
40	0.363	0.349	40	0.180	0.226	40	0.199	0.208
50	0.335	0.349	50	0.172	0.214	50	0.164	0.198
70	0.335	0.298	70	0.162	0.203	70	0.160	0.163
100	0.321	0.298	100	0.150	0.185	100	0.159	0.124
150	0.285	0.286	150	0.102	0.165	150	0.136	0.110
510	0.204		510	0.050		510	0.139	
1020	0.188		1020	0.045		1020	0.104	
3060	0.174		3060	0.030		3060	0.063	
15.1 MPa	0.125		5.8 MPa	0.023		5.0 MPa	0.031	
227.0 MPa	0.060		241.4 MPa	0.008		243.7 MPa	0.009	
	Sample 69'8"			Sample 83'11"			Sample 99'9"	
	(a)	(b)		(a)	(b)		(a)	(b)
0.1	0.374	0.404	0.1	0.397	0.384	0.1	0.366	0.375
5	0.293	0.293	5	0.279	0.309	5	0.255	0.274
10	0.251	0.265	10	0.271	0.285	10	0.230	0.262
15	0.225	0.178	15	0.242	0.271	15	0.202	0.226
20	0.210	0.146	20	0.217	0.255	20	0.175	0.188
30	0.199	0.122	30	0.195	0.223	30	0.157	0.159
40	0.190	0.109	40	0.178	0.201	40	0.147	0.146
50	0.185	0.101	50	0.165	0.184	50	0.141	0.140
70	0.176	0.093	70	0.149	0.162	70	0.132	0.128
100	0.169	0.085	100	0.142	0.144	100	0.126	0.123
150	0.159	0.078	150	0.128	0.124	150	0.118	0.114
510	0.069		510	0.067		510	0.091	
1020	0.056		1020	0.053		1020	0.068	
3060	0.042		3060	0.032		3060	0.051	
23.4 MPa	0.022		9.3 MPa	0.021		6.6 MPa	0.021	
229.2 MPa	0.010		238.2 MPa	0.007		239.0 MPa	0.007	

Table 1. (contd)

Matric Potential (-cm)	Water Content (cm^3/cm^3)		Matric Potential (-cm)	Water Content (cm^3/cm^3)	
	Sample 110'7"			Sample 117'6"	
	(a)	(b)		(a)	(b)
0.1	0.430	0.420	0.1	0.456	0.413
5	0.316	0.310	5	0.385	0.373
10	0.263	0.269	10	0.354	0.364
15	0.184	0.166	15	0.321	0.354
20	0.141	0.136	20	0.266	0.339
30	0.113	0.116	30	0.185	0.321
40	0.097	0.102	40	0.152	0.299
50	0.088	0.096	50	0.143	0.284
70	0.084	0.081	70	0.137	0.254
100	0.076	0.079	100	0.129	0.243
150	0.074	0.072	150	0.105	0.236
510	0.076		510	0.078	
1020	0.055		1020	0.058	
3060	0.042		3060	0.042	
5.8 MPa	0.026		25.5 MPa	0.014	
219.7 MPa	0.007		214.0 MPa	0.007	
	Sample 126'			Sample 133'10"	
	(a)	(b)		(a)	(b)
0.1	0.354	0.369	0.1	0.280	0.282
5	0.226	0.257	5	0.244	0.252
10	0.166	0.188	10	0.254	0.252
15	0.137	0.150	15	0.257	0.249
20	0.118	0.132	20	0.257	0.242
30	0.114	0.118	30	0.246	0.230
40	0.106	0.109	40	0.237	0.219
50	0.099	0.104	50	0.234	0.213
70	0.097	0.099	70	0.222	0.201
100	0.096	0.092	100	0.203	0.189
150	0.087	0.083	150	0.196	0.178
510	0.073		510	0.155	
1020	0.064		1020	0.103	
3060	0.042		3060	0.064	
35.9 MPa	0.017		32.3 MPa	0.024	
220.6 MPa	0.008		193.5 MPa	0.011	

Table 2. Parameters for the van Genuchten Model Fit to Retention Data from Sediments from the Grout Well. K_{ls} is the conductivity reported in the previous memo, where the subscript ls indicates that the sample was laboratory-saturated but not necessarily fully saturated.

Sample	θ_s m3/m3	θ_r m3/m3	α 1/cm	n	K_{ls} cm/s
5'	0.38063	0.025	0.08632	1.31349	5.73×10^{-4}
19'6"	0.49929	0.022	0.54741	1.28139	8.88×10^{-4}
25'9"	0.51122	0.028	0.07607	1.38880	1.80×10^{-3}
29'	0.43473	0.023	0.15208	1.22993	2.41×10^{-5}
37'3"	0.52244	0.060	0.09123	1.28327	5.77×10^{-4}
46'4"	0.41833	0.008	0.17633	1.36246	2.99×10^{-4}
54'9"	0.45302	0.009	0.15633	1.39591	1.38×10^{-5}
69'8"	0.39198	0.010	0.39456	1.34559	1.21×10^{-3}
83'11"	0.38273	0.007	0.20954	1.34125	1.78×10^{-4}
99'9"	0.37234	0.007	0.48677	1.29968	2.24×10^{-4}
110'7"	0.42861	0.007	0.25119	1.60079	2.82×10^{-4}
117'6"	0.43028	0.007	0.10074	1.40147	3.64×10^{-3}
126'	0.36614	0.008	0.85217	1.34293	1.98×10^{-3}
133'10"	0.26327	0.011	0.01954	1.31828	2.76×10^{-5}

Table 3. Bulk Density Information

Sample	Bulk Density (g/cm^3)	
	Water Retention Cores	Conductivity Cores
5'6"	1.62, 1.75	1.79
19'6"	1.45, 1.36	1.61
25'9"	1.36, 1.31, 1.34, 1.31	1.43
29'	1.53, 1.50	1.83
37'3"	1.27, 1.29	1.38
46'4"	1.44, 1.61	1.72
54'9"	1.47, 1.42	1.66
69'8"	1.70, 1.62	1.82
83'11"	1.65, 1.68	1.80
99'9"	1.71, 1.69	1.84
110'7"	1.55, 1.58	1.89
117'6"	1.47, 1.59	1.44
126'	1.80, 1.76	1.82
133'10"	1.97, 1.96	2.03
Mean Value[a] =	1.53	1.68

(a) Water retention cores for the depths 126' and 133'10" were packed in the laboratory and were therefore not included in the calculation of the mean bulk density.

Table 4. Particle Size Analysis of Sample 25'9" by Wet Sieving. Material Less Than 50μ is Classified as Silt and Clay.

Sieve Number	Sieve Opening (u)	Material Passing Sieve (%)	
		Sample a	Sample b
10	2000	100	100
18	1000	100	100
35	500	92	88
60	250	52	18
140	106	21	4
200	75	14	4
270	53	10	3

REFERENCES

Arya, L. M. and J. J. Paris. 1981. "A Physicoempirical Model to Predict the Soil Moisture Characteristic from Particle-Size Distribution and Bulk Density Data." Soil Sci. Soc. Amer. J. 45(6):1023-1030.

Klute, A. 1986. "Water Retention: Laboratory Methods." In Methods of Soil Analysis, Part 1, ed. A. Klute, pp. 635-662, American Society of Agronomy, Madison, Wisconsin.

Operator's Manual for the CX-1. 1987. Decagon Devices, Inc., P. O. Box 835, Pullman, Washington, 99163.

Mualem, Y. 1976. "A New Model for Predicting the Hydraulic Conductivity of Unsaturated Porous Media." Water Resour. Res. 12(3):513-522.

van Genuchten, R. 1978. "Calculating the Unsaturated Hydraulic Conductivity with a New Closed-Form Analytical Model." Water Resour. Prog., Dept. of Civil Eng., Princeton Univ., Princeton, New Jersey.

Figure 1.

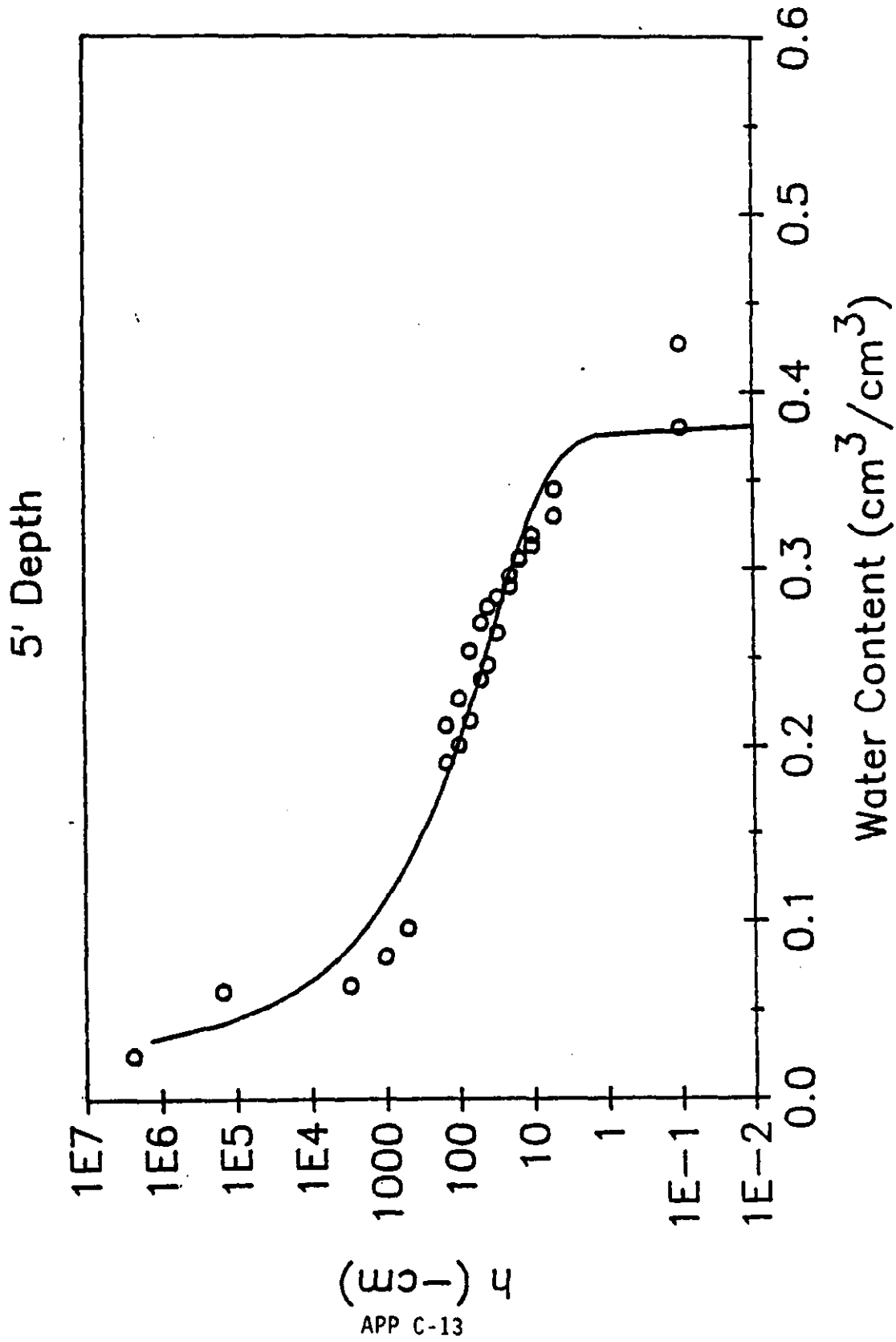
5' Depth
h (-cm)
1E7
1E6
1E5
1E4
1000
100
10
1
1E-1
1E-2
0.0
0.1
0.2
0.3
0.4
0.5
0.6
Water Content (cm3/cm3)

Figure 2.

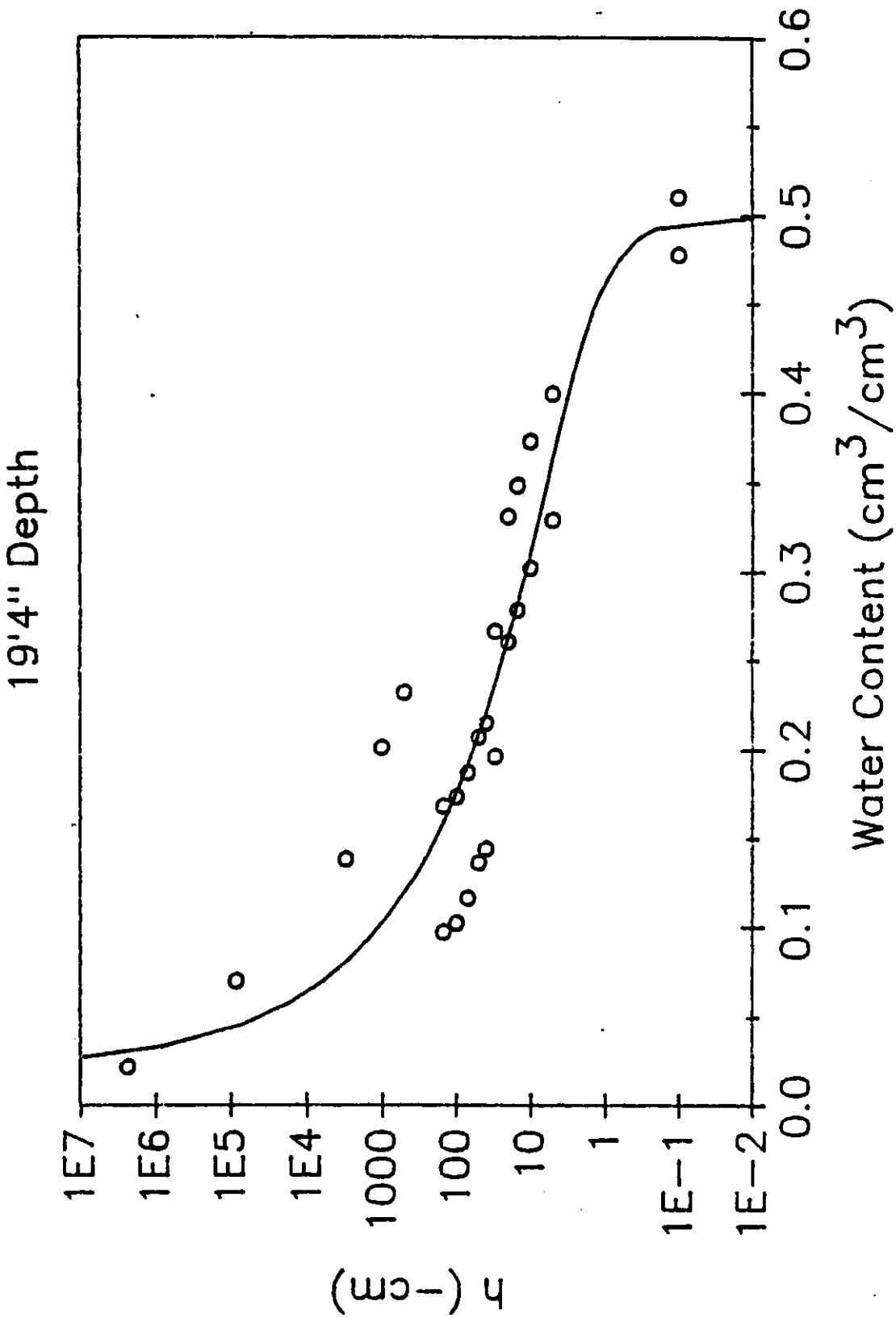
19'4" Depth
h (-cm)
1E7
1E6
1E5
1E4
1000
100
10
1
1E-1
1E-2
0.0
0.1
0.2
0.3
0.4
0.5
0.6
Water Content (cm3/cm3)

Figure 3.

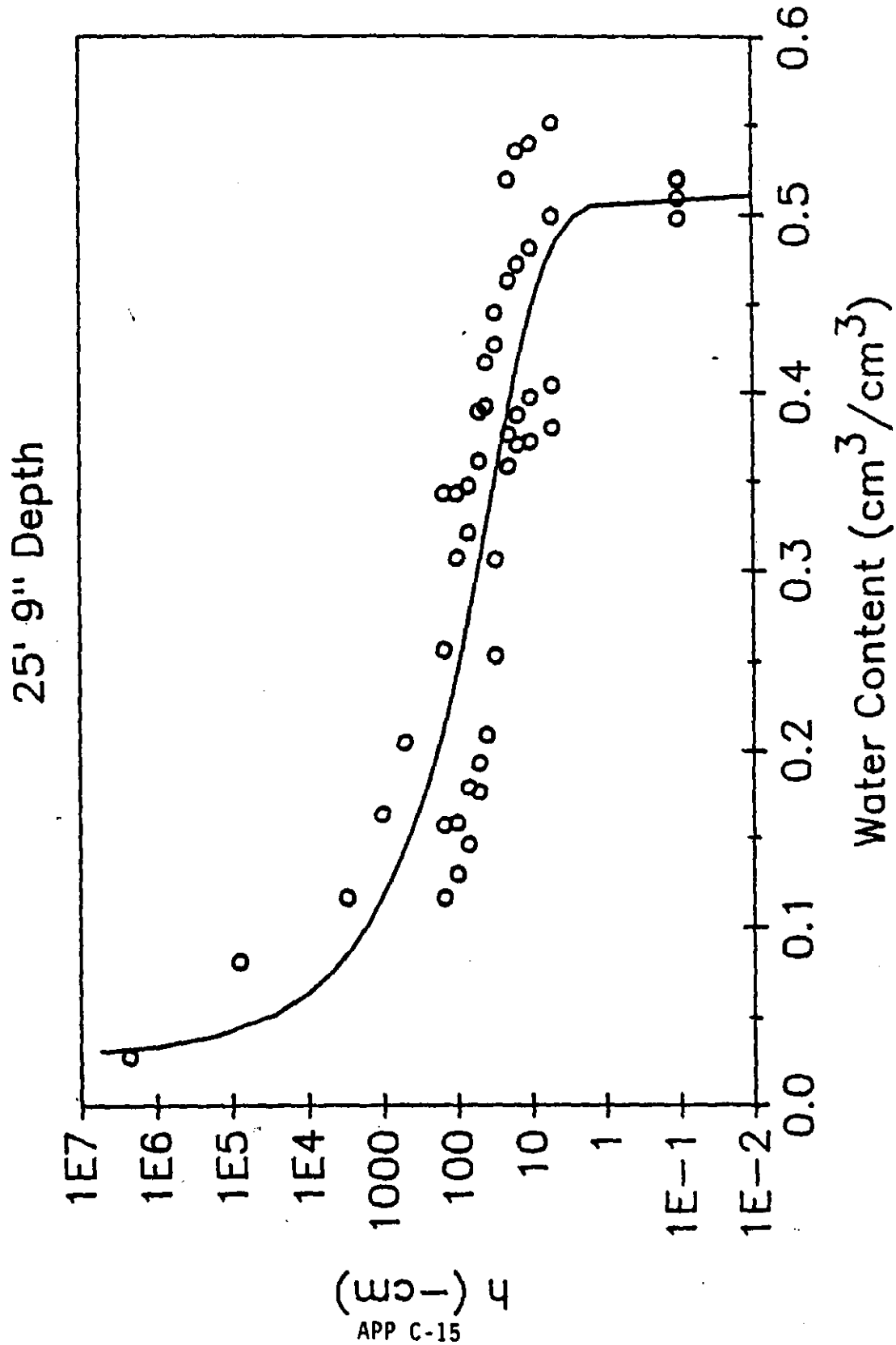
25' 9" Depth
h (-cm)
1E7
1E6
1E5
1E4
1000
100
10
1
1E-1
1E-2
0.0
0.1
0.2
0.3
0.4
0.5
0.6
Water Content (cm3/cm3)

Figure 4.

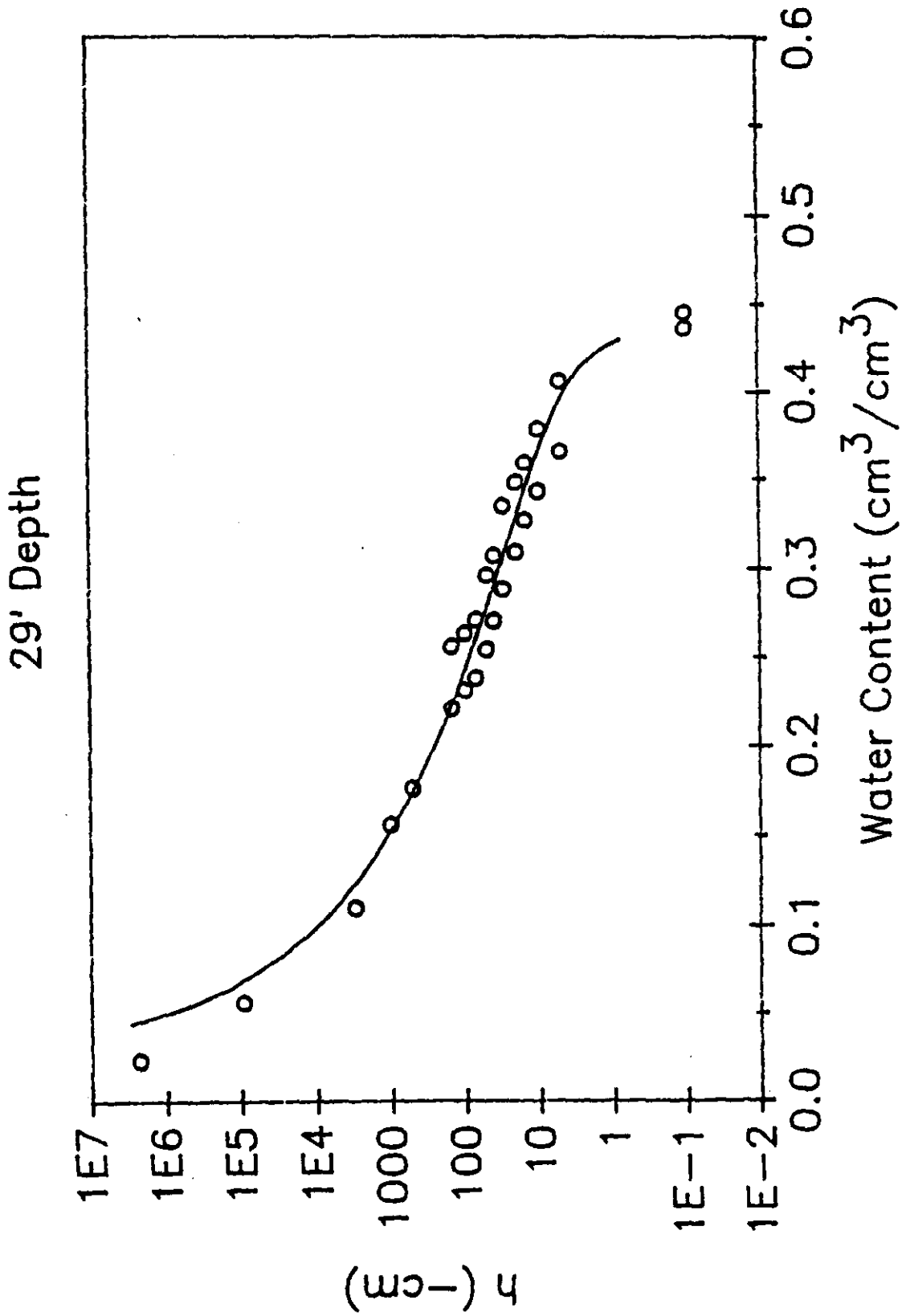
29' Depth
h (-cm)
1E7
1E6
1E5
1E4
1000
100
10
1
1E-1
1E-2
0.0
0.1
0.2
0.3
0.4
0.5
0.6
Water Content (cm3/cm3)

Figure 5.

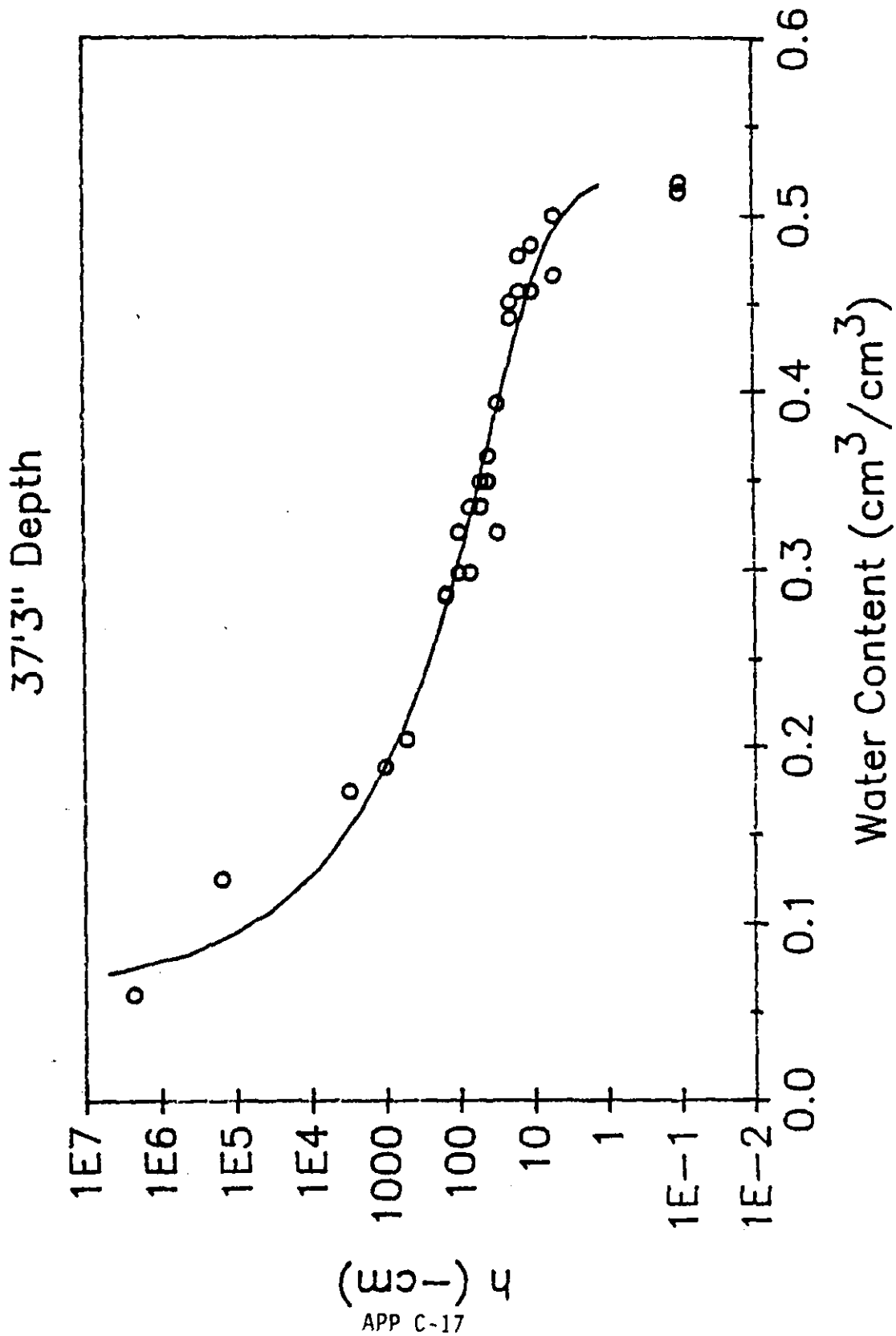
37'3" Depth
h (-cm)
1E7
1E6
1E5
1E4
1000
100
10
1
1E-1
1E-2
0.0
0.1
0.2
0.3
0.4
0.5
0.6
Water Content (cm3/cm3)

Figure 6.

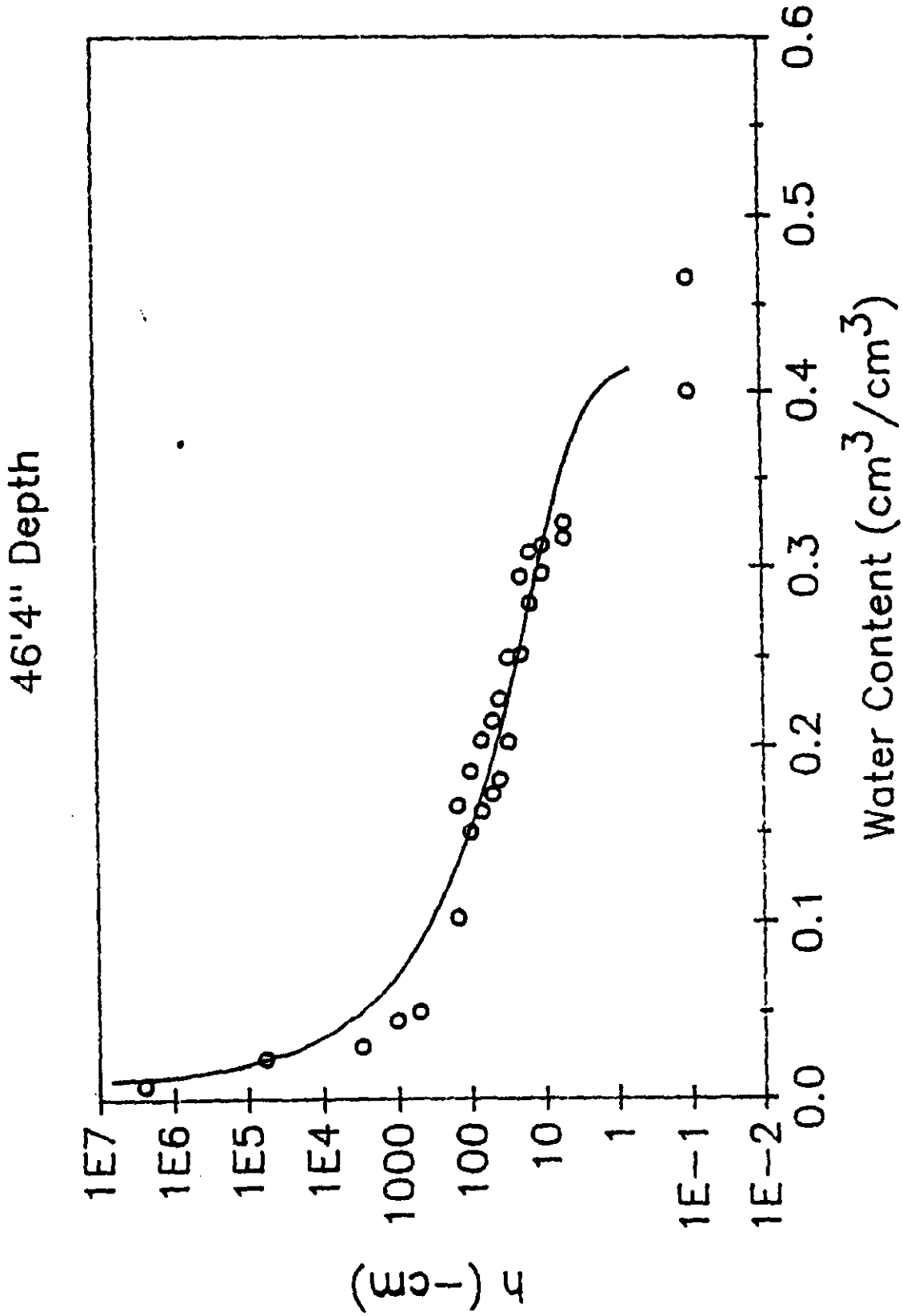
46'4" Depth
Water Content (cm^3/cm^3)
0.0
0.1
0.2
0.3
0.4
0.5
0.6
h (-cm)
1E7
1E6
1E5
1E4
1000
100
10
1
1E-1
1E-2

Figure 7.

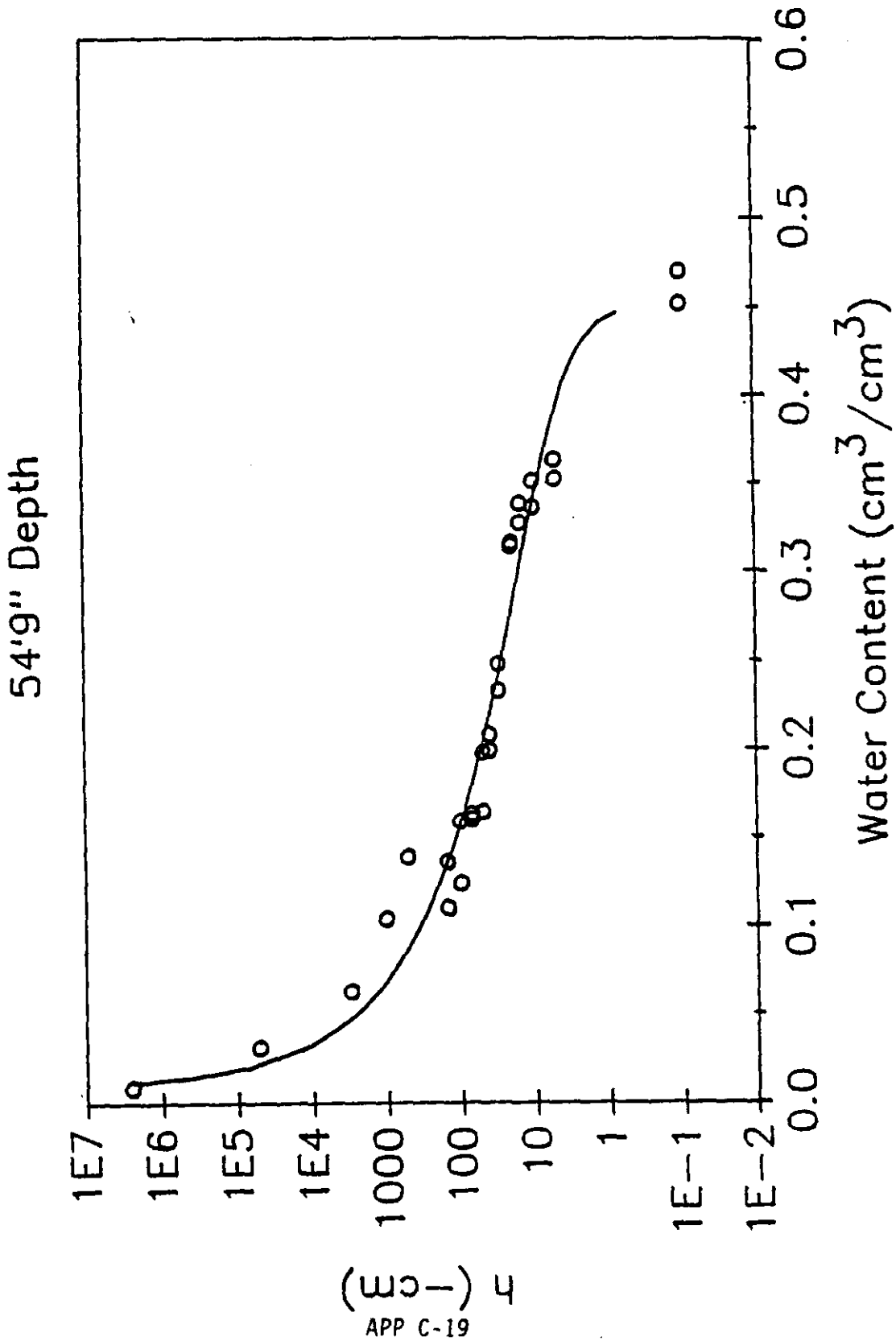
54'9" Depth
Water Content (cm^3/cm^3)
0.0
0.1
0.2
0.3
0.4
0.5
0.6
1E−2
1E−1
1
10
100
1000
1E4
1E5
1E6
1E7
h (−cm)

Figure 8.

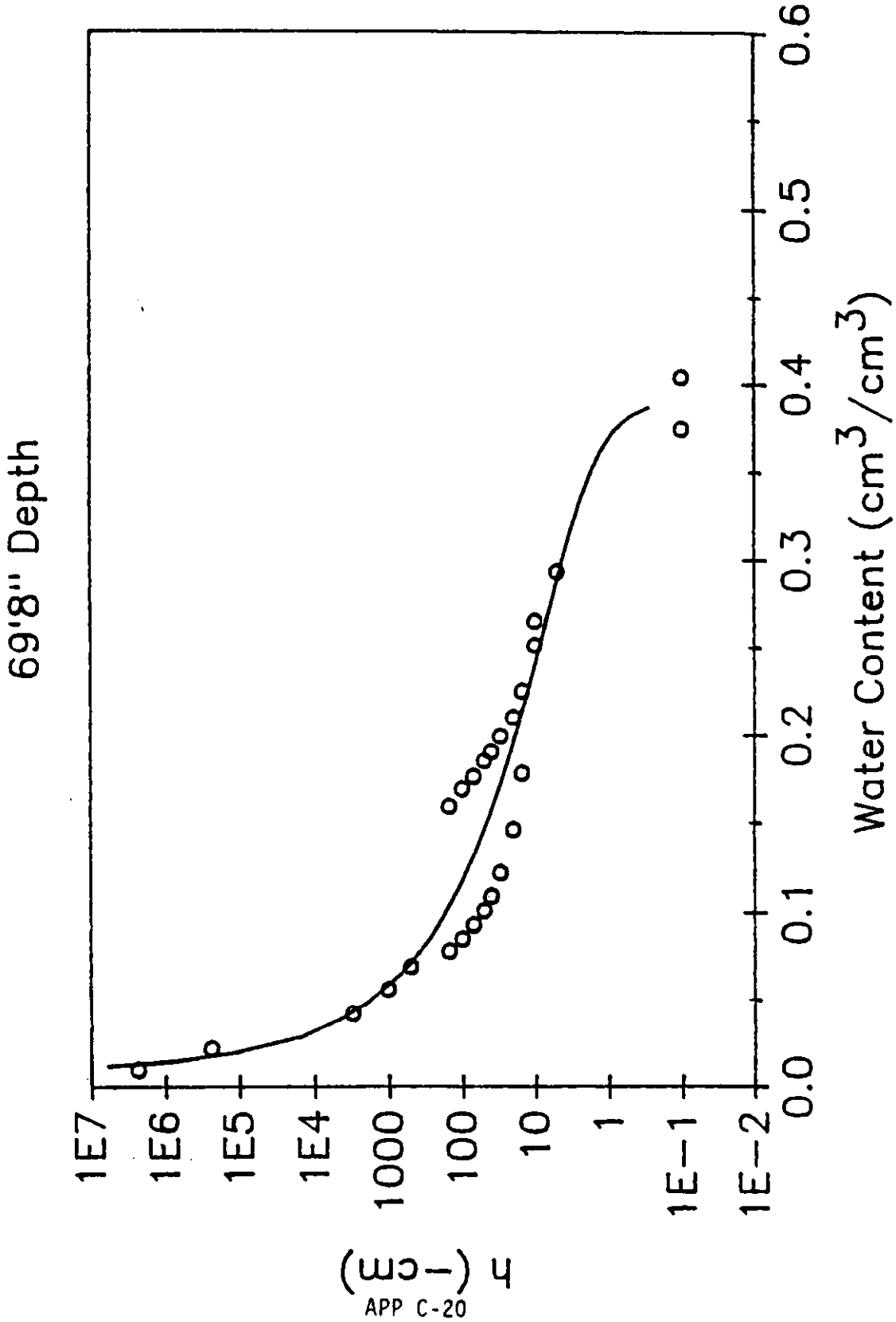
69'8" Depth
h (-cm)
1E7
1E6
1E5
1E4
1000
100
10
1
1E-1
1E-2
0.0
0.1
0.2
0.3
0.4
0.5
0.6
Water Content (cm3/cm3)

Figure 9.

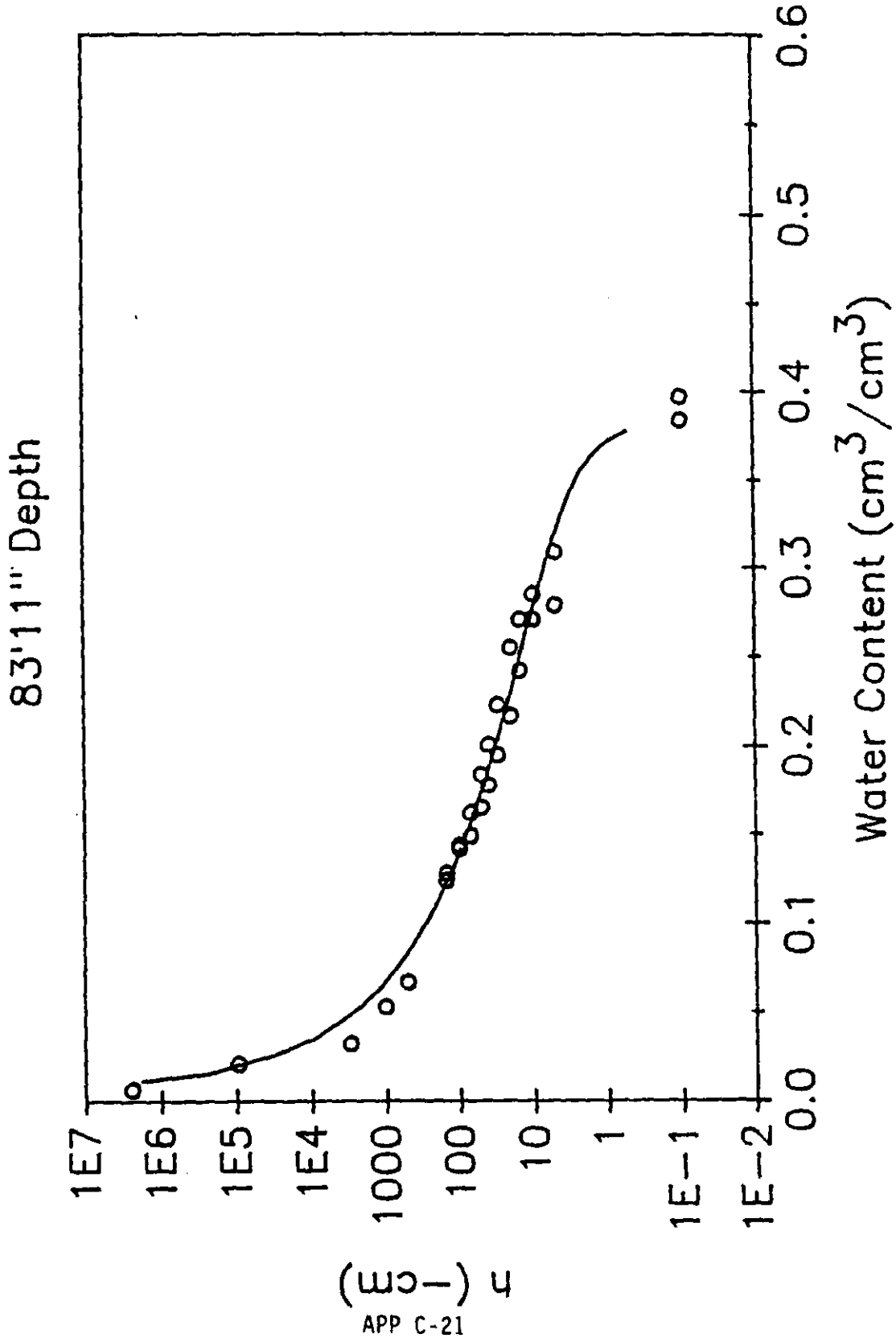
83'11" Depth
Water Content (cm^3/cm^3)
0.0
0.1
0.2
0.3
0.4
0.5
0.6
h (-cm)
1E7
1E6
1E5
1E4
1000
100
10
1
1E-1
1E-2

Figure 10.

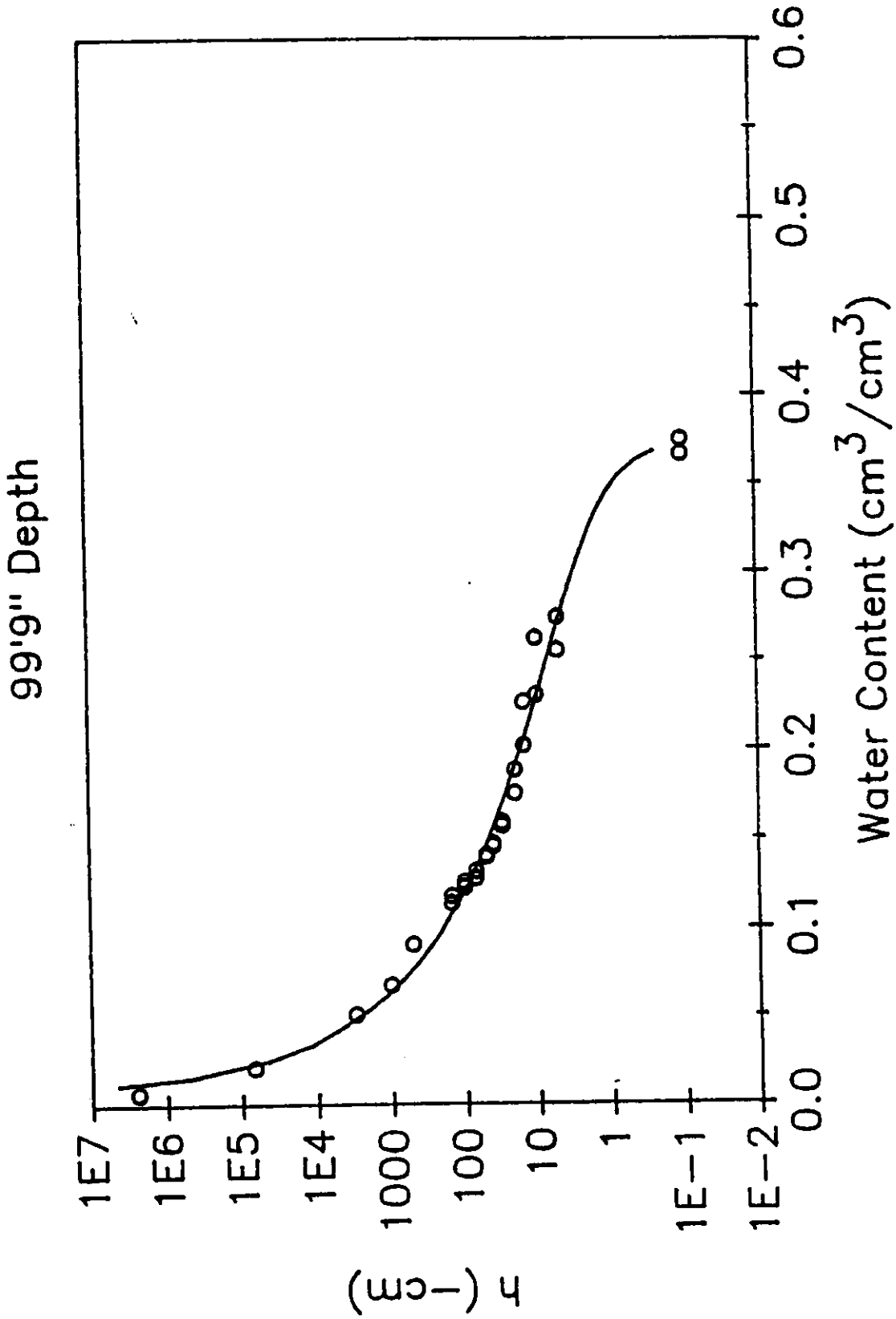
99'9" Depth
Water Content (cm^3/cm^3)
0.0
0.1
0.2
0.3
0.4
0.5
0.6
1E−2
1E−1
1
10
100
1000
1E4
1E5
1E6
1E7
ψ (−cm)

Figure 11.

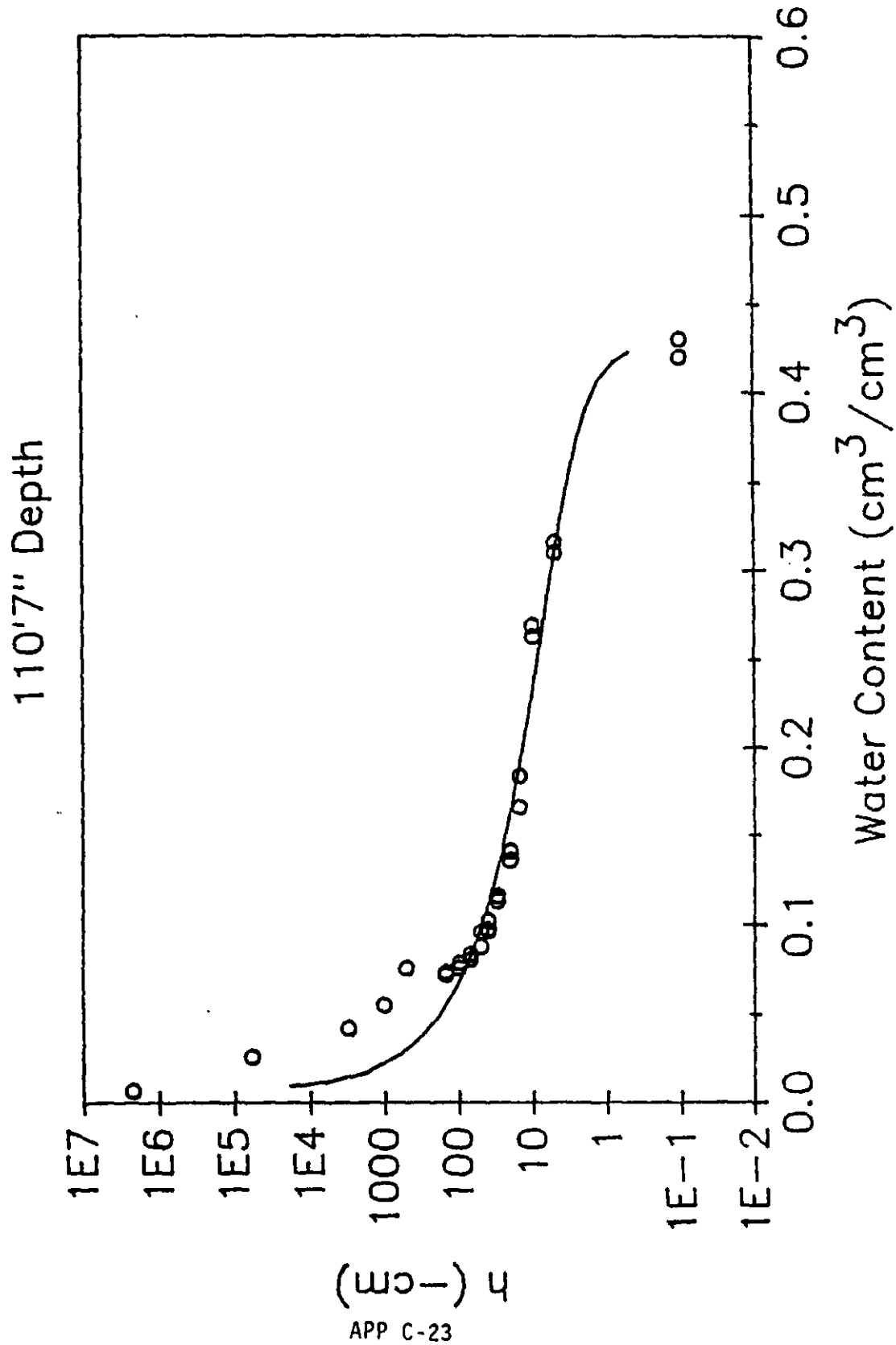
110'7" Depth
Water Content (cm^3/cm^3)
h (-cm)
0.0
0.1
0.2
0.3
0.4
0.5
0.6
1E7
1E6
1E5
1E4
1000
100
10
1
1E-1
1E-2

Figure 12.

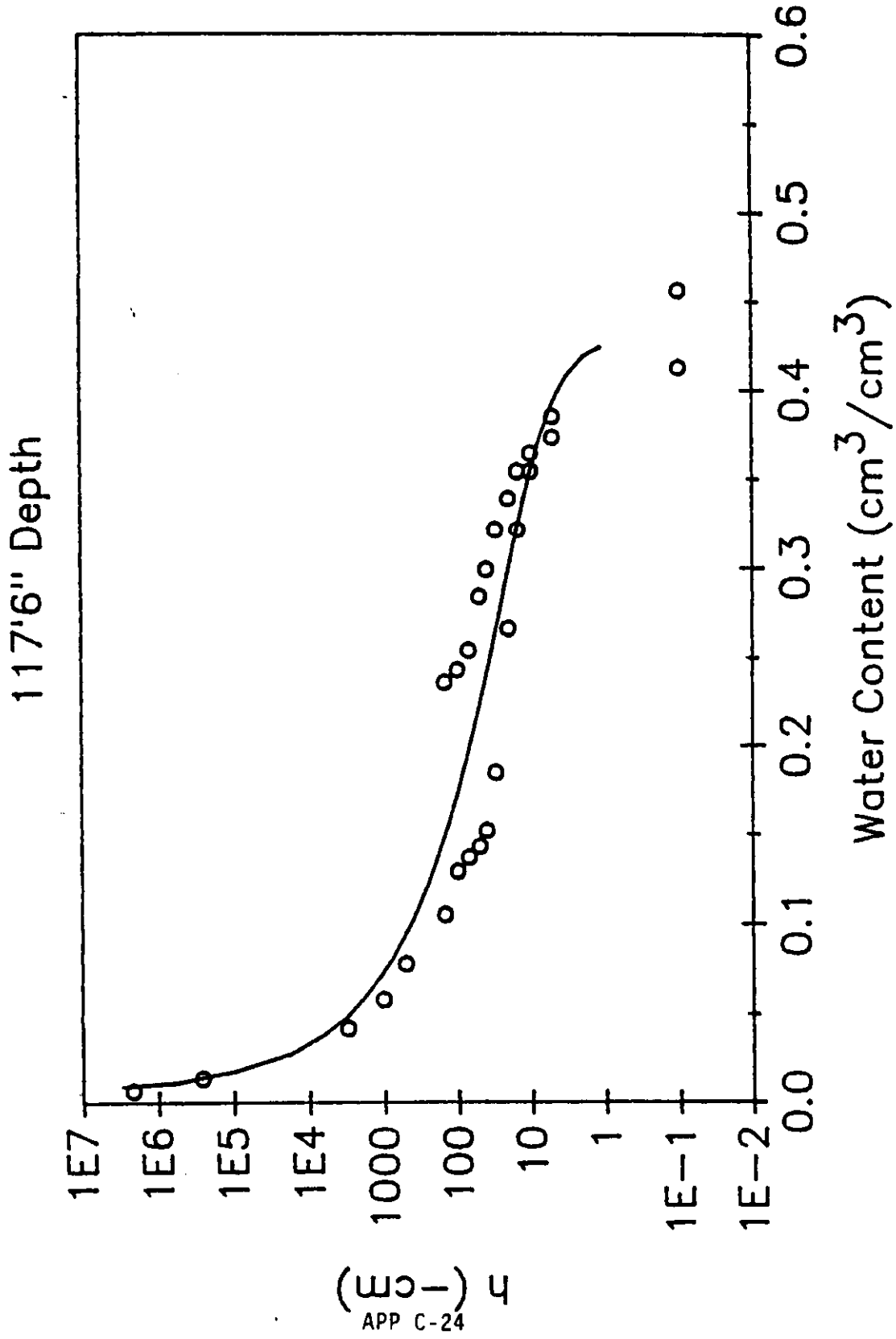
117'6" Depth
h (-cm)
1E7
1E6
1E5
1E4
1000
100
10
1
1E-1
1E-2
0.0
0.1
0.2
0.3
0.4
0.5
0.6
Water Content (cm3/cm3)

Figure 13.

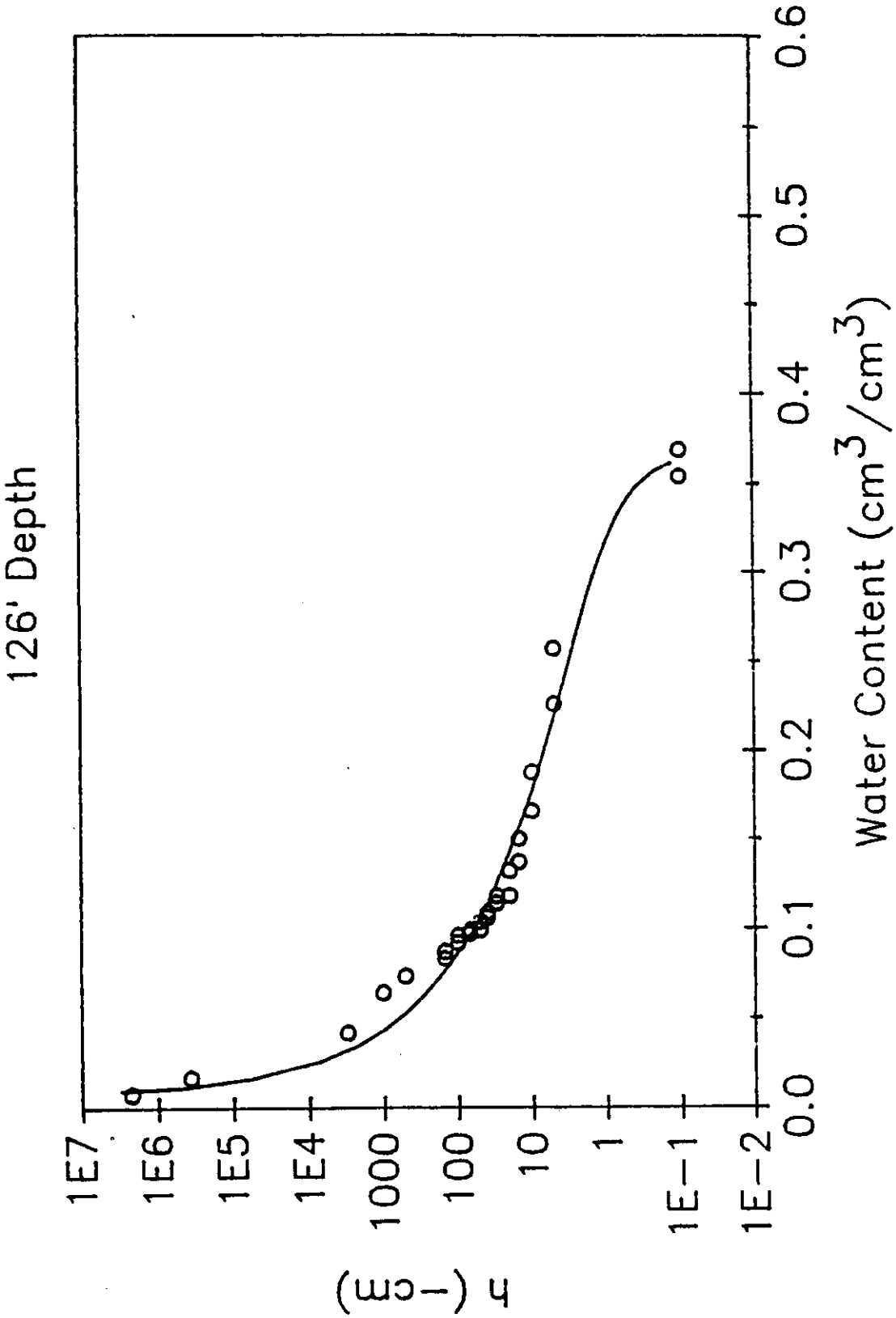
126' Depth
Water Content (cm^3/cm^3)
0.0
0.1
0.2
0.3
0.4
0.5
0.6
h (-cm)
1E7
1E6
1E5
1E4
1000
100
10
1
1E-1
1E-2

Figure 14.

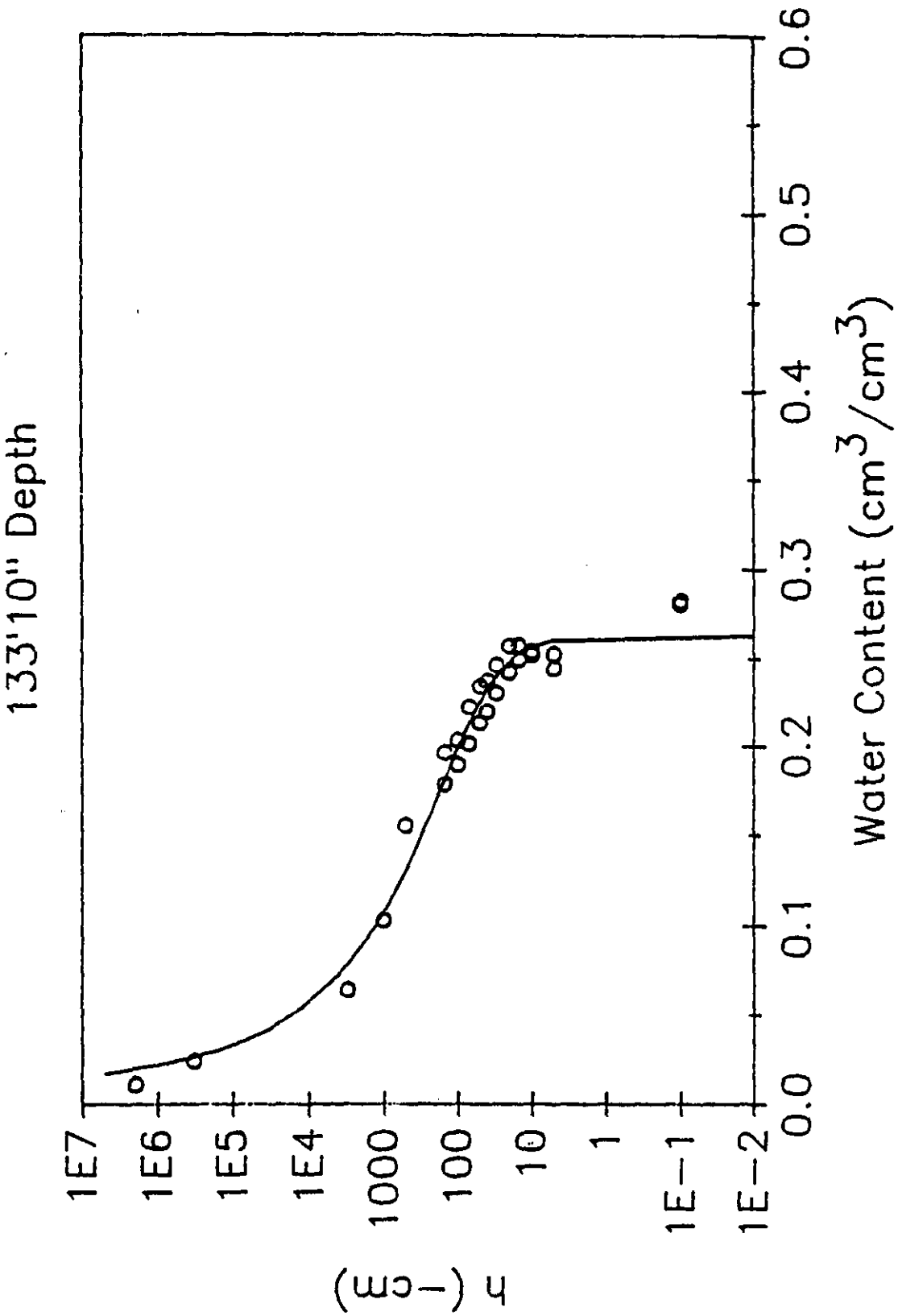
133'10" Depth
h (-cm)
1E7
1E6
1E5
1E4
1000
100
10
1
1E-1
1E-2
0.0
0.1
0.2
0.3
0.4
0.5
0.6
Water Content (cm3/cm3)

Figure 15.

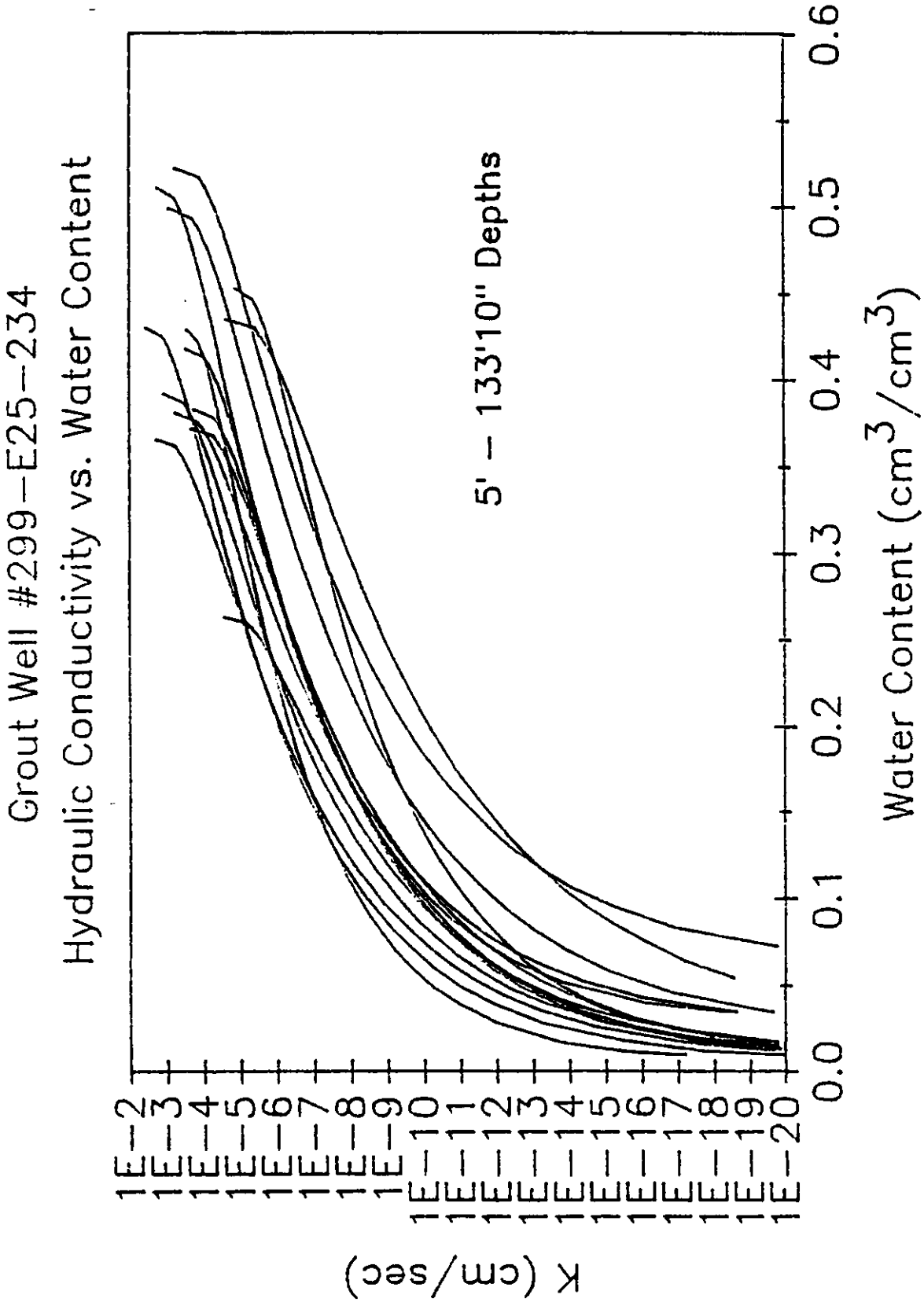
Grout Well #299-E25-234
Hydraulic Conductivity vs. Water Content
5' - 133'10" Depths
K (cm/sec)
1E-2
1E-3
1E-4
1E-5
1E-6
1E-7
1E-8
1E-9
1E-10
1E-11
1E-12
1E-13
1E-14
1E-15
1E-16
1E-17
1E-18
1E-19
1E-20
0.0
0.1
0.2
0.3
0.4
0.5
0.6
Water Content (cm3/cm3)

This page intentionally left blank.

DISTRIBUTION

Number of copies

OFFSITE

3 Battelle Memorial Institute
Project Management Division
505 King Avenue
Columbus, OH 43201

W. A. Carbeiner
R. A. Nathan
Technical Library

3 EG & G, Inc.
2151 North Blvd.
Idaho Falls, ID 83415

R. G. Baca
S. O. Magnuson
R. R. Seitz

1 Environmental Protection Agency
Office of Radiation Programs
(ANR-458)
401 M Street S.W.
Washington, DC 20460

Sheldon Meyers

5 S. W. Research Institute
Division 20, Center for
Regulatory Analysis
6220 Culebra Rd.
San Antonio, TX 78284

B. Sagar

1 United States Geological Survey
1201 Pacific Avenue, Suite 600
Tacoma, WA 98402

W. Staubitz

Number of copies

1 University of Arizona
Department of Soil and Water
Science
Tucson, AZ 85721

P. J. Wierenga

1 University of Arizona
Department of Water Resources
Building 11
Tucson, AZ 87521

S. P. Neuman

3 University of California
Earth Sciences Division
Lawrence Berkeley Laboratory
Berkeley, CA 94720

K. Pruess
C. F. Tsang
J. S. Wang

1 University of California
Lawrence Livermore National
Laboratory
P.O. Box 808
Livermore, CA 94550

L. D. Ramspott

1 SAIC
101 Convention Center Drive,
Suite 860
Las Vegas, NV 89109

U-Sun Park

Number of copies

ONSITE

9 U.S. Department of Energy-Richland Operations Office

M. J. Anthony	A6-95
G. J. Bracken	A6-80
R. D. Freeberg	A6-95
R. E. Gerton	A6-80
R. D. Izatt	A6-95
K. M. Thompson	A6-95
S. H. Wisness	A6-95
DOE/RL Public Reading Room (2)	A1-65

52 Pacific Northwest Laboratory

N. J. Aimo	K6-77
M. P. Bergeron	K6-77
L. L. Cadwell	P7-54
M. D. Campbell	K6-77
J. W. Cary	K6-77
C. R. Cole	K6-77
P. G. Doctor	K6-96
J. L. Downs	P7-54
J. W. Falco	K6-78
M. J. Fayer	K6-77
M. G. Foley	K6-84
M. D. Freshley	K6-96
G. W. Gee (10)	K6-77
J. M. Hales	K6-04
P. C. Hays	K6-86
D. J. Holford	K6-77
C. T. Kincaid	K6-77
R. R. Kirkham	K6-77
G. V. Last	K6-96
S. O. Link	P7-54
J. F. McBride	K6-77
E. M. Murphy	K6-77
R. W. Nelson	K6-77
W. E. Nichols	K6-77
W. T. Pennell	K6-98
M. L. Rockhold	K6-77
R. J. Serne	K6-81
C. S. Simmons	K6-77
R. L. Skaggs	K6-77
J. L. Smoot (5)	K6-77
J. D. Smyth	K6-25

Number of copies

Pacific Northwest Laboratory (cont.)

G. P. Streile	K6-77
J. E. Szecsody (5)	K6-77
Publishing Coordination	K1-11
Technical Report Files	P8-55

39 Westinghouse Hanford Company

M. R. Adams	H4-55
L. C. Brown	H4-51
J. W. Cammann	H4-54
M. P. Connelly	H4-54
H. F. Daugherty	R2-53
J. D. Davis	H4-54
A. J. Diliberto	R2-12
K. R. Fecht	H4-56
V. W. Hall	B2-15
C. H. Huang	R1-80
R. L. Jackson	H4-56
M. T. Jansky	H4-57
K. N. Jordan	B2-15
R. Khaleel	H4-54
N. W. Kline	H0-31
D. S. Landeen	H4-54
T. Legore	B4-63
R. E. Lerch	B2-35
H. E. McGuire	B2-35
B. E. Opitz	R1-19
M. G. Piepho	H0-54
S. J. Phillips	L7-10
W. H. Price	S0-03
R. E. Raymond	R1-62
J. F. Relyea	H4-54
P. D. Rittman	H4-54
W. A. Skelly	H4-55
J. C. Sonnichsen	H4-54
J. Sprouse	H4-17
N. R. Wing	H4-54
D. D. Wodrich	R1-48
R. D. Wojtasek	B2-15
J. C. Womack	R2-18
D. E. Wood	B2-19
Central Files	L8-04
EDMC	H4-22
Publications Services (3)	H4-17